

DIFFUSE REFLECTANCE INFRARED SPECTROSCOPY STUDIES  
OF THE AIR OXIDATION OF COAL SURFACES

E. L. Fuller, Jr. and N. R. Smyrl

Oak Ridge National Laboratory(\*)

Oak Ridge, TN 37831-2008

INTRODUCTION

Oxidation of coals is of concern to those interested in the weathering that begins as soon as the mined material is wrested from the humid, reducing, pressurized environment of the underground seam. The loss of energy content comprises an obvious economic impact to combustion processes. Flocculation and coking processes are both deleteriously effected whereas systematic information regarding the structure and reaction mechanisms can be obtained. This work is directed primarily to defining the surface structures and mechanisms occurring at the air/coal interface.

EXPERIMENTAL

Diffuse Reflectance Infrared Fourier Transform (DRIFT) spectroscopic analyses provide a wealth of information related to the chemical changes wrought in air oxidation of coals, as noted in the spectra of Figure 1. These spectra were obtained by direct observation of an aliquot of powder subjected to the temperature and chemical treatment in the reactor that resides continuously in the analytical beam in the DRIFT attachment within the infrared spectrometer. Detailed descriptions of the equipment and techniques have been reported elsewhere<sup>1,2</sup>. Each spectrum is presented in the  $\text{Log}[R(\text{sample})/R(\text{reference})]$ , "absorbance", format as noted in reference number 1. No numerical values are reported since they are not needed for the qualitative analyses discussed in this report.

RESULTS AND DISCUSSION

Examination of the spectra elucidates several features related to the mechanism of the oxidation of the powder surfaces:

(A) The oxidation progressively consumes the aliphatic hydrogen as witnessed in the loss of characteristic absorbance in the 3000-2800 wavenumber region, generally associated with interaction of the electromagnetic energy with the resonance -C-H, -CH<sub>2</sub> and -CH<sub>3</sub> stretching vibrations.

(B) Simultaneously there is an insertion of oxygen into the carbonaceous substrate to form carbonyl groups manifesting a marked enhancement of absorbance in the 1900-1600 wavenumber region, long known to be associated with the C=O vibrational

modes.

(C) The band at ca. 1550 wavenumbers due to the O-C-O and/or C-O-C bending mode is enhanced due to the oxygen enrichment of the coal structure in the surface regime penetrated by the reflecting infrared beam (see also Figure 2) In addition, the stretching vibrations of carboxylate salts are known to be manifest in absorption in this energy regime.

(D) The triplet at ca. 800 +/-50 wavenumbers (due to the out-of-plane bending mode of aromatic C-H) becomes less prominent due to the loss of "aromatic" character of the oxidized material. The residual doublet in this region is much akin to the lattice modes of kaolinitic clays, consistent with the hydroxyl bands noted below in (E).

(E) The broad triangular-shaped band 3600-2000 wavenumbers remains relatively unchanged, indicating relatively little or no change in the amount and/or distribution of hydrogen bonded O-H (phenolic, alcoholic, acidic, aquatic, etc.). The narrow bands (3600-3500 wavenumbers) of the clay mineral hydroxyl groups do become more distinct as the 3500 wavenumber feature is broadened.

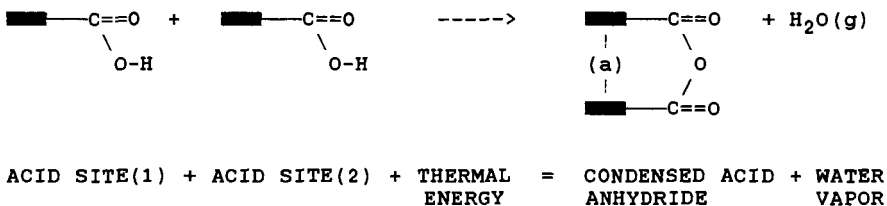
(F) The "aromatic" C-H band does not seem to be appreciably attacked by the oxygen treatment. Previous workers have generally attributed the band at 3000 to 3200 to an "aromatic" C-H vibrational mode. The peak value appears to shift from ca. 3050 to 3080 wavenumbers as aliphatic (-C-H) and olefinic (=C-H) entities are consumed. This is a tentative interpretation since the effect may involve another distinct type of aromatic C-H entity, not yet defined at this point in time.

Few, if any, techniques are individually able to provide as much information related to the oxidation of coals as does the in situ DRIFT technique. Additional quantitative data will be presented using the analytical techniques developed previously<sup>1</sup>.

These qualitative analyses are extremely informative and valuable in elucidating the process of weathering and resultant ramifications related to the processing of coals<sup>2</sup>. In addition a more detailed understanding is obtained by examining the difference spectra, depicting the changes induced with respect to the initial (unoxidized) material. Each of the difference spectra were obtained by direct subtraction without any arithmetic adjustment for sample size, geometric variations, etc. that pre present in other more classical infrared techniques<sup>1</sup>. By presenting the data in absorbance format (rather than Kubelka-Munk or remission units) we note that we have a distinctly direct ratiometric comparison to the reference material (rather than each mathematically ratioed to a diffusely reflecting reference material, KBr, CsI, NaCl, etc). The spectral changes can then be

observed in their own right on a much expanded scale and with a much more realistic interpretable background base line as noted in Figure 2. Now we can observe not only more accurate measures of the enhanced absorbance and more precise peak locations, but also delineate the progressive increase in the population of four (if not five) discrete carbonyl species based on observed inflection points in the curves formed by connecting the data points comprising the spectra.

These results are consistent with the successive oxygen insertion to form (1) aldo/keto groups, (2) acido groups, (3) acid anhydro groups, and finally (4) carbonato groups all as precursors to the ultimate release of the oxidized products of carbon dioxide and carbon monoxide. Earlier work at 400 C showed similar results albeit with faster rates<sup>1</sup>. In this work we note that the spectral distribution after 400 C oxidation differs from the 200 C result in additional transformation of the low wavenumber intensity to enhance the higher wavenumber bands (see Figure 3). This indicates that there is a greater mobility of the acido groups at 400 C to allow requisite juxtaposition of two precursors subsequent to expulsion of molecular water (dehydration) concomitant to the condensation to form the surface anhydride. This condition is contrasted to the homogeneous reactions in gas phases and/or liquid states where each of the reacting entities is completely mobile and the only activation barrier involves the energy to scission sigma bonds. A schematic representation of the surface reaction is presented below:



The initiation of the reaction requires enough energy to bring the acid entities to within a distance approaching "a" as well as the scission of both a C-O bond and an O-H bond either separately or in concert. Oxidation at 300 C yields intermediate results as shown by the 1810 and 1850 wavenumber feature in Figure 4. The results at 125 C show very little absorbance at 1850 wavenumbers, as revealed in the data of Figure 5. Subsequent elevation to the isothermal oxidation at 400 C is required to form the anhydro species. In view of the observations on more mobile configurations, "Phthalic acid melts with decomposition to the anhydride at temperatures ranging from 200 to 230°, depending on the rate of heating and the condition of the glass capillary surfaces."<sup>4</sup> This citation exemplarily refers to the bond

cleavage impediment with little or no migration barrier to the anhydride coalescence. The slight inflection at ca. 1850 wavenumbers is probably due to the small concentration of acid sites formed by oxidation of adjacent susceptible sites on the coal substrate. The migration of more dispersed acid entities is brought about only at the higher temperatures.

Further details and substantiation of the mechanisms are derived from the data of Figure 6. Here we note that the prolonged reaction at 125 C involved only minor amounts of water loss and the DRIFT spectra reveal marked loss of water due to the additional thermal activation to 400 C. These results are still of a qualitative nature but show the benefits of detailed examination to aid in our understanding of the oxidation of coals as related to the important chemical weathering processes, and precursor states to combustion at much higher temperatures.

Our project continues to develop the methodology and technique to acquire more details and more quantitative data. These results are for a single sample of a subbituminous coal from the Wyodak mine of the Roland/Smith seam, Gillette, Wyoming. Even this sample is unique in that it was acquired from a freshly opened mine face, hermetically sealed in a light tight container and maintained at 25 +/-3 C prior to these analyses. Additional studies on "real" materials will aid in their description with respect to our "reference" materials. Not to mention, the need to apply the versatile DRIFT technique to coals of other ranks. This work extends the affirmation, "Clearly, diffuse reflectance has overwhelming advantages in the characterization of high rank coals."<sup>5</sup> to a much broader extent. The major benefits arise from 1. ease of sample preparation, 2. reactions monitored without impediment of matrix (ie. KBr), 3. measurements possible in reaction medium (not inert gas as in photoacoustic), 4. reference spectrum acquired in vacuum, 5. inherently nondestructive (allows other supporting analyses on same aliquot), 6. the ability to acquire spectra over a wide range of temperatures (77 to 800 K, at present), and 7. direct measurements in either static (batch) or flowing (continuous) modes. The additional information provided by the DRIFT techniques relies on the vast amount of information obtained over the years via the more arduous classical procedures.

#### SUMMARY

Air oxidation of this sub-bituminous coal proceeds via oxygen insertion into the organic substrate progressively forming aldo/keto groups, acid groups and acid anhydride entities while consuming the hydrogen of the aliphatic hydrocarbon entities. The amount of anhydride is limited (a minority of the total oxidized sites), and serves to measure the number or adjacent susceptible sites on the coal surface. Above ca. 200 C there is sufficient activation to impart the mobility to allow the acid functionalities to come together and dehydrate to form the condensed anhydride species. Above 400 C the anhydro groups

predominate in the steady state production of carbon dioxide and water vapor. These studies show the merits of the in situ, real time DRIFT techniques for the unique definition of the chemistry and structure of coals.

#### REFERENCES

1. E. L. Fuller, Jr., N. R. Smyrl, and R. L. Howell, Chemistry and Structure of Fuels: Reaction Monitoring with Diffuse Reflectance Infrared Spectroscopy, in "Chemical, Biological and Industrial Applications of Infrared Spectroscopy" edited by James R. Durig, Wiley-Interscience, 1985.
2. E. L. Fuller, Jr. and N. R. Smyrl, Chemistry and Structure of Coals: Diffuse Reflectance Infrared Spectroscopy Equipment and Techniques, FUEL, 64, 1143-1149, (1985).
3. E. L. Fuller, Jr. and N. R. Smyrl, Diffuse Reflectance Infrared Fourier Transform, DRIFT, Studies of Coal Preparation Techniques (Preliminary Results), ORNL/CF-88/27, March 1988.
4. L. F. Fieser and M. Fieser, "Organic Chemistry" D.C. Heath and Co, 1944, p670.
5. P. Painter, B. Bartges, D. Plasizynski, T. Plasizynski, A. Lichtus, and M. Coleman, "Novel Methods for FTIR Analyses of Coal" ACS Fuel Chem. Prep. 31 65 (1986).

(\*) Operated by Martin Marietta Energy Systems, Inc. for the Department of Energy under contract No. DE-AC05-84OR21400.

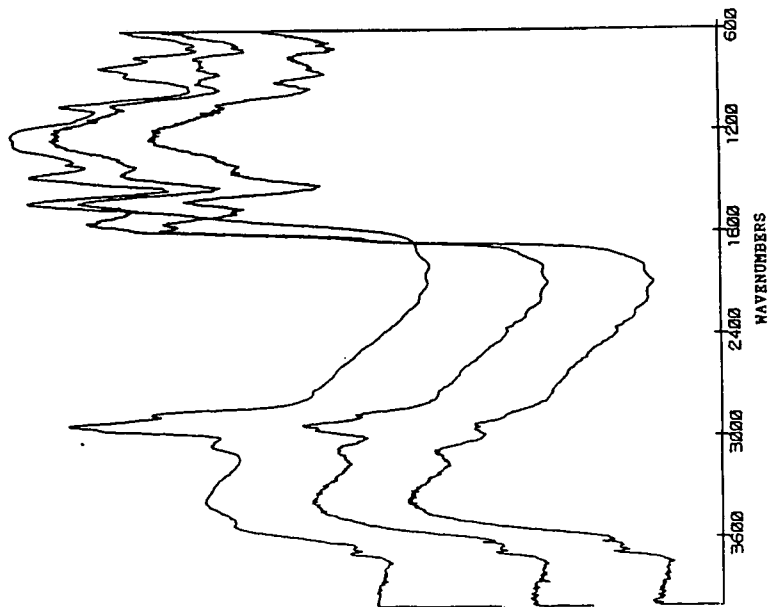


Figure 1. REPRESENTATIVE DRIFT SPECTRA FOR 200 C AIR OXIDATION OF WYODAK COAL POWDER. A. Original (unoxidized) material in vacuo, 200 C; B. 23 hours, 200 C, 100 cc/min; C. 129 hours, 200 C, 100 cc/min.

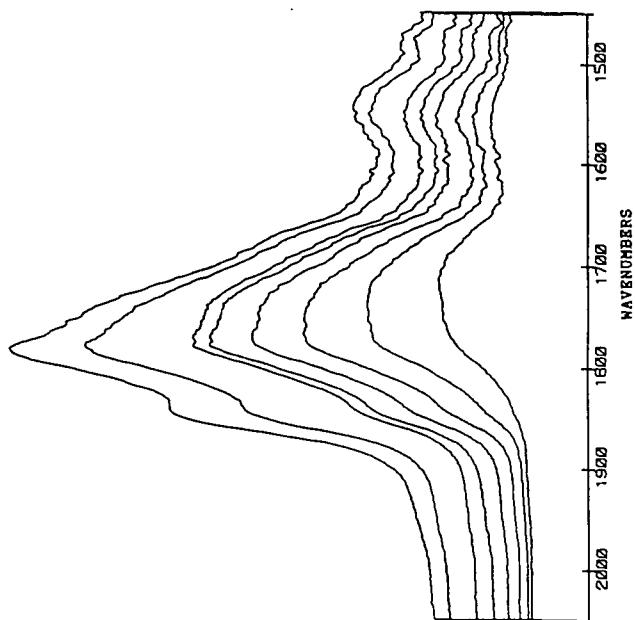


Figure 2. DRIFT DIFFERENCE SPECTRA FOR 200 C OXIDATION OF WYODAK POWDER. Successive spectra for 2, 4, 7, 10, 13, 23, 46, and 129 hours exposure (100 cc/min) isothermally in the beam of the spectrometer.

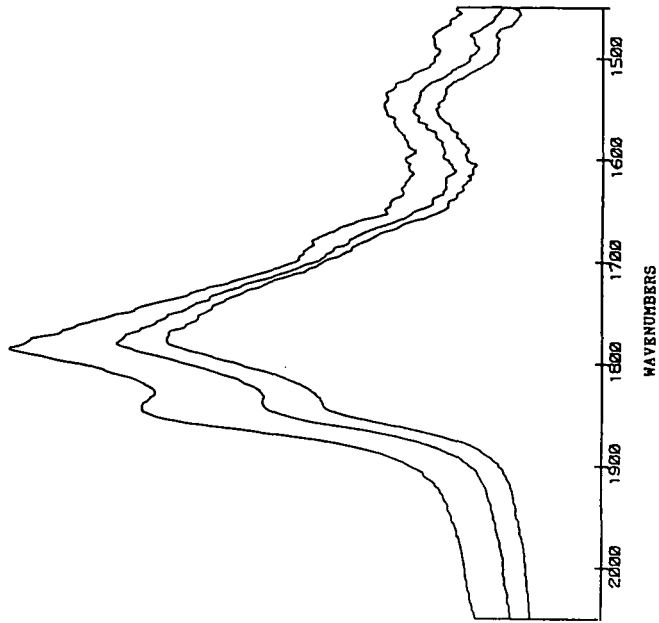


Figure 4. DRIFT DIFFERENCE SPECTRA FOR 300 C AIR OXIDATION OF WYODAK COAL POWDER. Spectra acquired after 1, 2, and 18 hours in situ exposure to 100 cc/min air flow.

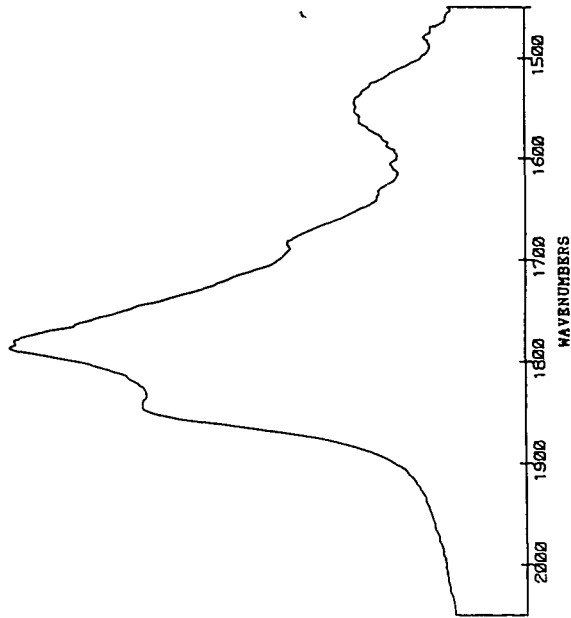


Figure 3. DRIFT DIFFERENCE SPECTRUM FOR 400 C IN SITU OXIDATION OF WYODAK. One hour isothermal exposure at 100 cc/min flow of air through reaction cell.

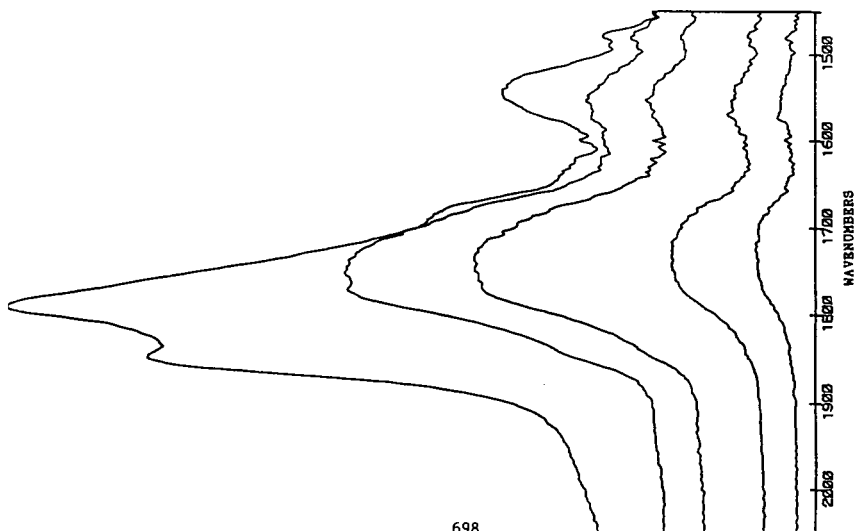


Figure 5. DRIFT DIFFERENCE SPECTRA FOR 125 C ISOTHERMAL OXIDATION OF WYODAK COAL POWDER AND SUBSEQUENT 400 C. Spectra acquired after 24, 48, 124, and 188 hours at 125 C where steady state conditions prevail. The uppermost curve was acquired after an additional 17 hours isothermal reaction at 400 C at the same 100 cc/min delivery of air reactant.

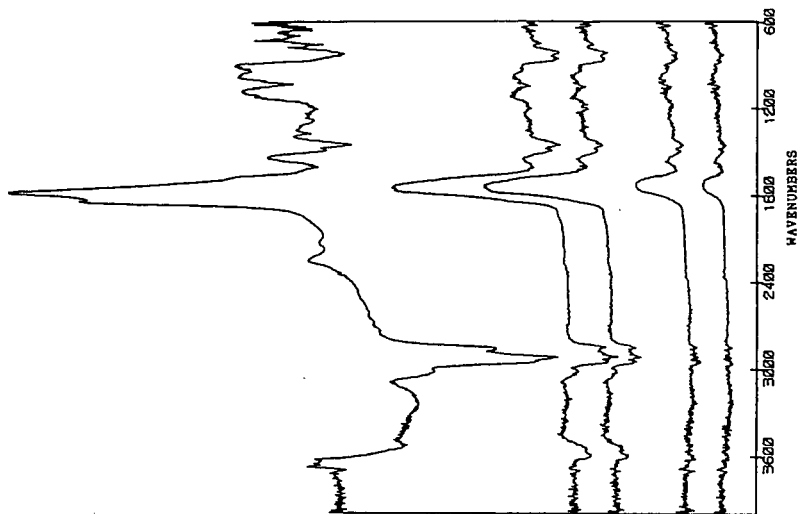


Figure 6. ENTIRE DRIFT DIFFERENCE SPECTRA FOR THE 125/400 C AIR OXIDATION OF WYODAK COAL POWDER. The relevant data are presented in Figure 5. Low temperature oxidation proceeds to the organic acid state and subsequent higher temperatures are required to dehydrate to the acid anhydride state as the precursor to carbon dioxide formation.

## LOW-TEMPERATURE COAL WEATHERING

M. M. Wu, R. A. Winschel and G. A. Robbins

### CONSOLIDATION COAL COMPANY

Research & Development

4000 Brownsville Road

Library, PA 15129

### ABSTRACT

Illinois 6 coal (hvBb) was weathered for up to 330 days at 25 and 80°C with humid air. Its behavior was compared with Pittsburgh Seam (hvAb) and Horsepen Seam (mvb) coals weathered under the same conditions. The weathering rate showed a strong dependence on temperature and coal rank. At 25°C, the Illinois 6 coal showed much more substantial changes in chemical and physical properties upon weathering. Spectroscopic data indicate that the concentration of organic oxygen groups in the coal may eventually level off. Two potential causes of this behavior are proposed. Thermal (non-oxidative) treatment at 80°C has little effect on the chemical and physical properties of a fresh hvAb coal.

### INTRODUCTION

Weathering can alter organic and mineral constituents of coal, change its chemical and physical properties and affect its utilization (1). Extensive laboratory research has been performed to study this important phenomenon. However, published studies have come to significantly different conclusions concerning the chemical nature of coal weathering (or oxidation). The rate of changes in coal properties induced by coal weathering or oxidation are dependent on temperature. Most reported coal weathering simulation experiments have been conducted at temperatures greater than 100°C to accelerate the oxidation rate. However, the reaction mechanism is reportedly different at temperatures above and below 70 to 80°C (2,3).

Three separate coal weathering reactions (two oxidative and one thermal) were recently proposed by Gethner (4,5) based on a coal oxidation study conducted at temperatures of 25 to 100°C. The rate of each reaction had a different temperature dependency. Gethner concluded, and we concur, that ill-defined or poorly controlled coal weathering or oxidation experiments can result in inaccurate conclusions (5). In addition to temperature, coal weathering is also known to depend on coal rank, humidity and oxygen partial pressure (1,3,6). The work reported here is a systematic study of coal weathering performed at realistic conditions. Different ranks of coal, including Illinois 6 (hvBb), Pittsburgh Seam (hvAb) and Horsepen Seam (mvb) coals, were weathered for up to 500 days at 25 to 80°C with humid air under well-controlled conditions. The work with Pittsburgh Seam and Horsepen Seam coals was reported previously (7). This paper includes the recent results of this study, most of which were obtained using the Illinois 6 coal. For present purposes, we will define oxidative weathering as the progressive changes in coal properties that occur as coal is exposed to humid air at temperatures of 80°C or less.

In addition to oxidative weathering, experiments were also performed with a different Pittsburgh Seam coal and a slightly weathered Illinois 6 coal under

flowing humid N<sub>2</sub> at 80°C. The objective of these tests was to observe any non-oxidative, thermal effects on coal properties and chemical structural changes. This paper also includes recent results of this study.

## EXPERIMENTAL

The experimental apparatus and procedures used in the weathering study were described previously (7). The non-oxidative experiment was carried out using N<sub>2</sub> instead of air at otherwise the same conditions. The Illinois 6 coal used in this study is the natural -28 mesh portion of fresh run-of-mine (ROM) coal from a deep mine in Jefferson County, Illinois. The Pittsburgh Seam coal used in the non-oxidative weathering study is the natural -28 mesh portion of fresh ROM coal from a deep mine in Monongalia County, West Virginia. Analyses of these two coals are listed in Table 1. Properties of the Pittsburgh Seam and Horsepen Seam coals used in the oxidative study were reported elsewhere (7).

## RESULTS AND DISCUSSION

### OXIDATIVE WEATHERING

Changes in elemental composition (H,C,O) observed upon weathering occurred more rapidly for the Illinois 6 coal (hvBb) than for the Pittsburgh Seam (hvAb) and Horsepen Seam (mvb) coals, as shown below.

<u>Weathering Time at 80°C, Days</u>	<u>Illinois 6</u>		<u>Pittsburgh Seam</u>		<u>Horsepen Seam</u>	
	<u>0</u>	<u>46</u>	<u>0</u>	<u>45</u>	<u>0</u>	<u>51</u>
Carbon, wt % MAF	81.8	78.6	82.9	81.1	89.3	87.7
Hydrogen, wt % MAF	5.2	4.7	5.5	5.2	5.0	4.9
Oxygen, wt % MAF (diff.)	9.9	14.0	7.2	9.5	3.1	4.9

These values indicate that rates of change in elemental compositions with weathering time are dependent on coal rank (6).

The FTIR oxidation index is defined as the ratio of the integrated intensity of the carbonyl band (1635-1850 cm<sup>-1</sup>) to that of the C-H stretching band (2745-3194 cm<sup>-1</sup>) in the diffuse reflectance FTIR spectrum of coal (7,8). Increases in the oxidation index upon weathering can be attributed to the progressive oxidation of C-H groups to carbonyl groups as the coal weathers (8,9). The oxidation index is plotted in Figure 1 as a function of weathering time at 80°C for the three coals. The oxidation index of Illinois 6 coal not only increases more rapidly with weathering time, but it also has a higher initial value than Pittsburgh Seam and Horsepen Seam coals. This indicates that both the initial value and the rate of change with time of the oxidation index are rank dependent.

The rate of change with time of the oxidation index also depends on weathering temperature. In Figure 2, the oxidation index of Illinois 6 coal is plotted as functions of weathering time and temperature. Changes are rapid at 80°C, and slow, but experimentally significant, at 25°C. Significant changes in the oxidation index of coals weathered at 25°C were observable for the Illinois 6 coal but, as reported previously (7,10), not for the Pittsburgh Seam and Horsepen Seam coals.

Gieseler maximum fluidity was found to be one of the most sensitive indicators of oxidation for the higher rank coals (7,8). However, the lower rank Illinois 6 coal has essentially no fluidity, even when fresh. Though free swelling index (FSI) measurements are less sensitive to weathering than Gieseler fluidity, they do provide an indication of the effect of weathering on the thermoplastic properties (7,8). Figure 3 shows that the rate of change with weathering time of the free swelling index (FSI) of Illinois 6 coal is much greater at 80°C than at 25°C; however, even at 25°C, changes were significant. In contrast, there was very little change in the FSI of Pittsburgh Seam (7) and Horsepen Seam (10) coals weathered at 25°C. This again demonstrates the rank dependency of coal weathering. The FSI and oxidation index of weathered Illinois 6 coal are compared in Figure 4. Figure 4 shows that there is a general linear relationship between the oxidation index and FSI of Illinois 6 coal weathered at both 25 and 80°C, as also noted previously by Huffman et al. (9). The alkali extraction test (11) also shows a general linear relationship with oxidation index for the weathered Illinois 6 coal (Figure 5). Alkali extraction test results are expressed as percent transmittance at 520 nm.

As shown in Figure 1, the oxidation index of Illinois 6 coal weathered at 80°C appears to level off after about 46 days weathering. Results of X-ray photoelectron spectroscopic (XPS) characterizations of the coal weathered at 80°C are consistent with this observation. Table 2 lists the surface elemental compositions of the Illinois 6 coal weathered at 80°C for 0, 46 and 80 days. Organic oxygen was calculated by the method of Perry and Grint (12) in which inorganic oxygen is subtracted from total oxygen assuming inorganic oxygen is associated with Si and Al in oxide forms (12). The organic O/C ratio increased from 0.15 to 0.23 after 46 days weathering at 80°C (Table 2). As shown in Figure 6, an asymmetric C<sub>1s</sub> peak with a shoulder at high binding energy (287-292 eV) was observed by XPS, indicating that carbon-oxygen functional groups were generated upon weathering for 46 days at 80°C. This is in agreement with FTIR results that show production of carbonyl groups. As weathering time increased from 46 to 80 days, only a slight increase in organic O/C ratio, from 0.23 to 0.24, was observed (Table 2). In addition, there was no significant change in XPS C<sub>1s</sub> spectrum of the coal between 46 and 80 days (Figure 6).

There are at least two possible explanations for this observation. First, it may be that after 46 days at 80°C, most of the active sites originally available for oxidation had reacted, i.e., few active sites were available for further oxidation at these conditions. Painter et al. (13) reported that coal oxidation is indeed site selective. They concluded that benzylic sites are most easily oxidized to carbonyl groups. Low-temperature weathering work by Larsen et al. (2) supported this concept.

A second possibility is that after 46 days at 80°C, the rate of carbonyl production is matched by the rate of carbonyl destruction, e.g., by decarbonylation and decarboxylation. Gethner (4,5) noted the importance of decarbonylation and decarboxylation reactions during coal oxidation. The rate of carbonyl destruction must depend on the concentration of carbonyl groups. As oxidation proceeds, carbonyl concentrations increase and thus, the rate of carbonyl destruction should increase as well. Eventually, a state may be reached in which the rates of carbonyl production and destruction are equal.

At this point, our data do not confirm or refute either explanation. Additional work is under way to gain a better understanding of this.

## NON-OXIDATIVE WEATHERING

A reaction mechanism involving thermal decomposition of carbon-oxygen functional groups (e.g., decarboxylation) was proposed by Gethner (4,5). He noted that this reaction was independent of the oxidative reactions that occur during low-temperature oxidation (4,5). Non-oxidative thermal effects on coal properties and chemical structural changes were examined by treating a Pittsburgh Seam coal under flowing humid nitrogen at 80°C for 48.4 days. No significant changes in elemental compositions were observed over the duration of the test. In addition, Gieseler maximum fluidity, Audibert-Arnu dilatation, FTIR oxidation index and alkali extraction measurements all show little or no change. The Gieseler maximum fluidity and the oxidation index of the Pittsburgh Seam coal treated at 80°C in flowing humid N<sub>2</sub> are plotted as functions of time in Figure 7. These data show that the changes in coal properties that were noted in the oxidative weathering tests with Pittsburgh Seam coal are dependent on the presence of oxygen. Purely thermal effects, except perhaps those involving newly formed oxidized components, were negligible. Since thermal (non-oxidative) effects may be rank dependent, a similar test is now being performed with a slightly weathered Illinois 6 coal.

## REFERENCES

1. Cox, J. L. and Nelson, C. R., ACS Div. Fuel Chem. Prepr. 29 (1), 102 (1984).
2. Larsen, J. W., Lee, D., Schmidt, T. and Grint, A., Fuel, 65, 595 (1986).
3. Yohe, G., Illinois State Geological Survey, Report of Investigations, 207, 1958.
4. Gethner, J. S., Fuel, 66, 1091 (1987).
5. Gethner, J. S., Appl. Spectrosc., 4, 50 (1987).
6. Schmidt, L. D., Elder, J. L., David, J. D., Ind. Eng. Chem., 32, 548 (1940).
7. Wu, M. M., Robbins, G. A., Winschel, R. A. and Burke, F. P., Energy & Fuels, 2, 150 (1988).
8. Huffman, G. P., Huggins, F. E., Dunmyre, G. P., Pignoco, A. J., and Lin, M-C, Fuel, 64, 849 (1985).
9. Huggins, F. E., Huffman, G. P., Dunmyre, G. P. and Lin, M-C, Fuel Process. Technol., 15, 233 (1987).
10. Wu, M. M., Winschel, R. A. and Robbins, G. A., "Weathering Effects on the Thermoplastic and Froth Flotation Properties of Bituminous Coal", Presented at the 47th Ironmaking Conference, Toronto, Ontario, Canada, April 18, 1988.
11. Lowenhaupt, D. E. and Gray, R. J, Int. J. Coal Geol., 1, 63 (1983).
12. Perry, D. L. and Grint, A., Fuel, 62, 1024 (1983).
13. Rhoads, C. A., Senfthe, J. T., Coleman, M. M., David, A., and Painter, P. C., Fuel, 62, 1387 (1983).

TABLE 1  
ANALYSES OF ILLINOIS 6 AND PITTSBURGH SEAM COALS

	Illinois 6	Pittsburgh Seam (a)
<u>Moisture, wt % as received</u>	2.76	0.64
<u>Proximate Analysis, wt % dry basis</u>		
Volatile Matter	35.74	37.24
Ash	5.30	12.07
Fixed Carbon (Diff)	58.96	50.69
<u>Ultimate Analysis, wt % MAF basis</u>		
Carbon	81.76	84.22
Hydrogen	5.23	5.74
Nitrogen	1.96	1.62
Sulfur, Total	1.19	3.54
Pyritic	0.51	1.97
Sulfate	0.03	0.05
Organic (Diff)	0.65	1.52
Oxygen (Diff)	9.86	4.88
<u>Heating Value, Btu/lb, MAF basis</u>	14,560	15,031
<u>Wet Screen Analysis, wt %</u>		
<u>Tyler Mesh</u>		
28 x 48 mesh	37.8	26.4
48 x 100 mesh	31.0	32.0
100 x 200 mesh	17.8	19.1
-200 mesh	13.4	22.5

(a) This coal used only in the non-oxidative test.

TABLE 2  
FTIR OXIDATION INDEX AND SURFACE COMPOSITION BY XPS  
OF ILLINOIS 6 COAL WEATHERED AT 80°C

Weathering Time, Days	FTIR Oxidation Index	Atomic Percentage								Organic O/C Ratio
		O								
		C	Total	Organic	S	N	Na	Si	Al	
0	1.26	75.0	19.3	11.2	0.1	0.8	0.3	2.7	1.8	0.15
46	2.76	68.0	24.6	15.9	0.3	1.1	0.4	3.0	1.8	0.23
80	3.26	68.3	25.3	16.7	0.3	1.1	0.3	3.0	1.7	0.24

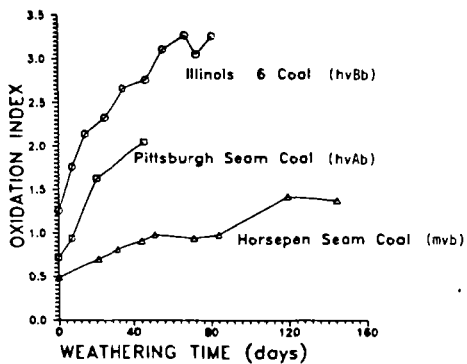


Figure 1. Oxidation Index vs Weathering Time for Coals Weathered at 80°C.

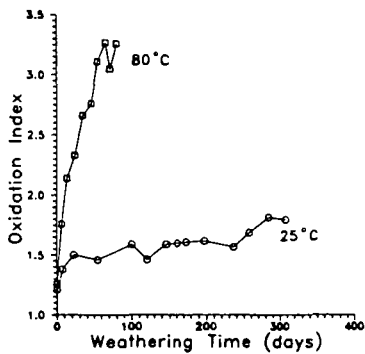


Figure 2. Oxidation Index of Ill. 6 Coal vs Weathering Time and Temperature.

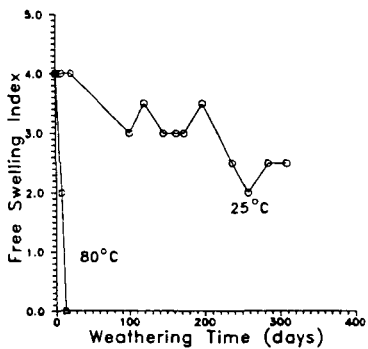


Figure 3. Free Swelling Index of Ill. 6 Coal vs Weathering Time and Temperature.

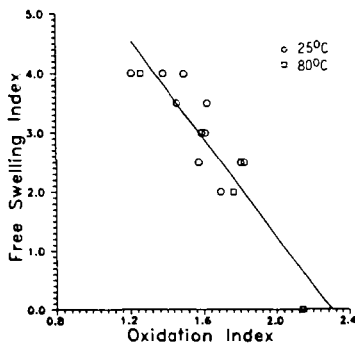


Figure 4. Free Swelling Index of Ill. 6 Coal vs Oxidation Index.

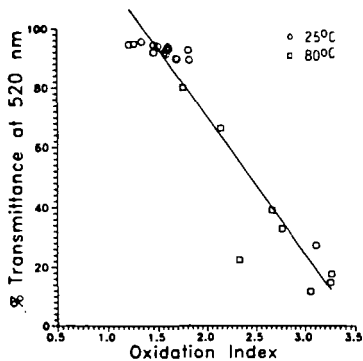


Figure 5. Alkali Extraction Test Results for Weathered Ill. 6 Coal vs Oxidation Index.

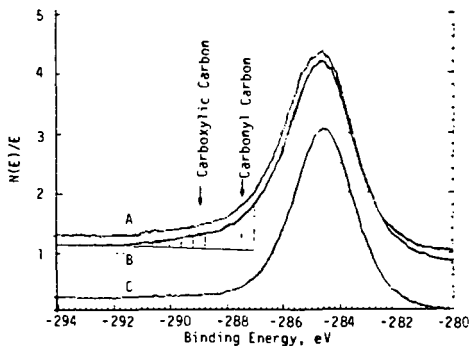


Figure 6. XPS  $C_{1s}$  Spectra of Ill. 6  
 A) Coal weathered at  $80^{\circ}C$  for 46 days.  
 B) Coal weathered at  $80^{\circ}C$  for 80 days.  
 C) Fresh Coal.

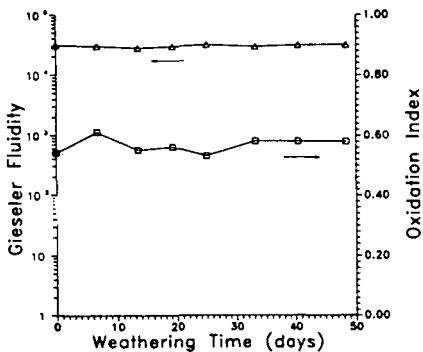


Figure 7. Gieseler Fluidity and Oxidative Index vs Time for Pittsburgh Seam Coal in the  $80^{\circ}C$  Non-Oxidative Weathering Test.  
 $\Delta$  Gieseler Fluidity  
 $\square$  Oxidation Index

# Application of X-Ray Photoelectron Spectroscopy to Coal Oxidation Kinetics

S. R. Kelemen and H. Freund

Exxon Research & Engineering Company, Annandale, NJ 08801

## Abstract

Several aspects of the oxidation kinetics of Illinois # 6 bituminous and Wyoming Powder River Basin subbituminous coal were quantified between 295-398K. XPS was used to determine the changes in the amount of surface organic oxygen and provide an oxygen functional group distribution. GC analysis of the gas phase products and weight changes from TGA experiments were used to place the XPS results in the context of bulk oxidation. The oxidation of Illinois # 6 coal produced mostly solid oxidation products. The rate of increase exhibited Arrhenius behavior with an apparent activation energy of 11.4 kcal/mole. Oxidation of Wyoming Powder River Basin coal at 398K gave mainly gaseous products and a slightly faster total oxidation rate relative to Illinois #6 coal. The amount of oxidized organic sulfur determined by XPS can be used to evaluate the total extent of coal oxidation.

## I. Introduction

Oxidation reactions of coal which occur in air near room temperature contribute to the self heating of coal and produce detrimental changes to many coal properties. Both solid and gaseous species are produced as oxidation products.<sup>(1)</sup> After oxidation many aspects of the solid coal have been investigated and several properties can be used to gauge the extent of oxidation. These include the determination of the changes in the amount of oxygen by difference, by neutron activation analysis<sup>(2)</sup> and by XPS analysis of the coal surface.<sup>(3,4)</sup> Relative changes in the properties of coal have also been used to measure oxidation. These include free swelling index,<sup>(5)</sup> Gieseler fluidity,<sup>(6,7)</sup> PH,<sup>(8)</sup> FTIR signatures<sup>(9)</sup> and changes in pyrolysis response.<sup>(10,11)</sup>

Despite the many available approaches it is very difficult to quantify the kinetics of low temperature oxidation,  $T < 350\text{K}$ . The total amount of solid oxidation products after several days near room temperature can be small.<sup>(12,13,23-25)</sup> There has been a greater number of oxidation studies performed at higher temperatures,  $T > 350\text{K}$ . The connection between high and low temperature oxidation reactivity is not well established and few have adopted a unified approach to characterize both solid and gaseous oxidation products.

We have quantified several aspects of the oxidation of Illinois # 6 coal and Powder River Basin coal between 295-398K. XPS was used to determine the changes in surface organic oxygen. GC analysis of gas phase products was carried out in conjunction with XPS measurements in order to provide a more complete description of the oxidation process. Thermal Gravimetric Analysis (TGA) results help place the XPS information in the context of bulk oxidation.

## II. Experimental

Illinois # 6 coal and Powder River Basin coal were obtained from the Exxon Research and Engineering Company Baytown Texas coal sample library.<sup>(26)</sup> Upon receipt, the sealed consignment was transferred to a nitrogen drybox. 100-200 mesh cuts were prepared and stored in the drybox for later use.

XPS spectra were obtained with an ion pumped Vacuum Generators ESCALAB instrument using non-monochromatic MgK $\alpha$  radiation. The source was operated at 300W, 20ma, 15KV. A complete XPS analysis took approximately 4 hours. The coal samples were mounted to a metallic sample block by means of double-sided Scotch nonconducting tape. An energy correction was made due to sample charging based on the C(1s) peak at 284.8 (eV) and the unoxidized organic sulfur 2p peak at 164.0 (eV). Samples were introduced using the standard diffusion pumped VG ESCALAB fast entry air lock. As previously observed with other coal samples<sup>(3,4,27,28)</sup> the elemental composition of the sample remained nearly constant during the measurement period; however, longer-term exposure to the X-ray beam produced damage as evidenced by decreases in the initial amount of carboxyl carbon and by subsequent increased vulnerability to surface oxidation at ambient conditions. New samples were obtained for measurement at every point in the oxidation sequence.

Data acquisition and processing were by means of a VGS 2000 software package using multi-scan averaging. The spectra were obtained at 0.9 eV resolution. Elemental concentrations were obtained relative to carbon calculated from the areas of the XPS peaks corrected for atomic sensitivity. The sensitivity factors relative to C(1s) were determined from VG sensitivity tables and experimentally measured standards.

The organic composition of the starting coal derived from an XPS measurement was compared to a standard bulk determination. The comparison for Illinois # 6 coal is shown in table I and for Powder River Basin coal in table II. Both coals have XPS derived organic nitrogen and organic sulfur values in very good agreement with bulk values. The amount of surface organic oxygen also compares favorably with bulk derived values. The amount of organic oxygen was derived from XPS results by taking into account inorganic contributions. The amount of oxygen associated with silicon and aluminum were taken as SiO<sub>2</sub> and AlO<sub>1.5</sub>. With recognition of the surface oxidation of pyrite, the amount of oxygen associated with the inorganic sulfate (2p) signal was taken as SO<sub>4</sub>. The difference between the pyrite iron (2p) signal and sulfate sulfur (2p) signal was associated with oxygen as FeO<sub>1.5</sub>.

While there is little inorganic sulfur in Powder River Basin coal it is known from bulk analysis that nearly 1/3 of the total sulfur in this Illinois # 6 coal exists as inorganic forms with the majority as pyrite. Table I also shows that there is a large discrepancy between the surface and bulk values of pyritic and sulfate sulfur for Illinois # 6 coal. The value for surface pyritic sulfur is based on the absence of the pyritic iron (2p) signal. These differences are most likely a result of the surface oxidation of pyrite. The XPS sulfur spectrum from I # 6 coal showed a sulfur 2p peak centered about 171.3 eV. This peak was substantially reduced by a brief water wash at room temperature. The broad peak is interpreted to arise from ferrous and ferric sulfates. The reactivity of coal following the water wash was

identical to the untreated coal. The sulfate peak and the associated iron (2p) signal is shifted by  $\sim 1.5$  eV to higher binding energy than the reported literature value.(29,30) This discrepancy is most likely due to a slightly enhanced sample charging of these inorganic components in our samples. We could not observe the iron (2p) signal due to iron pyrite.

We deconvoluted the sulfur (2p) spectrum using a single peak to represent the unresolved 2p spin doublet. We used a mixed Gaussian-Lorentzian line shape and a peak width at half maximum of 2.60 eV for each sulfur species. The organic part of the sulfur 2p spectrum showed two main peaks that occur at 164.0 eV and 168.3 eV. The 164.0 eV peak is characteristic of a variety of unoxidized organic species which includes thiophenes, sulfides and mercaptans. While oxidation to produce sulfoxides (166.0 eV)(31) and sulfonic acid (169.2 eV)(32) will contribute to the development of the main 168.3 eV sulphur (2p) peak, the dominant oxidation products appear as sulfones(168.0).(31-34)

XPS difference curves were made using the C(1s) lines whose areas were normalized to the value of the clean starting spectrum. The following methodology was used to deconvolute the positive peak in each carbon (1s) difference spectrum. We use a mixed Gaussian-Lorentzian line shape and a peak width of 1.80 eV at half maximum for each peak. Four peaks are used in the deconvolution that occur at 286.3 eV, 287.5 eV, 289.0 eV, and 285.2 eV. The 286.3 eV represents carbon bound to a single oxygen bond (i.e. ethers, hydroxyls, hydroperoxides), the 289.5 eV peak to carbon bound to two oxygen bonds (i.e. carbonyl) and the 289.0 eV peak to carbon bound to three oxygen bonds (i.e. carboxyl).(35-40) The intensity of the 285.2 eV peak is fixed to the 289.0 eV peak intensity and represents the carbon adjacent to carboxyl carbon and is referred to as a  $\beta$  peak.

Oxidation experiments for XPS kinetic studies were done in air with  $<25\%$  relative humidity. Oxidation experiments with gas phase analysis were done in a quartz reactor contained within a furnace. The outlet of the dead-ended reactor was connected to a Bellows pump and a recirculation loop. A gas sample could be taken from the recirculation loop for GC analysis via an evacuated 2 cc gas sample valve. The gas chromatograph used for product analysis was a Hewlett Packard 5840 equipped with a thermal conductivity and a FID detector. The separation column was Porapack Q. Samples were introduced into the quartz reactor vessel and evacuated to  $1 \times 10^{-3}$  Torr. The sample size was 100 mg. The reactor volume was then pressurized to 200 kPa with helium. Prior to oxidation the fresh coal samples were heated at the appropriate reaction temperature in He for 18 hours; thereafter the amount of thermal decomposition products were negligible compared to those produced in oxidizing environments. The samples were evacuated to  $1 \times 10^{-3}$  Torr before being pressurized to 200 kPa with the reactant gas mixture which consisted of  $\sim 6.7\%$  oxygen in Helium. Periodic evacuation and pressurization with new reactant gas was done in order to avoid the build-up of excessive amounts of products and to keep the reactant  $O_2$  partial pressure nearly constant. The closed recirculation reactor arrangement enabled the build-up of products over

long times. The loss of the portion of product gas due to gas sampling was corrected in the product analysis. TGA experiments were done by flowing dry air in a Dupont model 951 thermogravimetric analyzer.

### III. Results

We have monitored the increases in the amount of organic oxygen as a function of time and temperature. The results for Illinois # 6 coal are shown in Figures 1 and 2. The curve through the data points at each different temperature is based on a theoretical first order expression with a common asymptote corresponding to 0.085 maximum surface  $O/C$  atom ratio increase, or in other words an increase of 8.5 oxygens per 100 carbons. An Arrhenius plot using the XPS derived rate information is shown in Figure 3. The line through the data corresponds to an activation energy of 11.4 kcal/mole and pre-exponential of  $4.9 \times 10^6 (O/C) (day)^{-1}$ .

We have measured the corresponding changes in weight as a function of time up to 7 days at 398K. A comparison of these results with the XPS data is shown in figure 4. The same theoretical first order curve is used to fit the TGA data as the XPS data but with an asymptote of 5.0 wt.%  $O/C$  increase. The same expression provides an excellent fit to the TGA data.

We have measured the changes in gas composition which occur under similar experimental conditions following oxidation for 2 days at 398K. Table III shows the changes in the number of gaseous molecules expressed relative to carbon. The Illinois # 6 coal contains 70.87 wt% carbon. With this information we have determined the wt% increase and oxygen atom ratio increase relative to carbon expected on the basis of GC data. We compare the results in Table IV to other experimental information. There is good agreement between the GC and TGA results for the wt% increase. IR analysis of the gas phase shows the presence of a small amount of CO. We did not quantify the weight loss due to CO evolution. The total hydrocarbon production is three orders of magnitude below the levels of  $CO_2$  and  $H_2O$  and therefore was not considered. The increase in the surface oxygen concentration is 1.4 times greater than the bulk oxygen increase predicted from an oxygen balance using gas phase data. The fact that the surface enhancement is actually rather small and the similarity of the TGA and XPS kinetics imply that oxidation occurs throughout the bulk and that the surface oxidation process is a reflection of the bulk phenomenon.

The changes that occur in the XPS Carbon (1s) line shape can be related to the changes in the nature of the oxygen functional groups. The use of a difference spectrum facilitates the observation of the changes induced by oxidation. Examples of a C (1s) difference spectrum are found in figure 5 and were obtained after air oxidation of Illinois # 6 coal at 398K. The negative peak in each spectrum occurs near 284.7 eV. A decrease in intensity at this energy is indicative of a decrease in the amount of unoxidized carbon atoms. The presence of positive peaks at higher binding energies is associated with increases in the amount of oxygen functionalities. The fact that the positive going features are different in each spectrum indicates that the functional group distribution changes during the course of oxidation at 398K. Table V

shows the increases in the number of functional groups following oxidation. The information was obtained from the results of the deconvolution of the C (1s) spectrum, the deconvolution of the sulfur (2p) spectrum and the increase of total organic oxygen. Increases in the amount of oxygen associated with carbonyl and carboxyl types are obtained directly from the C (1s) difference spectrum. The amount of oxygen associated with sulfur species comes from the intensity increase in the sulfur (2p) sulfone peak. The amount of oxygen associated with groups bound to carbon by a single bond (i.e. ether, hydroxyl and hydroperoxides etc.) is obtained from the difference between the amount of total organic oxygen and the amount of oxygen associated with carboxyl, carbonyl, and oxidized sulfur.

After approximately 10 days at 398K, the oxygen concentration reaches a plateau. There are, however, changes that happen at longer oxidation times. We find that the carboxyl and oxidized organic sulfur concentration increases while that of the other types decline. Analysis of the gas phase changes, contained in table III, confirm that there is little change in the bulk oxygen to carbon ratio over the same period. The results also show that the Illinois coal continues to participate in oxidation reactions at long times; however, O<sub>2</sub> is consumed at a much slower rate. CO<sub>2</sub> and H<sub>2</sub>O are the main gaseous oxidation products. While there are significant changes in the surface oxygen functional group distribution, the total amount of bulk organic oxygen remains nearly constant.

Following oxidation at 294K for 170 days we find that the majority of oxygen increase is associated with the formation of carboxyl structures. Oxidized surfaces produced at slightly higher temperatures and shorter times also show that increases in carboxyl oxygen is responsible for the majority of oxygen increase.

We have used XPS to monitor the changes in the amount of organic oxygen after oxidation of Powder River Basin coal between 294K and 398K, Figure 6. There is very little increase in oxygen concentration even after 170 days at 298K. There is also very little change in the oxygen functional group distribution. Higher temperature oxidation resulted in the build-up of surface products but at much lower levels than that previously observed with Illinois # 6 coal. The changes in surface oxygen concentration were not amenable to a simple kinetic description. The lines in Figure 6 represent a linear connection of data points.

Despite the small or negligible increases in total organic oxygen near room temperature, the relative increase in the amount of oxidized organic sulfur can be substantial. Figure 7 shows the sulfur 2p spectrum of fresh Powder River Basin coal and a spectrum following air oxidation at 295K. The 164 eV peak is due to unoxidized organic sulfur. A peak develops near 168 eV following oxidation and is attributed to the presence of oxidized organic sulfur.

Analysis of the changes in the gas phase composition, Table VI, show that the oxidation of Powder River Basin coal is dominated by gaseous products. These results also support the XPS finding that there are only slight changes in the amount of organic oxygen during the initial oxidation period at 398K.

## Discussion

We have found that the oxidation of Illinois # 6 coal produces mainly solid oxidation products. A single kinetic expression was used to model the surface oxidation kinetics between 398K and 295K. TGA and GC gas phase analysis showed that the surface oxidation kinetics reflected bulk oxidation behavior.

Recent FTIR work on thin sections of Illinois # 6 coal indicated the presence of two kinetically distinct oxidative reaction sequences.(23-25) A slow oxidation process was extensively characterized at 393K but was difficult to measure below 343K.(23-25) A fast oxidation process was found to occur over two days at 295K but was complete after 30 minutes at 343K. This reaction is believed to result in a very small net decrease in the amount of organic oxygen. Both the fast and slow oxidation processes can contribute to the observed oxidation response of coal. We were unable to identify the fast oxidation process using XPS. This failure places an upper limit of 0.01 O/C change associated with this process. In another study(12) of Illinois # 6 coal, an increase of 2.4 oxygens per 100 carbons was observed after oxidation for 56 days under external ambient conditions. Nonalkylatable oxygen was the main product, presumably ether oxygen. In the present study near room temperature carboxyl was the main oxygen surface species.

The rate of increase of total oxidation products of Illinois # 6 coal exhibits Arrhenius behavior with an apparent activation energy of 11.4 kcal/mole. Non-isothermal studies(18) of bituminous and subbituminous oxidation, at a heating schedule of  $5^{\circ}\text{C min}^{-1}$ , demonstrate Arrhenius behavior for  $\text{O}_2$  consumption above 413K. The apparent activation energy is between 10.0 and 13.2 kcal/mole. Lower temperature oxidation was characterized by much lower activation energies attributed to the influences of diffusion-controlled processes or to physical absorption.(18) A study(22) of subbituminous coal oxidation kinetics demonstrated Arrhenius behavior between 303K-343K with activation energies between 15 to 20 kcal/mole. Apparent global activation energies between 12.6 and 24.5 kcal/mole were found based on calorimetric data for a variety of coals of different rank.(46) The energies were determined from data obtained between 373K-423K so as to minimize contributions due to the heat of wetting.

It is generally believed that the oxidation of coal proceeds by way of a free radical oxidation mechanism.(12,14,16-18,21,23-25,41-45) E.S.R. work provides experimental evidence for the changes in free radical population during coal oxidation.(41,42) The variety of oxygen functionalities that we have observed can be accounted for within the framework of a free radical mechanism.(14,16,44,45) It is known that mineral oxidation reactions occur simultaneously with organic oxidation in coal.(6,29,47-53) The catalytic participation of inorganic components toward low temperature organic oxidation has been considered(52,53) but not confirmed. Low temperature inorganic reactions are generally regarded as separate processes. Nevertheless, the presence of inorganic matter complicates the interpretation of the oxidation kinetics based solely on gas phase oxygen uptake or heat release.

Most agree that a radical chain oxidation mechanism, involving decomposition of hydroperoxides, explains coal oxidation behavior at moderate temperatures. The dominant reactions that take place near room temperature are less certain. We find that our XPS results fit a single kinetic expression. The oxygen functional group distribution observed at 295K after long times is similar to that found after shorter oxidation periods at 398K. We therefore conclude that under our experimental conditions the same basic chemistry occurs over the temperature range. Consideration of the errors associated with the XPS measurement enables us to place an upper limit of 0.01 O/C surface increase that can be associated with faster oxidation processes.

The oxidation behavior of Illinois # 6 coal changes at long times at 398K. The surface and bulk oxygen concentration remains nearly constant but CO<sub>2</sub> and H<sub>2</sub>O are still being produced. The total oxidation rate is much slower than the well defined kinetic process found at earlier times. The surface functional group distribution changes. The amount of oxidized organic sulfur continues to rise along with carboxyl oxygen, while other species decline.

We have made a limited study of Powder River Basin Coal. The initial oxidation at 398K gives mainly gaseous products. The total extent of oxidation after 2 days is 1.3 times that found with Illinois # 6 coal. We have monitored the changes in the surface composition at lower temperatures and find only small changes in the amount of organic oxygen. An earlier study indicated a high selectivity toward gaseous products for a low rank coal.<sup>(1)</sup> Previous work on this coal<sup>(13)</sup> at room temperature indicated that the change in bulk oxygen content was small. Chemical decarboxylation was offset by increases in the amount of nonalkylatable organic oxygen. Despite the small changes in total organic oxygen, we have found a substantial relative increase in the amount of oxidized organic sulfur.

### Conclusions

- 1) A single kinetic expression can be used to describe the surface oxidation of Illinois # 6 coal from 398K to 295K.
- 2) The surface oxidation kinetics observed at 398K reflects bulk oxidation behavior. We were unable to identify any faster oxidation process for Illinois # 6 coal. This failure places an upper limit of 0.01 O/C on the amount of surface oxygen change that can be associated with faster oxidation processes.
- 3) A much slower oxidation process was identified at 398K after reacting Illinois # 6 coal for long times. The total surface oxygen concentration remains nearly constant but the oxygen functional group distribution shifts towards carboxyl and oxidized sulfur. CO<sub>2</sub> is the main gaseous product.
- 4) The initial oxidation of Powder River Basin coal at 398K produces mainly gas. The total oxidation after 2 days is 1.3 times greater than observed with Illinois # 6 coal.
- 5) There is a significant relative increase in the amount of oxidized organic sulfur during 295K oxidation of Powder River Basin coal. The total amount of organic oxygen remains almost constant.

## References

- 1) P. D. Swann and D. G. Evans, Fuel 58 (1979) 276.
- 2) W. D. Ehmann, D. W. Koppenaal, C. E. Hamrin, Jr., W. C. Jones, M. N. Prasad and W. Z. Tian, Fuel 65 (1986) 1563.
- 3) D. T. Clark and R. Wilson, Fuel 62 (1983) 1034.
- 4) D. L. Perry and A. Gint, Fuel 62 (1983) 1029.
- 5) J. W. Larsen, D. Lee, T. Schmidt and A. Grint, Fuel 65 (1986) 595.
- 6) G. P. Huffman, F. E. Huggins, G. E. Dunmyre, A. J. Pignocco and M. Lin, Fuel 64 (1985) 849.
- 7) A. Grint and D. L. Perry, Proc. Int. Conf. Coal Sci. (1985) 879.
- 8) Y. Yun, B. Hoesterey, H. L. C. Meuzelaar and G. R. Hill. ACS Fuel Div. preprints 32 (1987) 302.
- 9) P. M. Fredericks and N. T. Moxon, Fuel 65 (1986) 1531.
- 10) B. S. Ignasiak, D. M. Clugston and D. S. Montgomery, Fuel 51 (1972) 76.
- 11) H. Iyuhara, R. Tanibata and S. Nishida, Proc. Inter. Conf. Coal Sci. (1985) 491.
- 12) R. Liotta, G. Brons, and J. Isaacs, Fuel 62 (1983) 781.
- 13) J. J. Isaacs and R. Liotta, J. Energy & Fuels 1 (1987) 349.
- 14) G. Alberts, L. Lenart and H. Oelert, Fuel 53 (1974) 47.
- 15) A. Y. Kam, A. N. Hixson and D. D. Perlmutter, Chem. Eng. Sci. 31 (1976) 815.
- 16) C. A. Rhoads, J. T. Senftle, M. M. Coleman and A. Davis, Fuel 62 (1983) 1387.
- 17) D. C. Cronauer, R. G. Ruberto, R. G. Jenkins, A. Davis, P. Painter, D. S. Hoover, M. E. Starsinic and D. Schlyer, Fuel 62 (1983) 1124.
- 18) D. C. Cronauer, R. G. Ruberto, R. S. Silver, R. G. Jenkins, I. M. K. Ismail and P. Schlyer, Fuel 62 (1983) 1116.
- 19) T. Handa, T. Nishimoto, M. Morita and J. Kodama, Fire Sci. Tech. 5 (1985) 21.
- 20) T. Nishimoto, M. Hosoya, J. Kodama, and M. Morita, Fire Sci. Tech. 5 (1985) 123.
- 21) W. S. Kalema and G. R. Gavalas, Fuel 66 (1987) 158.

- 22) M. Rahman, A. R. Hasan and D. N. Baria, Chem. Eng. Commun 46 (1986) 209.
- 23) J. S. Gethner, Fuel 64 (1985) 1443.
- 24) J. S. Gethner, Applied Spectroscopy 41 (1987) 50.
- 25) J. S. Gethner, Fuel 66 (1987) 1091.
- 26) R. C. Neavel, S. E. Smith, E. J. Hippo and R. N. Miller, Fuel 65 (1986) 312.
- 27) D. T. Clark, R. Wilson and J. M. Quirke, Chemical Geology 39 (1983) 215.
- 28) D. T. Clark, and R. Wilson, Org. Geochem. 6 (1984) 455.
- 29) A. N. Buckley and R. Woods, Applied Surf. Sci 27 (1987) 437.
- 30) Handbook of X-ray and Ultraviolet Photoelectron Spectroscopy (Heyden & Sons Ltd., 1978).
- 31) C. E. Mixan and J. B. Lambert, J. Org. Chem. 38 (1973) 1351.
- 32) D. T. Clark and H. S. Munro. Polymer Degradation and Stability 8 (1984) 213.
- 33) J. A. Gardella, Jr., S. A. Ferguson and R. L. Chin, Applied Spectroscopy 40 (1986) 224.
- 34) H. R. Thomas, Ph.D. Thesis, University of Durham, U.K. (1977) 144.
- 35) D. T. Clark and H. R. Thomas, J. Polym. Sci. & Polym. Chem. Ed. 14 (1976) 1671.
- 36) D. T. Clark, B. J. Cromarty and A. Dilks, J. Polym. Sci. Polym. Chem. Ed. 16(1978) 3173.
- 37) D. T. Clark and A. Harrison, J. Polym. Sci. Polym. Chem. Ed. 19 (1981).
- 38) D. T. Clark, Adv. Polym. Sci. 24 (1977) 125.
- 39) D. T. Clark, J. Polym. Sci. Polym. Chem. Ed. 16 (1978) 791.
- 40) D. T. Clark and A. Dilks, J. Polym. Sci. Polym. Chem. Ed. 17 (1979) 957.
- 41) S. W. Dack, M. D. Hobday, T. D. Smith and J. R. Pilbrow, Fuel 63 (1984) 39.
- 42) S. W. Dack, M. D. Hobday, T. D. Smith and J. R. Pilbrow, Fuel 62 (1983) 1510.
- 43) P. C. Painter, R. W. Snyder, D. E. Pearson and J. Kwong, Fuel 59 (1980) 282.

- 44) H. A. W. DeVries, C. Bokhoven and H. N. M. Dormans, *Brennst. Chem.* 50 (1969) 289.
- 45) E. A. C. Chamberlain, G. Barrass and J. T. Therlaway, *Fuel* 55 (1976) 217.
- 46) A. C. Smith and C. P. Lazzara, U.S. Bu. Mines RI 9079 (1987).
- 47) R. G. Herman, G. W. Simmons, D. A. Cole, V. Kumicz and K. Klier, *Fuel* 63 (1984) 673.
- 48) F. E. Huggins, G. P. Huffman and M. C. Lin, *Int. J. Coal Geo.* 3 (1983) 157.
- 49) D. C. Frost, W. R. Leeder, R. L. Tapping and B. Wallbank, *Fuel* 56 (1977) 277.
- 50) R. G. Wiese Jr., M. A. Powell and W. S. Fyfe, *Chemical Geology* 63 (1987) 29.
- 51) D. A. Cole, G. W. Simmons, R. G. Herman, K. Klier and I. Cyako-Nagy *Fuel* 66 (1987) 1240.
- 52) D. E. Pearson and J. Kwong, *Fuel* 58 (1979) 63.
- 53) F. E. Huggins, G. P. Huffman, D. A. Kosmack and D. E. Lowenhaupt *J. Coal Geol.* 1 (1980) 75.

Table I

<u>Atom ratio relative to carbon x 100</u>	<u>I #6 coal Fresh XPS</u>	<u>I #6 coal Fresh Bulk Analysis</u>	<u>I #6 coal Water Wash XPS</u>
Organic Sulfur	1.68	1.45	1.65
Sulfate Sulfur	1.19	0.02	0.32
Pyritic Sulfur	0.00	0.62	0.00
Organic Oxygen	10.3	9.9	11.6
Nitrogen	1.4	1.4	1.4

Table II

<u>Atom ratio relative to carbon x 100</u>	<u>Powder River Basin Fresh XPS</u>	<u>Powder River Basin Fresh Bulk Analysis</u>
Organic Sulfur	0.42	0.47
Sulfate Sulfur	0.03	0.027
Pyritic Sulfur	0.00	0.005
Organic Oxygen	19.3	20.1
Nitrogen	1.1	1.0

Table III

Changes in the gas composition after oxidation  
of Illinois #6 coal at 398K

<u>Time</u>	<u>2 Days</u>	<u>13 Days</u>	<u>48 Days</u>
O <sub>2</sub> /carbon (x100)	-1.74	-5.48	-8.73
CO <sub>2</sub> /carbon (x100)	0.33	1.68	4.46
H <sub>2</sub> O/carbon (x100)	0.16	0.45	1.06
Change in Bulk oxygen/carbon (x100) based on GC data	2.7	7.1	6.9

Table IV

Comparison of the Changes found after  
oxidation of I #6 coal at 398K for 2 days

	<u>Wt%</u> <u>Increase</u>	<u>Oxygen atom</u> <u>ratio increase</u> <u>relative to carbon x100</u>
From GC Experiment	2.3	2.7
From TGA Experiment	2.7	---
From XPS Experiment	---	3.9

Table V

Amount of oxygen increase per 100 carbons Associated with Various Functional Types Following Air oxidation of Illinois #6 coal

<u>Oxidation Temperature</u>	<u>Oxidation Time</u>	<u>Total Organic Oxygen increase</u>	<u>Carboxyl</u>	<u>Oxidized Sulfur</u>	<u>Carbonyl</u>	<u>Ether hydroperoxide Alcohol</u>
295K	170 days	3.8	2.1	0.3	0.7	0.7
398K	15 days	8.2	4.2	0.7	2.6	0.7
398K	41 days	8.1	4.9	1.0	1.4	0.8
398K	54 days	8.6	6.4	1.3	0.4	0.5

Table VI

Changes in the gas composition after oxidation of Powder River Basin coal at 398K

<u>Time</u>	<u>2 Days</u>	<u>13 Days</u>
O <sub>2</sub> /carbon (x100)	-2.32	-6.33
CO <sub>2</sub> /carbon (x100)	2.10	5.37
H <sub>2</sub> O/carbon (x100)	0.47	1.45
Change in bulk oxygen/carbon (x100) based on GC data	-0.03	0.47

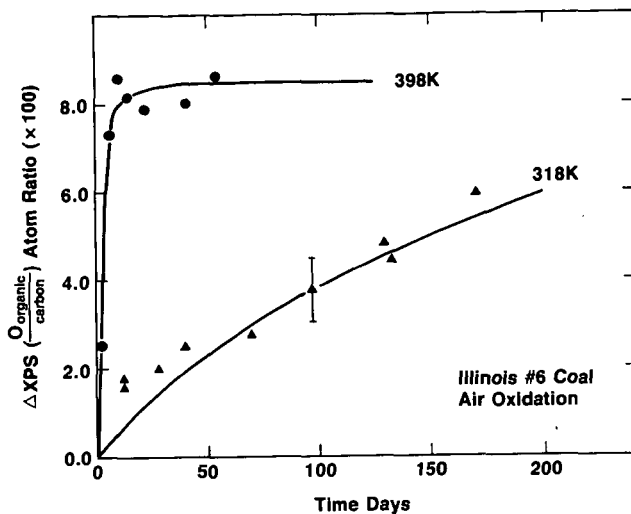


Figure 1. Change in the organic oxygen (1s) to carbon (1s) XPS atom ratio as a function of exposure time at 398K and 318K in air for Illinois # 6 coal

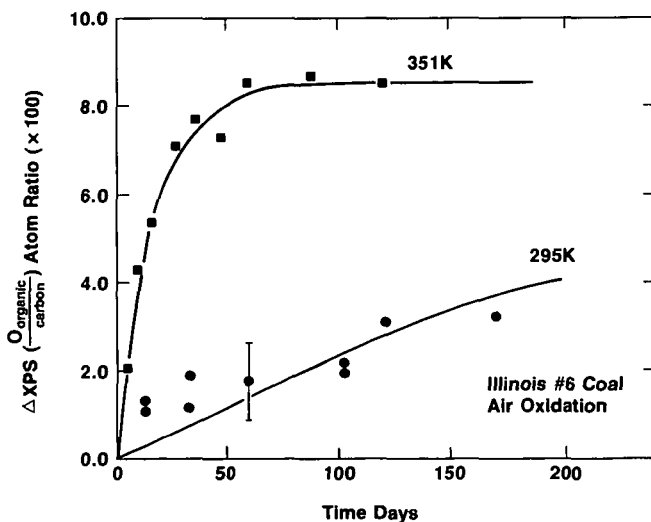


Figure 2. Change in the organic oxygen (1s) to carbon (1s) XPS atom ratio as a function of exposure time at 351K and 295K in air for Illinois # 6 coal

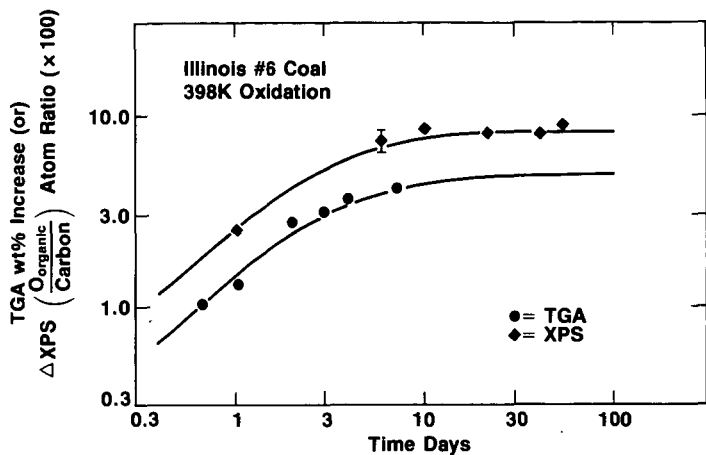


Figure 3. Comparison of the TGA wt% increase and the XPS oxygen (1s) to carbon (1s) atom ratio increase as a function of time at 398K for Illinois # 6 coal

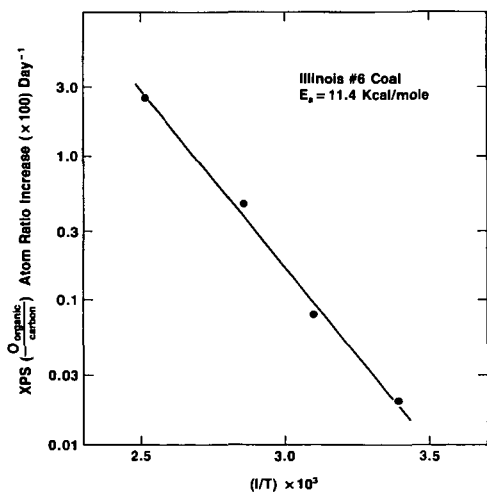


Figure 4. Arrhenius plot of the initial oxidation rate of Illinois # 6 coal based on the XPS data using a first order fit and common maximum O/C increase of 0.085

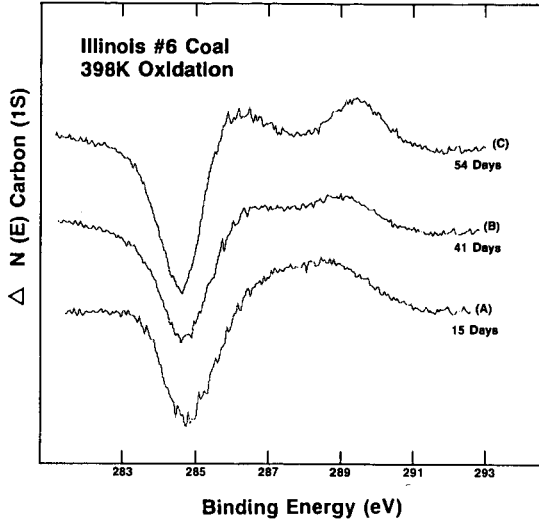


Figure 5. Change in the C (1s) spectrum following oxidation of Illinois # 6 coal for different times at 398K

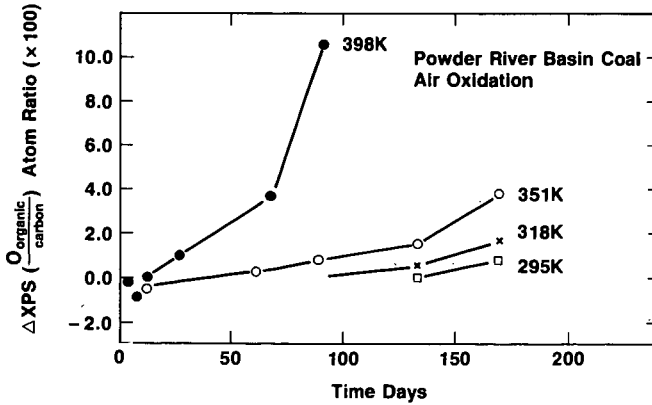


Figure 6. Changes in the Powder River Basin coal organic oxygen (1s) to carbon (1s) atom ratio as a function of exposure time in air at different temperatures.

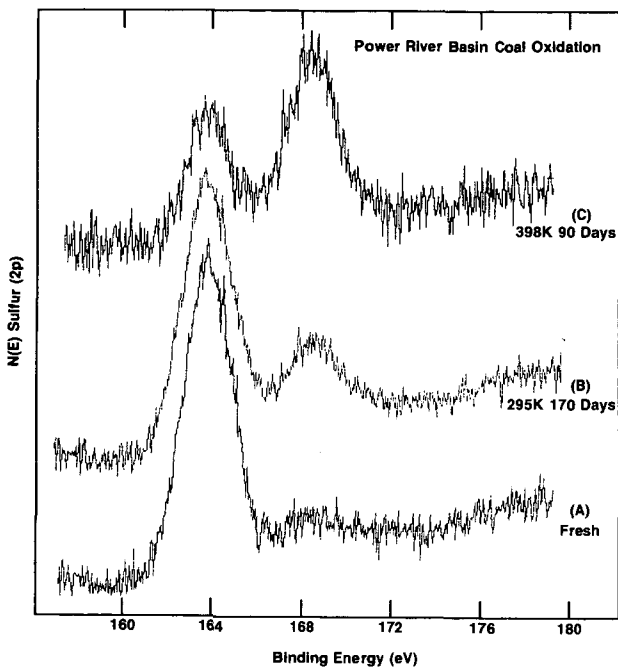


Figure 7. XPS sulfur (2P) spectrum from

- A) fresh Powder River Basin coal
- B) after oxidation for 170 days at 295K
- C) after oxidation for 90 days at 398K

## AN ESCA STUDY OF ALKALI-TREATED COAL SURFACES

J.P. Baltrus, J.R. Diehl, and J.R. D'Este  
Pittsburgh Energy Technology Center, U.S. Department of Energy  
P.O. Box 10940, Pittsburgh, Pennsylvania 15236-0940, U.S.A.

### ABSTRACT

The surface interactions of alkali with coal and mineral matter have been studied by ESCA to establish a basis for predicting the relative reactivity of alkali with sulfur during coal beneficiation processes. The speciation of sulfur in several coals doped with various alkali salts was determined and quantified following heating of the samples to 375°C in air or N<sub>2</sub> and after washing them with water. Organic and pyritic sulfur react with the alkali cation when heated, after which the sulfide or oxidized sulfur product can be washed from the coal. The extent of reaction between the alkali salt and sulfur is governed by the size of the cation and the electronic properties of the anion; larger alkali cations are more reactive, as are anions with stronger nucleophilic properties.

### INTRODUCTION

Over the years several processes employing alkali have been used for coal beneficiation (1). Presently the process for removing sulfur and ash from coal by treatment with molten caustics (MCL) is continuing to be developed as an alternative method for removing troublesome impurities from coal (1-4). Research has been conducted to determine the effects of process variables on the efficiency of the MCL system and to develop methods for analyzing and regenerating spent caustic (5-7). More fundamental studies have attempted to determine the mechanisms for interaction between the Na and K hydroxides and the components of coal, especially pyrite (8) and organosulfur (9,10).

This study focuses on the surface interactions of alkali with coal and mineral matter as studied by ESCA. Such interactions may be important in several processes in which coal and sulfur in coal are treated with alkali. Changes in the chemical state of the sulfur components of coal were monitored following deposition of various alkali hydroxides and sodium and potassium salts, and after subjecting the coals to various thermal treatments and washes.

### EXPERIMENTAL

Preparation of Alkali-Doped Samples. A Pittsburgh No. 8 hvAb coal (2.2% pyrite, 0.4% sulfate, 1.6% organic sulfur) and Rasa lignite (Yugoslavia) (approximately 11% organic sulfur) were ground in air to minus 100 mesh. A 0.75-g sample of coal was mixed with 1 mL of an aqueous solution containing enough NaOH or KOH to produce the desired alkali concentration in the coal. The alkali-doped coals were placed in a ceramic boat and dried overnight at 60°C in a flow of N<sub>2</sub>; coals were stored under air in a dessicator.

Four Pittsburgh No. 8 coal samples, the first containing 0.5% Na, the second containing 0.5% K, the third containing 0.25% Na and 0.25% K, and a fourth containing no added Na or K were analyzed after heating them to temperatures up to 375°C for one hour in flowing air or N<sub>2</sub>.

A quantitative study of the effects of washing on sulfur removal was carried out on Na-doped and (Na + K)-doped Rasa lignite that had been heated at 375°C for one hour in air or N<sub>2</sub>. The lignite samples were doped using the same procedure described above so that the final concentrations of alkali were approximately 5% Na and 5% Na plus 5% K, respectively. After heating, the samples were mixed with approximately 10% to 40% high-surface-area gamma alumina, which was used as an internal standard for monitoring changes in sulfur content during the wash procedure.

The Pittsburgh No. 8 coal was also doped with aqueous solutions of Na, K, Rb, and Cs hydroxides so that 0.75 g of coal contained  $1.62 \times 10^{-4}$  moles of one of the alkali metals. Another series of coal samples was impregnated with aqueous solutions of various Na and K salts (fluorides, chlorides, bromides, nitrates, acetates, and carbonates); the concentration of Na or K was 0.5% in each sample. All of the above samples were heated either in air or in nitrogen at 375°C for one hour.

Instrumentation. The coals were analyzed as powders mounted on double-sided sticky tape using a Leybold-Heraeus LHS-10 spectrometer. The magnesium anode was operated at 12 kV and 20 mA with the analysis chamber at a vacuum of  $2 \times 10^{-8}$  mbar or lower. The S 2p peaks were curve-fitted using the L-H DS-5 data system.

## RESULTS AND DISCUSSION

Thermal Treatments. The S 2p region was curve-fitted with two peaks: one at 169.7 eV due to oxidized sulfur, S<sub>(o)</sub>, most likely in the form of SO<sub>4</sub><sup>2-</sup>; and another at 164.0 eV due to unoxidized sulfur, S<sub>(u)</sub> (organic sulfur, pyrite, and elemental sulfur) (11). Table 1 shows the results of the curve-fitting analyses of the S 2p spectra for the non-doped, Na-doped, K-doped, and (Na + K)-doped coals after heating to various temperatures in air. It can be seen that heating the coal to higher temperatures in air resulted in the conversion of an increasing percentage of S<sub>(u)</sub> to S<sub>(o)</sub> ( $\%S_{(u)} = 100 - S_{(o)}$ ); the amount of S<sub>(o)</sub> was always greater for the alkali-doped coals. Higher S<sub>(o)</sub> values for Na-doped coals compared to K-doped coals may be due to the somewhat greater Na concentration, on a molar basis.

To investigate the role of oxygen in the oxidation of alkali-doped coals, the coals were heated in a flow of N<sub>2</sub>. Table 1 shows that little change in sulfur speciation occurred for the coal containing no alkali, in contrast to the decrease observed in the fraction of sulfur present as S<sub>(o)</sub> on heating the alkali-doped coals under N<sub>2</sub>. Bulk ASTM analyses showed no decrease in sulfur content on heating. The form of sulfur in the latter coals was hypothesized based on the results of subsequent experiments.

The percentages of S<sub>(o)</sub> are higher for the mixed-alkali-doped coals heated in air when compared to either the Na- or K-doped coals (Table 1). The creation of a eutectic mixture of Na and K hydroxides may enhance their contact with sulfur and promote S<sub>(o)</sub> formation.

Quantitative Determination of Sulfur Removal. Experiments employing Rasa lignite, which has a high sulfur content (approximately 11% S) that is almost exclusively organic, and Na or (Na + K) hydroxide were carried out to determine whether the alkali hydroxides were reactive toward organic sulfur and how much of the reaction products could be removed from the lignite by washing. The

percentages of  $S_{(o)}$  and  $S_{(u)}$  in the lignite before and after washing, and the S 2p/Al 2s intensity ratios, are reported in Table 2. There was a small increase in the percentage of  $S_{(o)}$  and a 22% decrease in the S 2p/Al 2s intensity ratio following washing for the Na-doped lignite heated in  $N_2$ . Therefore, heating of the Na-doped lignite in  $N_2$ , followed by washing, led to the removal, or conversion to  $S_{(o)}$ , of 34% of the total sulfur in the starting lignite. If one were to assume that all of the Na was converted to  $Na_2S$  upon heating the lignite in  $N_2$ , then 35% of the total sulfur in the lignite would have reacted. This would be in excellent agreement with the results obtained above if washing either oxidized the  $Na_2S$  to  $Na_2SO_4$  or removed it from the lignite. Complementary reductions in sulfur content were obtained for air-heated coal (Table 2) and by increasing the fraction of alkali in the coal.

Rasa lignite must be doped with either NaOH or KOH in order to observe oxidation of sulfur during heating, thereby indicating the importance of the alkali hydroxide for sulfur reactivity. In studies of MCL reactions of alkali with model organosulfur compounds, such as benzothiophene, have shown that nucleophilic attack by  $OH^-$  can lead to ring opening and formation of the Na or K salt of the organosulfur fragment (9,10). To systematically evaluate the effect of the alkali cation and its associated anion on the reactivity of sulfur in coal, two sets of experiments were performed. In the first experiment, a Pittsburgh No. 8 coal was doped with various Na and K salts and heated in air or  $N_2$  at 375°C for 1 hour. Coals doped with Na and K salts and heated in  $N_2$  showed no significant difference in the percentages of  $S_{(o)}$  and  $S_{(u)}$  ( $\%S_{(o)} = 14.3 \pm 2.4$ ) because formation of an alkali sulfide renders the reacted sulfur indistinguishable by ESCA from unreacted organosulfur and pyrite.

An easier comparison of the relative reactivity of alkali cations and anions towards sulfur, most importantly organic sulfur, in coal is achieved by heating the coals in air where the product is the alkali sulfate. Table 3 shows that for coals doped with Na salts and heated in air,  $F^-$ ,  $NO_3^-$ , and  $CO_3^{2-}$  were least effective for conversion of  $S_{(u)}$  to  $S_{(o)}$ , while the acetate salt was the most reactive. For coals doped with K salts,  $F^-$ ,  $Cl^-$ , and  $NO_3^-$  were least effective for  $S_{(o)}$  formation compared to acetate, which was most reactive. It is interesting to note that less conversion of  $S_{(u)}$  to  $S_{(o)}$  occurs in the presence of the small and highly electrophilic (less nucleophilic) anions,  $F^-$  and  $Cl^-$  (when associated with K) than in the presence of larger and less electrophilic  $Br^-$  and acetate anions. Studies of MCL employing model organosulfur compounds have shown that nucleophilic attack of the aromatic sulfur-containing ring is an important step in sulfur elimination (9,10). Therefore, while reactions between  $Br^-$  or acetate anions and the sulfur-containing moieties of coal may be sterically hindered, the stronger nucleophilic properties of these anions may play an important role in the overall reaction that leads to sulfur oxidation.

The effects of alkali cation size on the reactivity of the sulfur-containing components of coal can be seen in Table 4, which shows that as the size of the cation increases ( $Na^+ \rightarrow Cs^+$ ), the conversion of  $S_{(u)}$  to  $S_{(o)}$  for coal heated in air also increases. The extent of reaction of model organosulfur compounds under MCL conditions has been found to increase with cation size (9,10,12). The earlier studies proposed that the increased size of the cation may help to stabilize a reaction intermediate prior to sulfur elimination, thereby promoting the overall reaction.

## CONCLUSIONS

These experiments have shown that removal of sulfur from coal may be accomplished by doping with alkali hydroxides followed by heating to moderate temperatures and washing. The types of alkali salts used for treating coal surfaces are important in determining the nature and extent of sulfur reactivity.

## ACKNOWLEDGMENTS AND DISCLAIMER

The authors thank Bruce Utz and Yael Miron for helpful discussions. Reference in this report to any specific commercial product, process, or service is to facilitate understanding and does not necessarily imply its endorsement or favoring by the U.S. Department of Energy.

## REFERENCES

1. Wheelock, T.D.; Markuszewski, R. In "The Science and Technology of Coal and Coal Utilization"; Cooper, B.R., Ellington, W.A., Eds.; Plenum Press: New York, 1984; pp. 47-123.
2. Masciantonio, P.X., Fuel, 44, 269-275 (1965).
3. TRW Energy Development Group "Gravimelt Process Development," Final Report, DOE/PC/42295-T7 (DE84013743), June 1983.
4. Meyers, R.A.; Jones, J.F.; McClanathan, L.C., TRW Applied Technology Division, "MCL System Integration Project," Presented at Coal Utilization and Environmental Control Contractors' Review Meeting, Pittsburgh, PA, July 1987.
5. Markuszewski, R.; Mroch, D.R.; Norton, G.A.; Straszheim, W.E.; Am. Chem. Soc. Div. Fuel Chem. Prepr. Pap., 30, 41-48 (1985).
6. Criswell, C.D.; Mroch, D.R.; Markuszewski, R., Anal. Chem., 58, 319-21 (1986).
7. Markuszewski, R., "Chemistry of Caustic Regeneration in Chemical Coal Cleaning," Presented at Coal Utilization and Environmental Control Contractors' Review Meeting, Pittsburgh, PA, July 1987.
8. Chiotti, P.; Markuszewski, R., Ind. Eng. Chem., Process Des. Dev., 24, 1137-1140 (1985).
9. Utz, B.R.; Friedman, S.; Sobaczewski, S.K., in: Fossil Fuel Utilization, R. Markuszewski and B.D. Blaustein (Eds.), Am. Chem. Soc., Washington, DC, 1986, pp. 51-61.
10. Friedman, S.; Utz, B.R.; Nowak, M.A.; Fauth, D.J.; Schmidt, C.E., Proc.-Int. Conf. Coal Sci., 1987, 435-438.
11. Wagner, C.D., "Handbook of X-Ray Photoelectron Spectroscopy," Perkin-Elmer Corporation, Eden Prairie, MN, 1979.
12. Wallace, T.J.; Hofmann, J.F.; Schriesheim, A., J. Am. Chem. Soc., 85, 2739 (1963).

Table 1. Percentages of  $S_{(o)}$  as Determined by ESCA for a Pittsburgh No. 8 Coal Heated for 1 Hour at Various Temperatures.

<u>Temperature</u>	<u>Non-Doped Coal</u>	<u>Na-Doped Coal</u>	<u>K-Doped Coal</u>	<u>(Na + K)-Doped Coal</u>
Not Heated	30.7	37.5	32.6	45.8
100°C <sup>a</sup>	33.6	36.8	37.5	49.2
150°C <sup>a</sup>	38.0	43.1	43.1	57.2
250°C <sup>a</sup>	46.7	71.4	60.9	81.0
350°C <sup>a</sup>	58.6	82.7	77.0	84.5
375°C <sup>a</sup>	67.4	87.2	80.6	88.2
375°C <sup>b</sup>	31.5	14.6	15.9	23.5

<sup>a</sup>Heated in air.

<sup>b</sup>Heated in  $N_2$ .

Table 2. Percentages of  $S_{(o)}$  and  $S_{(u)}$  and S 2p/Al 2s Intensity Ratios as Determined by ESCA for a Heated-Treated<sup>a</sup> Rasa Lignite Before and After Washing.

	<u>Heated In Air</u>			<u>Heated In <math>N_2</math></u>		
	<u><math>S_{(o)}</math></u>	<u><math>S_{(u)}</math></u>	<u>S 2p/Al 2S</u>	<u>%<math>S_{(o)}</math></u>	<u>%<math>S_{(u)}</math></u>	<u>S 2p/Al 2S</u>
<u>Na-Doped (5% Na)</u>						
Before Washing	57.2	42.8	0.796 <sup>b</sup>	8.6	91.4	1.40 <sup>c</sup>
After Washing	15.5	84.5	0.584 <sup>b</sup>	16.0	84.0	1.09 <sup>c</sup>

<sup>a</sup>Heated at 375°C for 1 hour.

<sup>b</sup>Mixed with approximately 20%  $Al_2O_3$ .

<sup>c</sup>Mixed with approximately 10%  $Al_2O_3$ .

Table 3. Percentages of  $S_{(o)}$  and  $S_{(u)}$  as Determined by ESCA for Air-Heated,<sup>a</sup> Alkali-Doped Pittsburgh No. 8 Coal.

Anion	Na <sup>+</sup> Cation		K <sup>+</sup> Cation	
	%S <sub>(o)</sub>	%S <sub>(u)</sub>	%S <sub>(o)</sub>	%S <sub>(u)</sub>
OH <sup>-</sup>	87.2	12.8	80.6	19.4
F <sup>-</sup>	76.7	23.3	71.0	29.0
Cl <sup>-</sup>	85.3	14.7	74.4	25.6
Br <sup>-</sup>	88.2	11.8	82.7	17.3
NO <sub>3</sub> <sup>-</sup>	80.1	19.9	77.5	22.5
(C <sub>2</sub> H <sub>3</sub> O <sub>2</sub> ) <sup>-</sup>	94.9	5.1	89.9	10.1
CO <sub>3</sub> <sup>2-</sup>	81.1	18.9	78.9	21.1

<sup>a</sup>Heated at 375°C for 1 hour.

Table 4. Percentages of  $S_{(o)}$  and  $S_{(u)}$  as Determined by ESCA for Heat-Treated,<sup>a</sup> Alkali-Doped Pittsburgh No. 8 Coal.

Cation	Heated In Air		Heated In N <sub>2</sub>	
	%S <sub>(o)</sub>	%S <sub>(u)</sub>	%S <sub>(o)</sub>	%S <sub>(u)</sub>
None	67.4	32.6	31.5	68.5
Na <sup>+</sup>	87.2	12.8	14.6	85.4
K <sup>+</sup>	87.2	12.8	15.9	84.1
Rb <sup>+</sup>	91.4	8.6	26.4	73.6
Cs <sup>+</sup>	100.0	0.0	22.4	77.6

<sup>a</sup>Heated at 375°C for 1 hour.

## FTIR EXTERNAL REFLECTION STUDY OF SURFACE LAYERS ON COAL

J. A. Mielczarski, J. L. Yordan and R. H. Yoon

Department of Mining and Minerals Engineering  
Virginia Polytechnic Institute and State University  
Blacksburg, Virginia 24061

### ABSTRACT

An infrared reflection-absorption spectroscopy (IRAS) technique has been developed to study the structure of adsorbed surfactant layers on coal. Owing to the optical properties of coal, negative as well as positive absorption bands are observed in the recorded spectra which depend on the angle of incidence ( $\theta$ ) and the polarization of the incident radiation. Theoretical calculations make it possible to predict the changes in absorbance with  $\theta$  and polarization. These changes are a function of the optical properties of the coal and the adsorption layer. The application of the IRAS method to studies of the adsorption layer is presented for several systems, i.e., adsorption of sodium laurate and a nonionic surfactant on coal. In addition, the oxidation layer produced during low-temperature oxidation of coal has been investigated. The results obtained indicate that the IRAS method has an enormous potential for use in determining the structure of an adsorption layer on coal after different treatments.

### INTRODUCTION

Systematic studies of coal structure have been carried out in recent years. Since coal is a mixture of various organic and inorganic compounds which are non-crystalline and mostly insoluble, the standard analytical methods of structural determination are of little use. Thus, spectroscopic techniques such as transmission infrared (1,2) and NMR (3,4) are usually applied to characterize the structure of coal and its derivative products.

In most coal cleaning processes, such as froth flotation, the coal surface properties play an important role. Diffuse reflectance (DR) (5,6) and attenuated total reflection (ATR) (7,8) in infrared, and x-ray photoelectron spectroscopy (XPS) (9) are very surface-sensitive techniques and, hence, have been used to study the coal surface. Nevertheless, the study of the surface structure of coal is very difficult because the recorded spectra are the summation of the spectra of heterogeneous bulk coal and those of the surface layers.

In the present paper, the structure of surface layers on coal has been studied using the infrared reflection-absorption spectroscopy (IRAS) technique. To date most of the IRAS studies have been done to study metals surfaces (10-13) which strongly reflect the incident beam. Coal, on the other hand, shows low reflectivity relative to metals, and interpretation of the recorded spectra in terms of an oriented surface structure is more complicated. However, the theoretical analysis presented in this paper makes it possible to predict the changes in the absorbance of polarized light, which makes it easier to interpret the recorded spectra. Moreover, as shown in this work, the IRAS method provides a means of distinguishing the spectrum of the thin surface layer from that of the substrate, and provides a means of examining the flat surface of a large coal slab directly after treatment.

## EXPERIMENTAL

### Preparation of Thin Layer

Coal slabs 10x30 mm in size were cut by means of a diamond wheel using water as the cooling medium. The coal sample was from a Pittsburgh seam in West Virginia. Each specimen was wet-polished with emery paper (No. 600 and 1200) and washed in water in an ultrasonic bath.

For the study of adsorbed layers, the samples were immersed into 100 ml of  $2 \times 10^{-4}$  M solution of nonylphenolpolyethyleneglycol ether with a pH of  $7.2 \pm 0.2$  for 5 minutes or 12 hours, and for 1 hour in 100 ml of  $10^{-3}$  M sodium laurate with a pH of  $6.0 \pm 0.2$ . After adsorption, the samples were removed from solution, dried at room temperature and placed into the FTIR spectrometer to record the spectra.

Low-temperature oxidation of the coal specimens was carried out at 125°C in air for a period of 24 hours. The oxidized sample was examined spectrometrically and then treated with barium hydroxide (0.05 M) to change the surface carboxyl groups to ionic form. The spectrum of the sample was recorded again after this treatment.

The reagents used were nonylphenolpolyethyleneglycol ether (Tergitol NP-9), a nonionic surfactant obtained from Union Carbide Corporation, with an average of 9 ethylene glycol groups per molecule. The sodium laurate was obtained from Pfaltz and Bauer, Inc. Both reagents were used as received with no further purification. Double distilled water produced in an all-glass still was used in all the experiments.

### Measurement

The infrared spectra were recorded on a Perkin-Elmer Model 1710 FTIR spectrometer with an MCT detector using an external reflection attachment (Spectra Tech, Inc) with a single reflection. A wire grid polarizer (Harrick Scientific Company) was placed before the sample and provided polarization selection. The spectra were taken at  $4 \text{ cm}^{-1}$  resolution by co-adding 64 scans in the  $4000\text{--}500 \text{ cm}^{-1}$  region. The unit of intensity is given in terms of  $-\log(R/R_0)$ , where R and  $R_0$  are the reflectivities of the samples after different treatment and freshly exposed coal, respectively. The transmission spectra of lauric acid and coal in KBr pellets, and chloroform solution of Tergitol NP-9 were prepared and measured in the standard way.

### Calculation of Reflection-Absorbance

Figure 1 shows a model of the three-phase system investigated and the interaction of an electromagnetic wave with the system. The optical properties of each phase are characterized by the complex refractive index  $\hat{n}_j = n_j + ik_j$ , where  $n_j$  is the real refractive index and  $k_j$  is the absorption constant. The thin film has a thickness,  $d_2$ .

The theoretical calculation of the intensity of an absorption band in the reflection spectra is described in several papers (14-17). In this paper, a recently reported (17) theoretical analysis was used. The calculation was made for the following data: for ambient (air)  $n_1 = 1.0$  and  $k_1 = 0$ ; for the adsorption layer of lauric acid,  $n_2 = 1.5$  and  $k_2' = 0.3$  at  $1705 \text{ cm}^{-1}$ ; and for the adsorption layer of a nonionic surfactant,  $n_2 = 1.5$  and  $k_2'' = 0.38$  at  $1103 \text{ cm}^{-1}$ . The thickness of the adsorbed monolayer was assumed to be  $5 \times 10^{-9}$  m.

The optical constants of coal were calculated to be  $n_3 = 2.05$  and  $k_3 = 0.02$  at  $1800\text{ cm}^{-1}$ . These latter data were obtained on the basis of transmission spectra of KBr pellets of coal and measurements of the ratio of reflectivities of p- and s-polarization at different angles of incidence. These particular optical data for the three phases are only approximations of the real values and were chosen to simulate the optical properties of adsorption layers on coal.

## RESULTS AND DISCUSSION

### Adsorption of Nonylphenolpolyethyleneglycol Ether on Coal

The infrared transmission spectra of the coal and nonionic surfactant used in this study are shown in Figures 2 and 3, respectively. Figure 4 shows the reflection spectra of the thin surface film of Tergitol NP-9 on the coal after 12 hours of treatment time in a  $2 \times 10^{-4}\text{ M}$  solution. Since the absorbance was measured in terms of  $-\log(R/R_0)$ , any spectrum recorded showed the effect of the treatment. It should also be noted that no spectrum is recorded after only 5 minutes of treatment, indicating slow adsorption kinetics. It is shown that the intensity of the absorption bands vary with the polarization and the angle of incidence. The negative absorption bands observed in the recorded spectra are not unique for the system studied in the present work. Others were theoretically predicted (14,18) for low-absorption substrates and observed experimentally for water (16) and cuprous sulfide (17) substrates.

In order to explain the changes in IRAS spectra observed, theoretical calculation of the absorbance for the system has been carried out, and the results are shown in Figure 5. The solid lines represent the changes of absorbance ( $A$ ) at  $1100\text{ cm}^{-1}$ , as a function of the angle of incidence for both s-polarization ( $A_{\perp}$ ) and p-polarization ( $A_{\parallel}$ ). This calculation was performed for an isotropic layer of the nonionic surfactant. The experimental points obtained after 12 hours of adsorption from the  $2 \times 10^{-4}\text{ M}$  solution are shown as circles and crosses for s- and p-polarization, respectively. In general, a reasonable agreement between the experimental results and the theoretically predicted values is observed. For s-polarization, negative absorption bands are predicted and, in fact, only negative bands are observed. For s-polarization which has electric field components which are only parallel to the interface plane (Figure 1), only those molecular groups that have transition moment components parallel to the substrate surface can interact with the incidence radiation, allowing absorption to be observed. The difference between the relative intensity ratios of the observed bands in IRAS (Figure 4, s-polarization) and transmission spectra (Figure 3) indicates that adsorbed molecules are oriented on the surface of coal.

The same conclusion can be obtained from the spectroscopic results for p-polarization. An intense absorption band is observed at  $1103\text{ cm}^{-1}$  for p-polarization and at an 80-degree angle of incidence, while the calculated values of absorbance,  $A$ , under these conditions is close to zero (Figure 5). This discrepancy can be explained by consideration of the two components,  $E_{\parallel x}$  and  $E_{\parallel z}$ , of p-polarization of the incident beam (Figure 1). The theoretical calculation of the  $A_{\parallel x}$  and  $A_{\parallel z}$  components has been done in the same way as reported recently (17), and the results are shown in Figure 5 as dashed lines. According to this calculation, an intense positive absorption band should be obtained at an angle of incidence of 80 degrees for molecular groups which have transition moments parallel to the surface of the substrate. Since the absorption band at  $1103\text{ cm}^{-1}$  can be assigned to (C-O-C) stretching, the presence of this intense absorption band in the recorded spectra indicate that the polyethylene glycol part of the adsorbed molecule is positioned parallel

to the surface of the coal. However, the nonylphenol unit of the adsorbed molecule is inclined to the plane of substrate.

#### Thin Layer of Lauric Acid on Coal

The adsorption was performed from  $10^{-3}$  M solution of sodium laurate at pH  $6.0 \pm 0.2$ . Under these conditions, the reagent exists in solution as lauric acid ( $pK=4.7$ ). It was found that a significant part of surfactant was deposited on the coal surface from a thin film of solution during drying of the sample.

The reflection spectra of the thin film of lauric acid on coal are shown in Figure 6. Theoretical calculations performed for the coal-lauric acid system (Figure 7) allow an explanation of the results obtained in a similar way as was discussed for the non-ionic surfactant. Generally good agreement is observed between the experimental data and the theoretical analysis. This agreement also suggests that the lauric acid molecules in the thin layer on the surface of coal are randomly oriented. Data presented in Figure 7 was calculated for a thin layer of  $50 \text{ \AA}$ . Since the experimental intensities for the absorption bands are nearly 5 times higher than those calculated, the thickness of the lauric acid could be considered to be as thick as  $250 \text{ \AA}$ . The real thickness of the lauric acid layer is probably much thinner. Various reasons for the discrepancy between real and theoretically calculated values have been discussed recently (17).

#### Low-Temperature Oxidation of Coal

During the oxidation, the following changes in the reflection spectra (Figure 8) are observed: the bands at  $1700$ ,  $1555$  and  $1180 \text{ cm}^{-1}$  appear and the intensity of the band at  $1440 \text{ cm}^{-1}$  decreases. These results indicate that the oxidation products, such as carbonyl and carboxyl groups (band at  $1700 \text{ cm}^{-1}$ ), ionized  $-\text{COO}^-$  groups (band at  $1550 \text{ cm}^{-1}$ ) and C-O groups in ether, alcohol or phenyl (band at  $1180 \text{ cm}^{-1}$ ), are formed while the aliphatic groups (band at  $1440 \text{ cm}^{-1}$ ) present in the coal are oxidized.

The band at  $1700 \text{ cm}^{-1}$  is markedly distorted due to the anomalous dispersion of the refractive index of the oxidation products. Notably, band shape distortion when using the reflection method has also been reported (19).

For p-polarization at a 70-degree angle of incidence, positive absorption bands in the spectrum are observed. However, for the other measurement conditions, i.e., different angles and polarization, only negative absorbances are recorded (Figure 8). Hence, for oxidized coal samples, the negative and positive absorption bands appeared at the same angle of incidence and polarization as was found for the adsorption layer from solution (Figures 4 and 6).

The barium hydroxide-treated oxidized coal sample shows intense absorption bands at  $1550$  and  $1400 \text{ cm}^{-1}$  (Figure 9). These bands can be assigned to asymmetric and symmetric stretching vibrations of the COO group, respectively. A notably strong increase in the intensities of these bands is due to the change of the  $-\text{COOH}$  groups to the ionized  $-\text{COO}^-$  form.

A significant increase in the intensity of the band at  $1555 \text{ cm}^{-1}$  after oxidation (Figure 8) relative to the band at  $1440 \text{ cm}^{-1}$  could indicate that the ionic groups  $-\text{COO}^-$  which are formed during the oxidation process are oriented with both of the oxygen atoms oriented toward the ambient (air).

## CONCLUSIONS

The infrared reflection-absorption spectroscopy (IRAS) method has been developed for characterizing the surface layer on coal. The absorbance is shown to be a function of the optical properties of the coal and the surface layer, as well as of the angle of incidence and the polarization of the incident beam.

The results obtained show that the IRAS method makes it possible to determine both the chemical nature and the structure of the adsorbed layers on the coal substrate.

## REFERENCES

1. Painter, P. C., Starsinic, M. and Coleman, M. M., 1985. in Fourier Transform Infrared Spectroscopy, Vol. 4 (J. R. Ferraro and L. J. Basile, Eds.), Academic Press, New York, p. 169 and references therein.
2. Gethner, J. S., 1987. Appl. Spectrosc., 41:50.
3. Fredericks, P. M., Warbrooke, P. and Wilson, M. A., 1983. Org. Geochem., 5:89.
4. Painter, P. C., Kuchn, D. W., Starsinic, M., Davis, A., Havens, J. R. and Koenig, J. L., 1983. Fuel, 62:103.
5. Fuller, M. P., Hamadeh, I. M., Griffiths, P. R. and Lowenhaupt, D. E., 1982. Fuel, 61:529.
6. Smyrl, N. R. and Fuller, E. L., 1987. Appl. Spectrosc., 41:1023.
7. Mielczarski, J. A., Denca, A. and Strojek, J. W., 1986. Appl. Spectrosc., 40:998.
8. Bubnowskaia, L. M., Popov, W. K. and Rusianova, 1982. Koks i chemia, 5:9.
9. Perry, D. L. and Grint, A., 1983. Fuel, 62:1024.
10. Golden, W. G., 1985. in Fourier Transform Infrared Spectroscopy, Vol. 4 (J. R. Ferraro and L. J. Basile, Eds.), Academic Press, New York, Chapter 8.
11. Swalen, J. D. and Rubolt, J. F., 1985. in Fourier Transform Infrared Spectroscopy, Vol. 4 (J. R. Ferraro and L. J. Basile, Eds.), Academic Press, New York, Chapter 7.
12. Mielczarski, J. A. and Leppinen, J., 1987. Surface Science, 187:526.
13. Liedberg, B., Carlsson, C. and Lundstrom, I. J., 1987. Coll. Inter. Science, 120:64.
14. McIntyre, J. D. E., 1973. in Advances in Electrochemistry and Electrochemical Engineering, Vol. 9 (R. M. Muller, Ed.), Wiley Interscience, New York, Chapter 2.
15. Allara, D. L., Baca, A. and Pryde, C. A., 1978. Macromolecules, 11:1215.
16. Dluhy, R. A., 1986. J. Phys. Chem., 90:1373.
17. Mielczarski, J. A. and Yoon, R. H., 1988. J. Phys. Chem.; submitted.
18. Hansen, W. N., 1970. Symp. Faraday Soc., 4:27.
19. Porter, M. D., Bright, T. B., Allara, D. L. and Kuwana, T., 1986. Anal. Chem., 58:2461.

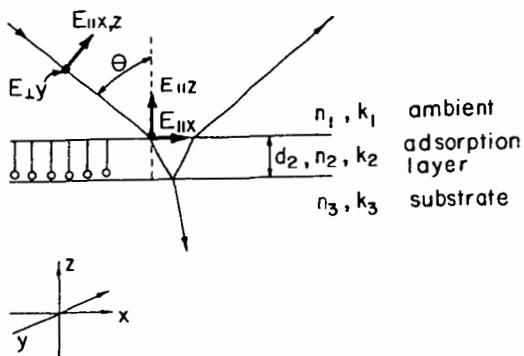


**Figure 1.** Electric field vectors in a three-phase system. Parallel (p) ( $E_{\parallel z}$ ,  $E_{\parallel x}$ ) and perpendicular (s) ( $E_{\perp y}$ ) components are shown for incident radiation.

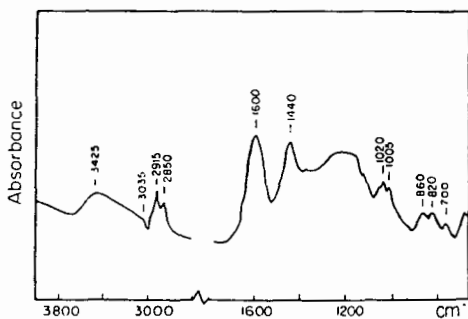


**Figure 2.** Transmission spectrum of Pittsburgh seam coal.

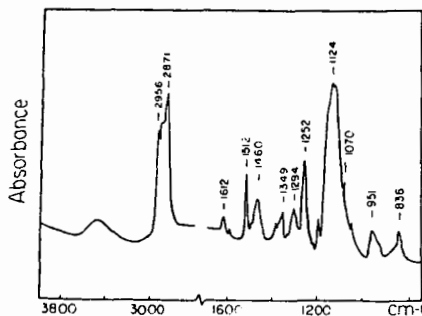


**Figure 3.** Transmission spectrum of nonylphenolpolyethyleneglycol ether.

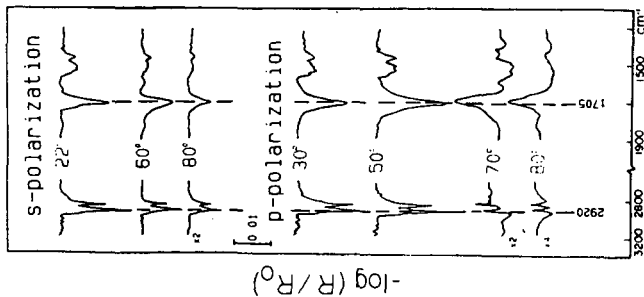


Figure 6. IRAS spectra of lauric acid layer on coal recorded at various angles of incidence with s- and p-polarization.

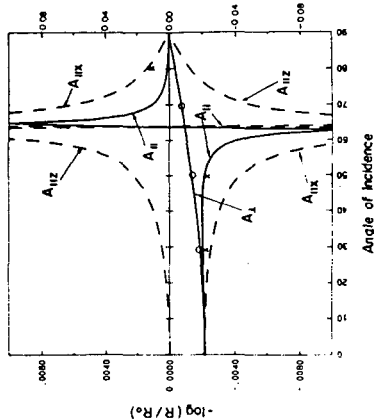


Figure 5. Calculated absorbance for hypothetical layer of nonylphenolpoly-ethylene glycol ether ( $n_2 = 1.5$ ,  $k_2 = 0.36$ ,  $\lambda = 9.09$ ,  $d_2 = 5 \times 10^{-9}$  m) on coal ( $n_3 = 2.05$ ,  $k_3 = 0.02$ ) (solid and dashed lines). Experimental results (note different absorbance scales) shown as circles for s-polarization and as crosses for p-polarization.

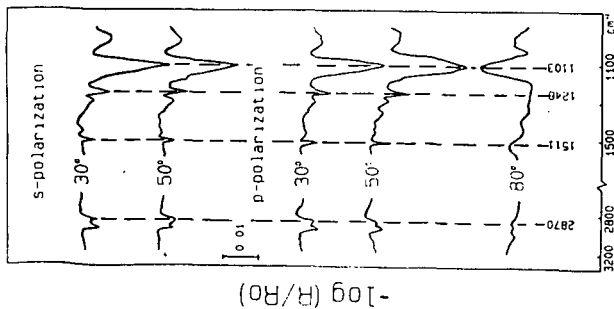


Figure 4. IRAS spectra of the adsorbed layer of nonylphenolpoly-ethylene glycol ether on coal recorded at various angles of incidence with s- and p-polarization.

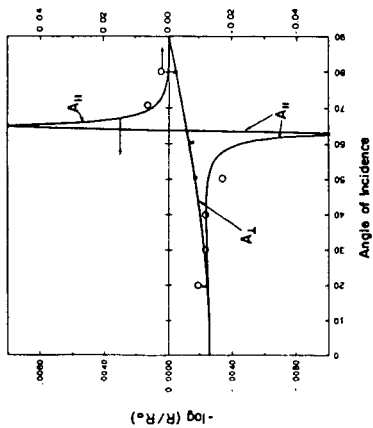


Figure 7. Calculated absorbance for hypothetical layer of lauric acid ( $n_2 = 1.5$ ,  $k_2 = 0.3$ ,  $\lambda = 5.85$ ,  $d_2 = 5 \times 10^{-9}$  m) on coal ( $n_3 = 2.05$ ,  $k_3 = 0.02$ ) (solid lines). Experimental results (note different absorbance scales) shown as circles for s-polarization and as crosses for p-polarization.

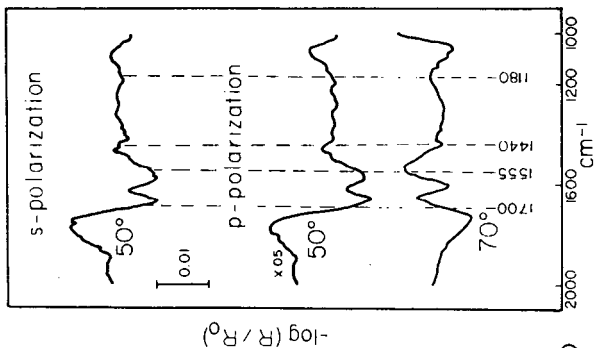


Figure 8. IRAS spectra of low-temperature oxidized coal recorded at different angles of incidence for s- and p-polarization.

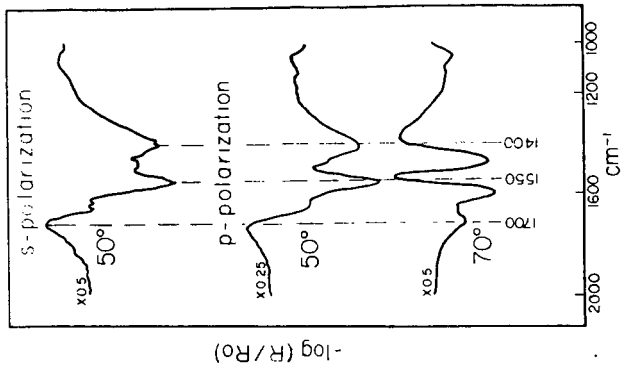


Figure 9. IRAS spectra of barium hydroxide treated oxidized coal recorded at different angles of incidence for s- and p-polarization.

APPLICATION OF THE DUBININ-ASTAKHOV EQUATION TO THE EVALUATION OF THE  
BENZENE AND CYCLOHEXANE ADSORPTION ISOTHERMS ON STEAM GASIFIED  
HUMIC ACIDS CHARs FROM BROWN COAL

Teresa Siemieniewska, Kazimierz Tomków, Jan Kaczmarczyk, Andrzej Albiniaak  
Institute of Chemistry and Technology of Petroleum and Coal, Techni-  
cal University, Gdańska 7/9, 50-306 Wrocław, Poland

Yves Grillet

Centre de Thermochimie et de Microcalorimétrie du CNRS, 26, rue du  
141 RIA, 13003 Marseille, France

Michèle François

Centre de Recherches sur la Valorisation des Minerais, École Natio-  
nale Supérieure de Géologie, BP 40, 54501 Vandoeuvre Cédex, France

#### INTRODUCTION

The Dubinin's theory of volume filling of micropores (1) is ap-  
plied to the evaluation of adsorption isotherms to characterize the  
capillary structure of microporous carbonaceous solids (2-15). Re-  
cently, this theory is frequently represented by the Dubinin-Astak-  
hov (DA) equation (16):

$$W = W_0 \exp \left[ - (A/\beta E_0)^n \right] \quad (1)$$

where  $W$  is the volume of micropores filled with the adsorbate at  
temperature  $T$  and relative pressure  $p/p_0$ ,  $W_0$  is the total volume of  
micropores,  $A = RT \ln(p/p_0)$  is the differential molar work of adsorp-  
tion. The product  $\beta E_0$  is equal  $E$ , where  $E_0$  and  $E$  are characteristic  
adsorption energies for a standard and a chosen adsorptive, respec-  
tively. The coefficient  $\beta$  is a similarity factor, related to the ad-  
sorptives ( $\beta$  is usually calculated as the ratio of molar volumes or  
parachores of the adsorptives), and it enables the characteristic  
curves (plots of  $W/W_0$  versus  $A$ ) of different adsorptives on the same  
solid to be superimposed. The value of the parameter  $n$  is chosen so  
that the experimental data would fit equation 1.

The proper choice of  $n$  may present some difficulties. Also, the  
question arises, if the rectilinearity of the plot in the coordi-  
nates corresponding to the logarithmic form of equation 1:  $\ln W$  ver-  
sus  $(A/\beta E_0)^n$ , even if it should be attained for a given  $n$ , can be  
considered as a sufficient indication for the physicochemical vali-  
dity of the resulting parameters  $W_0$  and  $\beta E_0$ .

The aim of this work was to establish, for a suite of carbona-  
ceous materials, the values of  $n$  for which a satisfactory agreement  
would be obtained between the experimental adsorption data and the  
DA equation, trying also to verify the obtained DA parameters refer-  
ring to related results calculated, or obtained experimentally, in-  
dependently.

As adsorptives benzene (frequently used as standard) and cyclo-  
hexane (to avoid the presence of  $\pi$  - electrons in the molecule)  
were chosen. To have a suite of samples characterized by a systema-  
tically changing porosity, humic acids steam gasified chars were  
prepared with varying burn-offs. Humic acids from brown coals can be  
obtained with a low mineral matter content and they are thought to  
be representative for the organic substance of low rank coals. Ad-  
ditionally, two industrial active carbons, described elsewhere (17)  
were investigated.

#### EXPERIMENTAL

Humic acids (HA) were obtained from a Polish humodetrinitic  
brown coal (containing about 70 wt %, daf, HA), by extraction with  
diluted NaOH solution, followed by precipitation with hydrochloric

was taken. The lower limit of  $p/p_0$  results from our possibility of accurate adsorption measurements; the higher limit is connected with the fact that at relative pressure above 0.1, before the beginning of the hysteresis loop, capillary condensation might, in some cases, occur, due to the tertiary process of adsorption in wider micropores (20). For each of the assumed value of  $n$ , correlation coefficients were calculated, and for each of the adsorbate/adsorbent system the correlation coefficients were closest to unity when  $n=2$  (in a few cases  $n=1.5$  or  $n=2.5$ ) was chosen (upper part of figure 5). This indicates that the best coincidence of experimental points with the DA equation is achieved, within the considered limits of relative pressures, for  $n=2$  (if integrars are to be considered). However, this does not necessarily mean that the values of  $W_0$  and  $\beta E_0$  corresponding to  $n=2$  are of true physicochemical significance.

Applying, for the calculation of the values of  $n$ , the method of Dubinin(21), for benzene adsorption on HA 850/10 ... HA 850/85 the following values were obtained:  $n=6$ ,  $n=6$ ,  $n=5$ ,  $n=3$  and  $n=4$ , and on the charcoals 208 C and 264:  $n=6$  and  $n=4$ . Similar values of  $n$  were obtained for cyclohexane adsorption on these samples.

To gain some additional information concerning the validity of the values of  $W_0$  obtained for  $n=2$  (and also to check the remaining  $W_0$  values), an independently calculated value of the volume of micropores was necessary. We thought this purpose might be served by the volume of micropores, as given in figures 3 and 4 ( $V_{mic}$ ). We tried also to assess the position of the values of  $V_m$  calculated by application of the Brunauer, Emmett and Teller(BET) equation(22) in relation to the respective values of  $V_{mic}$ . Because in the BET coordinates practically no straight lines were obtained from the isotherms in figures 3 and 4, a modification of the BET procedure, according to Joyner, Weinberger and Montgomery (23) was applied.

It appears that here the values of  $V_m$  (according to the theory of BET,  $V_m$  is the monolayer capacity of the adsorbent) are in a very good agreement with respective values of  $V_{mic}$ , the correlation coefficient being equal 0.998 (figure 6 a). This means that  $V_m$ , in case of the investigated samples, might represent the volume of adsorbate contained in the micropores only, not including the adsorption in the monolayer of the mesopores ( $V_{Smes}$ ). If to the values of  $V_m$  the values of  $V_{Smes}$  are added, an approximate position of point B of the isotherms in figures 1 and 2 is reached. This is seen in Table II, where the amounts adsorbed are expressed directly in mmol/g.

Table II. Benzene adsorption (mmol/g) and corresponding  $p/p_0$

Sample	$a_{mic}$ (p/p <sub>0</sub> )	$a_m$ (p/p <sub>0</sub> )	$\{a_m + a_{Smes}\}$ (p/p <sub>0</sub> )	$a_0$ (p/p <sub>0</sub> )
HA 850 10	1.43 (0.10)	1.43(0.10)	1.53 (0.22)	1.40(0.07)
HA 850 25	2.77 (0.07)	2.73(0.06)	2.92 (0.18)	2.77(0.07)
HA 850 50	4.26 (0.05)	4.27(0.05)	4.76 (0.16)	4.34(0.06)
HA 850 75	4.99 (0.05)	4.93(0.04)	5.71 (0.14)	5.12(0.06)
HA 850 85	4.95 (0.04)	4.94(0.04)	5.81 (0.16)	5.04(0.05)
Charcoals:				
208 C	4.23 (0.08)	4.23(0.08)	4.42 (0.16)	4.27(0.09)
264	3.25 (0.06)	3.40(0.08)	3.90 (0.19)	3.32(0.07)

For all the investigated samples correlation coefficients were calculated for the relationships between  $W_0$  obtained for different values of  $n$  and the respective values of  $V_{mic}$  and  $V_m$ . In all cases

acid. The carbonization was carried out at a rate of 5°C/min to the final temperature of 850°C. The obtained char, designed as HA 850, was gasified, in a thermogravimetric apparatus, with steam at 800°C to following burn-offs: 10, 25, 50, 75 and 85 %. The obtained samples were designed as: HA 850/10..... HA 850/85. Active carbons: charcoal 208 C and charcoal 264, based on coconut shell and on coal, correspondingly, were obtained from the firm Sutcliffe Speakman Ltd. Sorption measurements of benzene and cyclohexane were carried out at 25°C in a gravimetric vacuum apparatus (McBain quartz springs). Mercury porosimetry was used for the determination of macropore volumes of the steam gasified HA chars.

#### RESULTS AND DISCUSSION

The characteristic of samples is presented in Table I.

Table I. Proximate and ultimate analyses ( wt % )

Sample	Proximate analysis			Ultimate analysis		
	Moisture	Ash	Volatile matter	C	H	(O+N+S <sub>o</sub> ) <sub>diff</sub>
		dry	daf	daf	daf	daf
Brown coal	52.1 <sup>4)</sup>	9.5	57.1	70.8	6.0	23.2
HA	6.3	0.4	53.2	69.1	6.0	24.9
HA 850	1.1	0.6	1.7	97.1	0.5	2.4
HA 850 10	0.5	0.7	1.8	96.3	0.7	3.0
HA 850 25	0.6	0.8	1.7	96.3	0.7	3.0
HA 850 50	0.6	1.2	1.6	96.4	0.7	2.9
HA 850 75	0.7	2.4	1.6	97.6	0.6	1.8
HA 850 85	0.6	3.0	0.8	98.6	0.7	0.7
Charcoals:						
208 C	6.2	5.4	3.2	96.1	1.2	2.7
264	4.7	14.8	3.0	95.4	1.1	3.5

<sup>4)</sup> Total moisture of raw coal.

Isotherms of benzene and cyclohexane adsorption are given in figures 1 and 2. Basing on the desorption branch of the benzene isotherms, the pore size distributions of mesopores were calculated (18,19). The volume of micropores ( $V_{mic}$ ) was calculated as the difference between the Gurvitch volume (the amount adsorbed at  $p/p_0 = 0.96$ , corresponding to the effective radius of 50 nm, was taken) and the volume of mesopores. Within the micropores volumes, the volumes of super- and ultramicropores were distinguished, in which primary and secondary (cooperative) adsorption processes occurred (20). The results are shown in form of bar graphs in figures 3 and 4. For the HA steam gasified chars, also the volumes of macropores are indicated. With increasing burn-offs systematic changes of each kind of considered porosity are visible.

On the basis of standard adsorption isotherms on a non-porous carbon black - Spheron 6-2700, the benzene and cyclohexane isotherms in figures 1 and 2 were corrected, subtracting at successive relative pressures the respective amounts adsorbed on the surface of mesopores ( $S_{mes}$ ). The values of  $S_{mes}$  for the samples HA 850/10 ... ..HA 850/85 are: 25.3, 51.1, 133.2, 206.6 and 228.8 m<sup>2</sup>/g, and for the charcoals 208 C and 264: 49.0 and 132.3 m<sup>2</sup>/g, respectively.

The corrected isotherms were used to calculate the values of  $W_0$  and  $\beta E_0$  according to the DA equation, assuming different values of the exponent  $n$ , from 1 to 6. The results are shown in figure 5. For these calculations the relative pressure region between 0.01 and 0.1

the best correlation was obtained, if  $W_0$  values corresponding to  $n=2$  were considered. It follows from figure 6 b, that there exists almost an identity between the  $W_0$  values calculated from the DA equation for  $n=2$  and the respective  $V_{mic}$  and  $V_m$  values. For all the investigated samples, if  $W_0$  is calculated for  $n=2$ , for benzene adsorption: points of the plots  $V_m=f(W_0)$  and  $V_{mic}=f(W_0)$ , and for cyclohexane adsorption: points of the plot  $V_m=f(W_0)$ , are placed on a straight line which passes almost through the origin of the coordinate system with a slope very close to 1. This is not the case, if for the calculation of  $W_0$  in the DA equation other values of  $n$  are used.

Examples of DA plots for  $n=2$ , for chosen samples, are presented in figure 7. These plots confirm the proper choice of the upper limit of the relative pressure region ( $p/p_0=0.10$ ) considered for calculations.

An attempt was made to determine the micropore volumes of the samples, employing the  $\alpha_s$ -method (20), using Spheron6-2700 as standard. For samples with a low surface area of mesopores (HA 850/10, HA 850/25 and charcoal 208 C) a fairly good agreement was obtained with  $W_0$  values for  $n=2$ .

To test the validity of the values of  $\beta E_0$  obtained for  $n=2$ , the method presented by Stoekli and Kraehenbuehl (6,8) was applied. The enthalpies of immersion in organic liquids ( $-\Delta H_{im}$ )<sub>mic</sub> of microporous solids with negligible external and mesopore surface areas can be related to the characteristic energies of adsorption ( $\beta E_0$ ) according to the equation:

$$(-\Delta H_{im})_{mic} = \beta E_0 (\sqrt{\pi}/2)(1 + \alpha T) \quad (2)$$

where  $\alpha$  is the thermal expansion coefficient of the adsorbate at temperature  $T$ ; for benzene and cyclohexane the values of  $\alpha$  were taken as  $8.87 \times 10^{-4}$  and  $9.80 \times 10^{-4} \text{ K}^{-1}$ , respectively, calculated on the basis of their densities at the boiling and critical points (21).

$(-\Delta H_{im})_{mic}$  is expressed in the same units as  $\beta E_0$ , e.g. in kJ/mol. In order to express the enthalpy per mass unit, e.g. in J/g, it is necessary to take account of the amount adsorbed in the micropores corresponding to this unit of mass, i.e.  $a_0 = W_0/d$  (where  $d$  is the density of the adsorbate, taken as the density of the adsorbate as liquid at corresponding temperature):

$$(-\Delta H_{im})_{mic} = (-\Delta H_{im})_{mic} \times a_0 \quad (3)$$

These calculations were carried out for the steam gasified HA chars. To the obtained values of  $(-\Delta H_{im})_{mic}$  corrections for the evolution of heat on the mesopore surface area were added:

$(-\Delta H_{im})_{Smes}$ . These corrections were calculated on the basis of the respective  $a_{mes}$  values of the HA chars and the  $\beta E_0$  values of Spheron 6-2700. The sum:  $(-\Delta H_{im})_{mic} + (-\Delta H_{im})_{Smes} = (-\Delta H_{im})$ , considered as the calculated total enthalpy of immersion of the char, was compared with the respective enthalpy value determined experimentally by microcalorimetric measurements (24). The results are shown in figure 8, and (with the exception of samples with highest burn-offs) a satisfactory agreement between the calculated and experimentally determined enthalpy values can be stated.

These considerations point to the fact that the values of  $W_0$  and  $E_0$  calculated from the DA equation with  $n=2$ , represent, in all probability, the real properties of the capillary structure of the investigated samples. Deviations obtained if other values of  $n$  are chosen, are shown in figure 9. Values of  $W_0$  and  $E_0$  for  $n=2$  are given in Table III (for benzene  $\beta=1$ ; for cyclohexane  $\beta=1.22$ ).

Table III. Parameters  $W_0$  ( $\text{cm}^3 \text{g}$ ),  $\beta E_0$  and  $E_0$  ( $\text{kJ mol}$ ) for  $n=2$

Sample	Benzene adsorption		Cyclohexane adsorption		
	$W_0$	$E_0$	$W_0$	$\beta E_0$	$E_0$
HA 850 10	0.125	28.6	0.074	24.9	20.4
HA 850 25	0.248	26.6	0.211	26.7	21.9
HA 850 50	0.388	23.0	0.381	21.1	17.3
HA 850 75	0.458	20.1	0.474	17.0	13.9
HA 850 85	0.451	19.9	0.458	14.2	11.6
Charcoals:					
208 C	0.382	29.1	0.350	23.6	19.3
264	0.297	18.6	0.313	13.9	11.4

A comparison of the  $W_0$  values resulting from adsorption of benzene (molecular sizes: 0.37 and 0.70 nm) and of cyclohexane (molecular sizes: 0.48 and 0.68 nm), indicates the presence of slit-like micropores of widths below 0.48 nm in the microporous system of the HA chars of low burn-offs and the charcoal 208 C. In all cases the values of  $E_0$  for benzene are higher from the respective values for cyclohexane.

#### CONCLUSIONS

- The parameters  $W_0$  and  $\beta E_0$ , calculated for the considered adsorption data, are in a satisfactory agreement with the independently calculated micropore volumes and calorimetrically determined enthalpies of immersion, if in the DA equation the exponent  $n=2$  is assumed.
- These results were obtained for micro- and mesoporous carbonaceous materials, which can be considered as being representative for the majority of active carbons.
- It is very probable that the values of  $W_0$  and  $\beta E_0$  for  $n=2$  are closely related to real properties of the capillary structure - the micropore volume and the integral enthalpy of immersion.

#### ACKNOWLEDGEMENTS

This work was sponsored by the Technical University of Wrocław and the Polish Academy of Sciences (Scientific Program CPBP 01.16).

#### REFERENCES

- Dubin, M.M. in Chemistry and Physics of Carbon (P.L. Walker, Jr., Ed.); Dekker: New York, 1966; Vol. 2, pp 51-120.
- Rand, B. J. Colloid Interface Sci. 1976, 56, 337-343.
- Huber, U.; Stoekli, H.F.; Houriet, J.P. J. Colloid Interface Sci. 1978, 67, 195-203.
- Dubin, M.M.; Stoekli, H.F. J. Colloid Interface Sci. 1980, 75, 35-42.
- Walker, Jr., P.L. Phil. Trans. R. Soc. London 1981, A300, 65-81.
- Stoekli, H.F.; Kraehenbuehl, F. Carbon 1981, 19, 353-356.
- Masters, K.J.; McEnaney, B. J. Colloid Interface Sci. 1983, 95, 340-345.
- Stoekli, H.F.; Kraehenbuehl, F. Carbon 1984, 22, 227-229.
- McEnaney, B.; Masters, K.J. Thermochemica Acta 1984, 82, 81-102.
- Stoekli, H.F.; Kraehenbuehl, F.; Lavanchy, A.; Huber, U. J. Chim. Phys. 1984, 81, 785-790.
- Ali, S.; McEnaney, B. J. Colloid Interface Sci. 1985, 107, 355-361.
- Carrott, P.J.M.; Roberts, R.A.; Sing, K.S.W. Carbon 1987, 25, 59-68.

13. Marsh, H. Carbon 1987, 25, 49-58.
14. McEnaney, B. Carbon 1987, 25, 69-75.
15. Barton, S.S. Carbon 1987, 25, 77-80.
16. Dubinin, M.M.; Astakhov, V.A. Izv. Akad. Nauk SSSR Ser. Khim. 1971 No 1, 5, 11.
17. Everett, D.H.; Parfitt, G.D.; Sing, K.S.W.; Wilson, R. J. appl. Chem. Biotechnol. 1974, 24, 199-219.
18. Pierce, C. J. Phys. Chem. 1953, 57, 149-152.
19. Kankare, J.; Jantti, O. Soumem Kemistilehti 1967, B40, 51-53.
20. Gregg, S.J.; Sing, K.S.W. Adsorption, Surface Area and Porosity; Academic Press: London, 1982.
21. Komarov, W.S. Adsorbents and their Properties (Russian language); Nauka i Tech.: Minsk, 1977; pp 231-239.
22. Brunauer, S.; Emmett, P.H.; Teller, E. J. Am. Chem. Soc. 1938, 60, 309-319.
23. Joyner, L.G.; Weinberger, E.B.; Montgomery, C.W. J. Am. Chem. Soc. 1945, 67, 2182.
24. Grillet, Y.; François, M.; Torralvo, M.J.; Guerrero, A.; Siemieniowska, T.; Tomków, K.; Kaczmarczyk, J.; Albinia, A. Proc. IUPAC Symposium on Characterization of Porous Solids, Bad Soden, F.R.G. 26-29 April 1987; Elsevier.

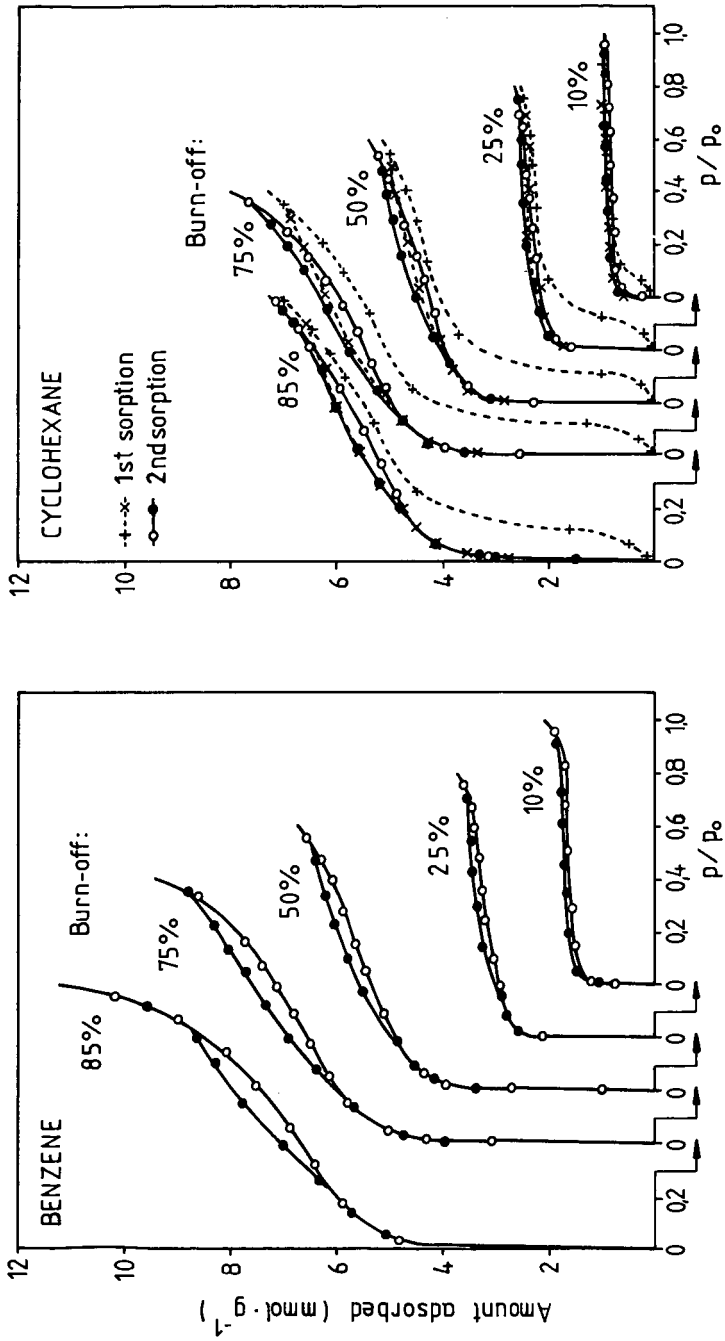


Figure 1. Benzene and cyclohexane sorption isotherms at 25°C on steam gasified (800°C) humic acids char HA 850.

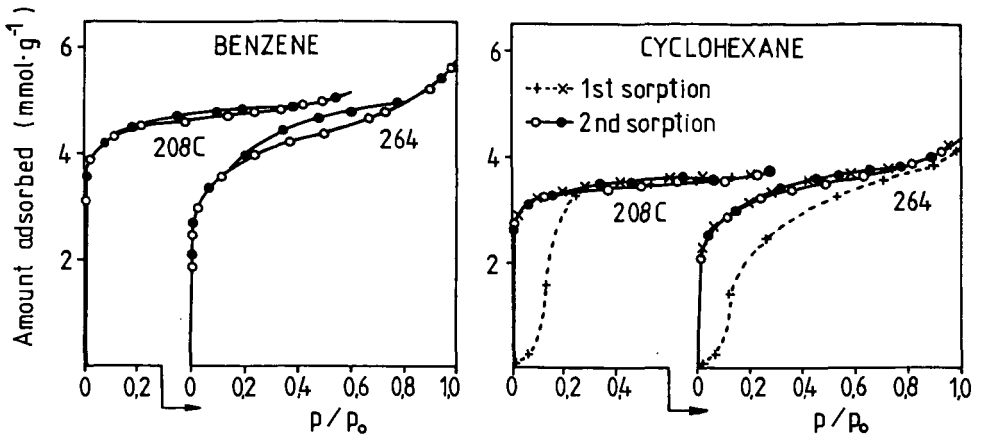


Figure 2. Benzene and cyclohexane sorption isotherms at 25°C on charcoals 208C and 264.

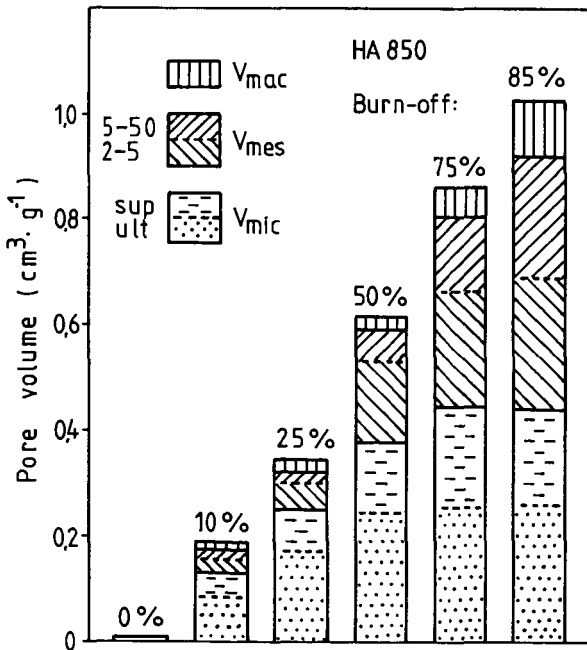


Figure 3. Influence of burn-off on the pore size distribution of steam gasified (800°C) humic acids char HA 850.

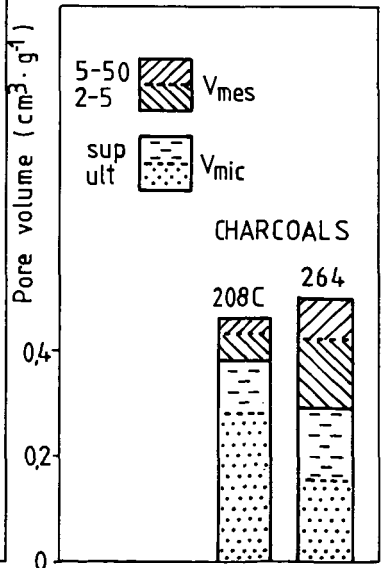


Figure 4. Pore size distribution in charcoals 208C and 264.

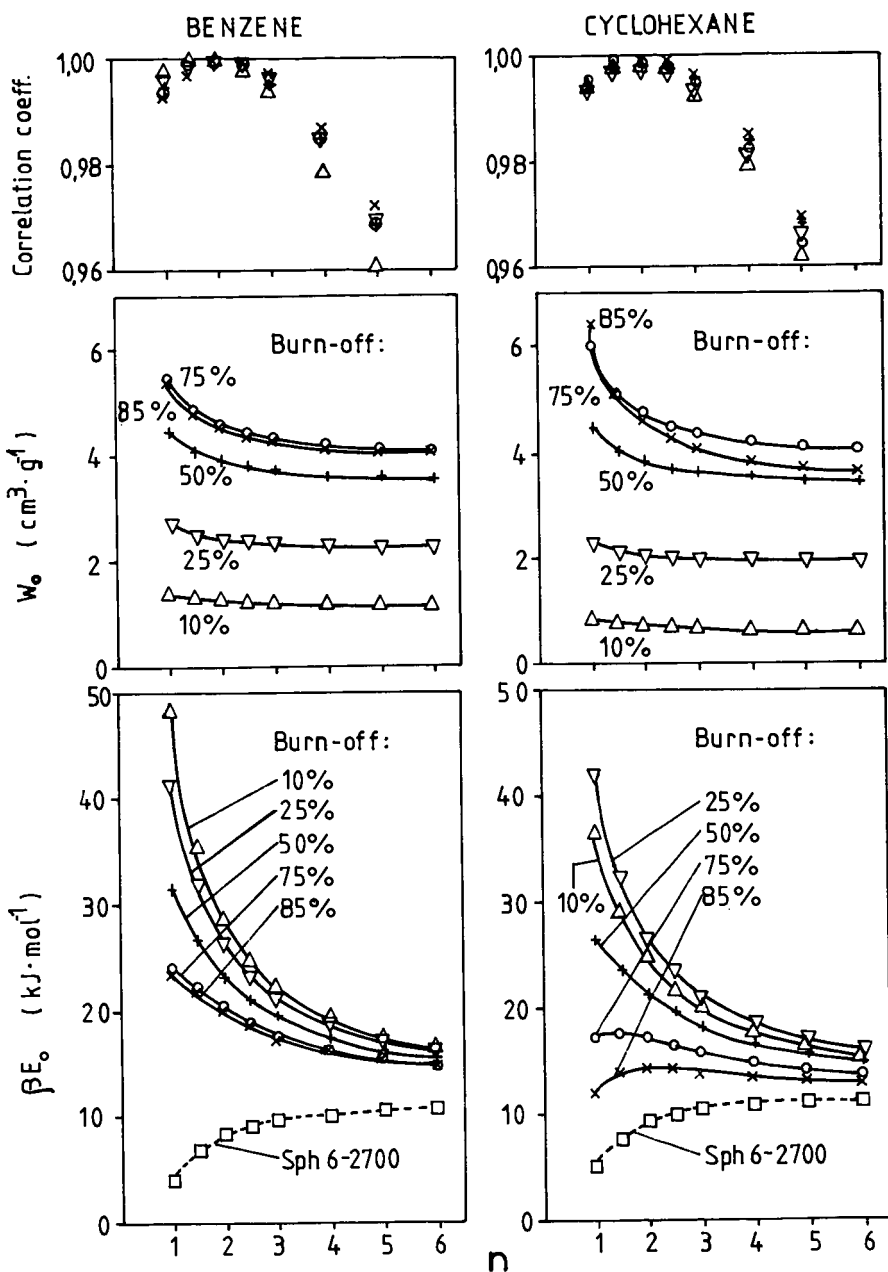


Figure 5. Influence of  $n$  used in calculations on the resulting values of  $W_0$  and  $\beta E_0$  of the DA equation.

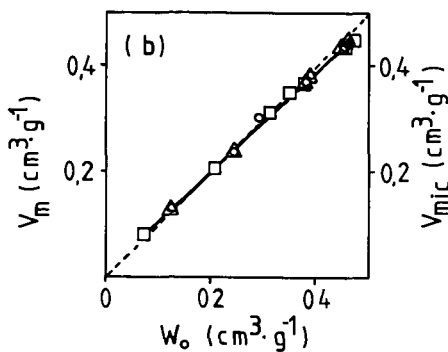
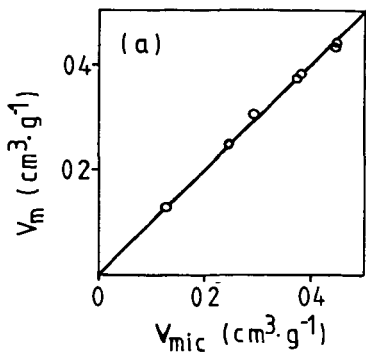


Figure 6. Plots: (a)  $V_m$  vs  $V_{mic}$  ( $\circ$ , benzene); (b)  $V_m$  vs  $W_o$  ( $\circ$ , benzene;  $\square$ , cyclohexane);  $V_{mic}$  vs  $W_o$  ( $\Delta$ , benzene).

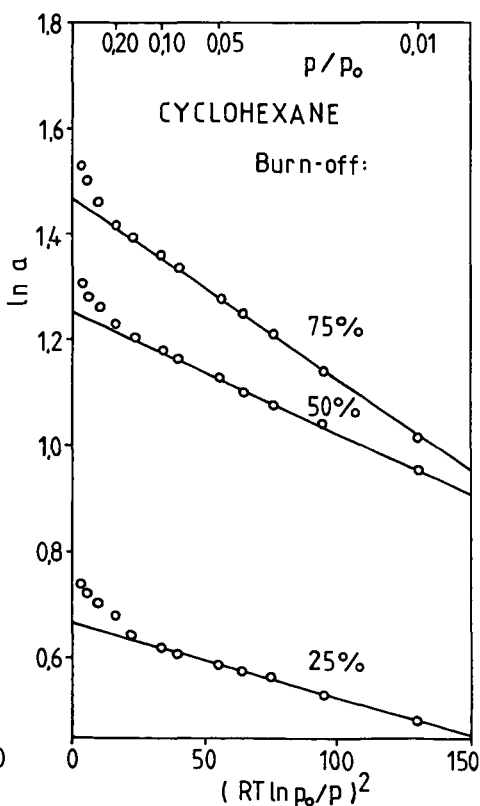
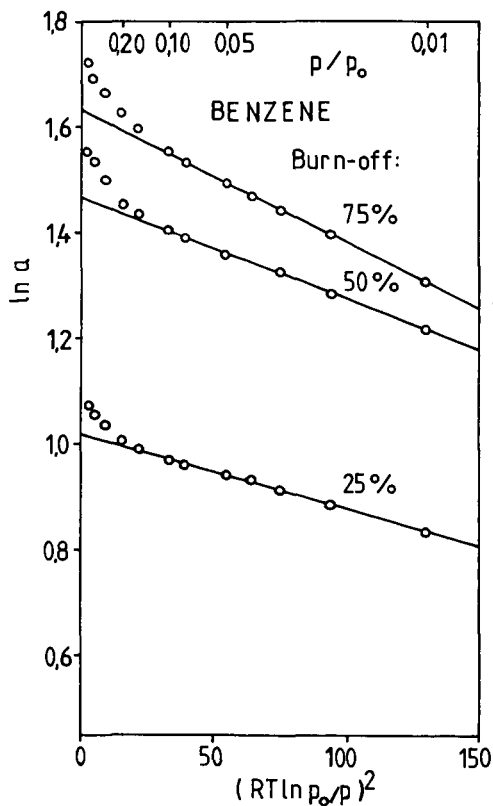


Figure 7. Plots:  $\ln a$  vs  $(RT \ln p_o/p)$  for steam gasified humic acids char HA850;  $a$  in  $\text{mmol}\cdot\text{g}^{-1}$ ,  $RT$  in  $\text{kJ}\cdot\text{mol}^{-1}$ .

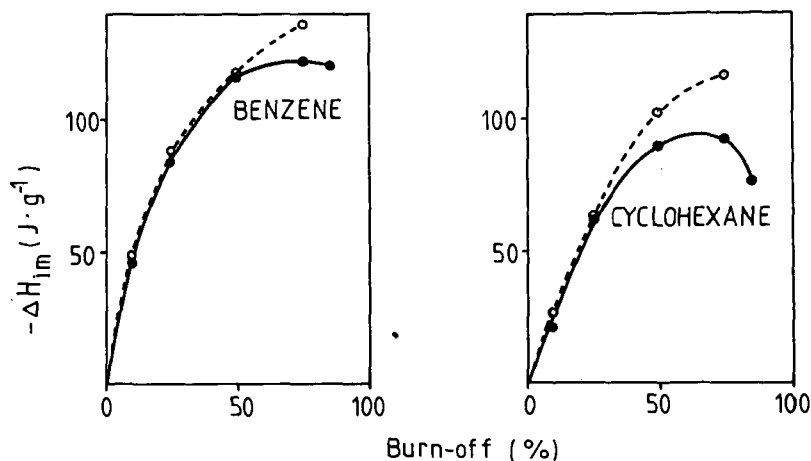


Figure 8. Enthalpies of immersion of steam gasified humic acids char HA 850:  $\circ$  - experimental and  $\bullet$  - calculated from parameters  $\beta E_o$  and  $W_o$  of the DA equation for  $n=2$ .

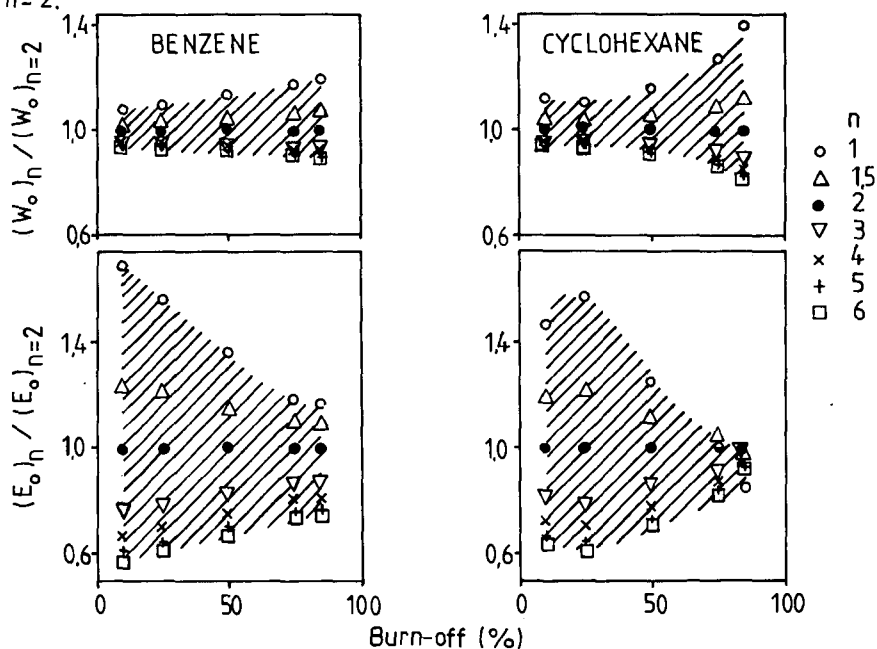


Figure 9. Influence of  $n$  in the DA equation on the ratios  $(W_o)_n / (W_o)_{n=2}$  and  $(E_o)_n / (E_o)_{n=2}$  for steam gasified humic acids char HA 850.

## CHARACTERIZATION OF COAL PARTICLE SURFACES BY FILM FLOTATION

D. W. Fuerstenau, J. Diao and J. S. Hanson  
Dept. of Materials Science and Mineral Engineering  
University of California  
Berkeley, CA 94720

### ABSTRACT

Because of the heterogeneity of coal, particles may vary in composition and, consequently, each particle may have its own unique set of surface properties. The distribution of surface properties of coal particles was determined through film flotation with a series of aqueous methanol solutions. This paper shows how such measurements of the critical wetting surface tension can be used to determine the contact angle ( $\theta$ ) of particles and the distribution of lyophobic sites on the surface of the particles. The mean contact angles calculated from film flotation results for sulfur, graphite and a number of different coals are in reasonable agreement with the values reported in the literature.

### INTRODUCTION

Characterization of coal particles in terms of their wetting properties is important for understanding the behavior of coal in such surface-based processes as flotation, agglomeration, filtration and dust abatement. The wetting properties of solids have commonly been studied by measuring contact angles on a flat surface (1) and determining the critical wetting surface tension from the well-known Zisman plot (2). This method has been very successful for assessing the wettability of homogeneous materials, such as polymers. However, because of the heterogeneity of coal, the results obtained using this approach by different researchers are inconsistent (3,4).

Because of the heterogeneity of coal, the properties of coal particles can range from those of a virtually pure inorganic mineral species to that of an organic material. Consequently, each particle may have its own unique set of surface characteristics. Standard measurements of liquid penetration rates, heat of immersion, immersion times, and freezing-front points can assess only average properties of particulate samples. Recently, a film flotation technique was developed wherein the fraction of particles that sink or float on liquids of different surface tensions can be determined (5,6), and from such determination the distribution of wetting surface tensions (surface energies) can be determined.

In this study, the distribution of the surface properties of coals was determined with 100 x 150  $\mu\text{m}$  particles by film flotation on a series of aqueous methanol solutions (of different compositions). By separating the particles into the lyophobic fraction (those remaining on the surface) and the lyophilic fraction (those imbibed into the solution) at each surface tension, the distribution of coal particles in relation to their wetting surface tension was determined. This paper shows how such information can be used to delineate the surface characteristics of the particles.

### THEORETICAL CONSIDERATIONS

The critical wetting surface tension of a solid is an important parameter that represents the wettability of the solid. It was defined by Zisman as the surface

tension of a liquid which forms a zero contact angle on the solid (2). In our earlier research (7,8), we have verified theoretically and experimentally that for practical film flotation, the critical wetting surface tension of coal particles can be taken to be the surface tension of the liquid at which the particles sink into the liquid and that the effect of particle size and density are negligible.

Since we are familiar with the concept of contact angle and because we cannot measure the contact angle of a small particle directly, it is useful to calculate it. The calculation is possible only when  $\gamma_c$  of the particles can be determined by film flotation. By using the Young equation

$$\gamma_{SV} - \gamma_{SL} = \gamma_{LV} \cos \theta \quad (1)$$

and the Neumann/Good equation of state (9):

$$\gamma_{SL} = \frac{(\sqrt{\gamma_{SV}} - \sqrt{\gamma_{LV}})^2}{1 - 0.15\sqrt{\gamma_{SV}\gamma_{LV}}} \quad (2)$$

we can calculate the contact angle of a particle for a liquid of a given surface tension,  $\gamma_{LV}$ , from the values of  $\gamma_c$  measured in the film flotation experiments. It has been shown that  $\gamma_c$  can be taken as being equivalent to  $\gamma_{SV}$  (9).

Because coal is a mixture of inorganic minerals and organic substances, the surface will appear as a patchwork assembly of carbonaceous material, hydrocarbon, oxygen functional groups and mineral matter. The carbonaceous and hydrocarbon materials contribute to the lyophobic character of coal, whereas the oxygen functional groups and mineral matter contribute to the lyophilic behavior of coal. Therefore, the Cassie-Baxter equation (10) for a composite surface can be used to account for the variation of the contact angle with coal rank (11,12).

To calculate the fraction of lyophobic sites on the surface of coal particles  $\alpha_{HB}$  and the fraction of lyophilic sites  $\alpha_{HL}$ , we assume that i) the lyophobic sites have a contact angle in water  $\theta_{HB} = 105^\circ$  (i.e. paraffin wax) and ii) the lyophilic sites have a contact angle in water  $\theta_{HL} = 0^\circ$ . Thus,

$$\alpha_{HB} + \alpha_{HL} = 1 \quad (3)$$

By using Eq. 3 and the Cassie-Baxter equation for a composite surface, we obtain

$$\cos \theta = \alpha_{HB} \cos \theta_{HB} + \alpha_{HL} \cos \theta_{HL} \quad (4)$$

and can calculate  $\alpha_{HB}$  and  $\alpha_{HL}$  of coal particles from their contact angles in water.

#### MATERIALS AND METHODS

Materials used in this study included a number of U.S. coals, Ceylon graphite (99.0% carbon) and sulfur (Nevada). For all materials 100 x 150  $\mu\text{m}$  particles were prepared by grinding the as-received materials in a small ceramic to avoid iron contamination, followed by sizing with sieves. Paraffin wax-coated coal particles were prepared by a simple vapor deposition procedure (11). Oxidation of the coal was carried out thermally in air for 19 hours at 200°C in a mechanical convection oven.

Film flotation experiments (5,6) were conducted by sprinkling the 100 x 150  $\mu\text{m}$  particles onto the surface of the aqueous methanol solutions, with compositions varying from pure water to pure methanol so that the surface tension could be controlled between 22.4 and 72.8 mN/m. For each solution, the fraction of particles remaining at the liquid/vapor interface was determined. All film flotation experiments were carried out at 20°C.

## RESULTS AND DISCUSSION

Because of the heterogeneity of coal, the wetting properties of coal particles may change continuously from that of lyophobic organic materials to those of the lyophilic inorganic matter. Figure 1 shows the cumulative distribution of Cambria #78 coal particles as a function of their critical wetting surface tension obtained by film flotation using aqueous methanol solutions. From the results in Fig. 1, the frequency distribution of Cambria #78 coal particles was determined as a function of their critical wetting surface tension and are presented in Fig. 2. These two figures clearly show the heterogeneous nature of coal particles.

From such distributions, four wetting parameters have been defined (5,6). The critical wetting surface tension of the most lyophobic particles in the assembly,  $\gamma_c^{\text{min}}$ , is the surface tension of the liquid at which none of the particles remains at the liquid surface. The critical wetting surface tension of the most lyophilic particles in the powder,  $\gamma_c^{\text{max}}$ , is the surface tension of the liquid at which all the particles remains at the liquid surface. The mean critical wetting surface tension of all particles,  $\bar{\gamma}_c$ , can be calculated from the film flotation frequency distribution using the equation:

$$\bar{\gamma}_c = \int \gamma_c f(\gamma_c) d\gamma_c \quad (5)$$

where  $\gamma_c$  is the critical surface tension of particles and  $f(\gamma_c)$  is the frequency distribution function.  $\bar{\gamma}_c$  represents the wettability of the assembly of particles. The standard deviation  $\sigma_{\gamma_c}$  of the frequency distribution function reflects the heterogeneity of the surface. High  $\sigma_{\gamma_c}$  values correspond to heterogeneous materials.

Figure 3 shows the frequency distribution of Cambria #78 coal particles as a function of their contact angle in liquids with surface tension of 60.0 and 72.8 mN/m, respectively. The contact angle of the particle for the given liquid surface tension was calculated from their  $\gamma_c$  using Eqs. 1 and 2. The weight percent of particles in different intervals of the contact angle was taken from the distribution presented in Fig. 2. The figure clearly shows that coal particles in an assembly have a wide range of contact angles and that the lower the surface tension of the liquid the smaller the contact angle of the coal particles. This distribution of contact angles serves to illustrate why the coal particles reside at the liquid/vapor surface in film flotation.

The surface composition of coal particles can be related to their wetting properties by calculating the fraction of lyophobic sites on the surface of the particles from their contact angles in water using Eqs. 3 and 4. The frequency distribution of Cambria #78 coal particles as a function of their percentage of lyophobic sites on the surface of the particles is given in Fig. 4. The weight percent of particles in the different intervals shown in Fig. 4 was again taken from Fig. 2. This figure shows that coal particles are covered by varying amounts of lyophobic materials and gives some insight into the extreme heterogeneity of the coal surface.

Table 1. Wetting parameters of as-received, wax-coated and oxidized Cambria #78 coal obtained from film flotation results.

Treatment	$\bar{\gamma}_c$ , mN/m	$\theta$ , deg.	$\alpha_{HB}$	$\sigma_{\gamma c}$ , mN/m
Wax-coated	25.3	100	0.92	2.60
As-received	43.0	68	0.49	4.53
Oxidized at 200°C for 19 hours	67.0	24	0.07	---

The validity of the film flotation method for characterizing particle surfaces was tested by conducting film flotation tests on wax-coated and oxidized Cambria #78 coal. Figure 5 shows the cumulative distribution of as-received, wax-coated and oxidized Cambria #78 coal particles as a function of their critical wetting surface tension as determined by film flotation. The wetting parameters calculated from the film flotation results are given in Table 1. It can be seen from Fig. 5 and Table 1 that the cumulative distribution of wax-coated coal particles moves to lower wetting surface tensions as compared with that of the as-received coal particles. Also  $\bar{\gamma}_c$  of wax-coated coal particles is less than that of as-received coal particles, and the value of  $\theta$  and  $\alpha_{HB}$  for wax-coated coal particles are higher than that of as-received coal particles. This increase in lyophobicity is due to the presence of additional lyophobic sites on the wax-coated coal. On the other hand, the cumulative distribution curve of oxidized coal particles moves to higher wetting surface tensions and its  $\bar{\gamma}_c$  value is higher than that of as-received coal particles. The value of  $\theta$  and  $\alpha_{HB}$  oxidized coal particles are smaller than that of as-received coal particles, indicating, as expected, that coal particles are more lyophilic when they are oxidized due to the destruction of lyophobic sites by the oxidation process. These findings serve to confirm our film flotation approach.

To further verify our new approach, the mean contact angle of a particle assemblage was compared with the values reported for direct measurements on the flat surface of a bulk sample. Since a flat surface of a bulk sample can be considered to be a composite of small particles with different contact angles, the contact angles

Table 2. The contact angles,  $\theta$ , of sulfur, graphite and coals in water calculated from film flotation results, and measured by captive-bubble (CB) and sessile-drop (SD) methods.

Mineral	Film Flotation $\theta$ , degrees	Contact Angle Measurement		
		$\theta$ , deg.	Method	Ref.
Sulfur	86	87	SD	(13)
Graphite	71	77	CB	(14)
Braztah Coal	87	90	SD	(15)
Somerset Coal	74	56	SD	(15)
Cambria #33 Coal	62	57	CB	(14)
		85	CB	(4)
		91	SD	(4)
Geneva Coal	81	72	SD	(15)
		86	SD	(15)
		64	CB	(14)

obtained from both methods should agree with each other if our approach is correct and if the polishing procedures used in preparing the flat surface do not change its wetting properties significantly. The contact angle of sulfur, graphite and various coals in water calculated from film flotation results are presented in Table 2. This table also shows the contact angle measured by captive-bubble and sessile-drop methods on a flat surface of the same samples in our laboratory. From this table it is seen that the two sets of values are in quite good agreement with each other, especially for the more homogeneous minerals. This further supports the model for the estimation of the contact angle of particles from their critical wetting surface tension.

#### SUMMARY AND CONCLUSIONS

The distribution of the critical wetting surface tension of an assemblage of particles was determined using the film flotation method. A model has been developed to estimate the contact angle of coal particles from the critical wetting surface tension distribution and to estimate the fraction of lyophobic sites on the surface of these particles from this calculated value. The estimated mean contact angle of particles is in good agreement with measured values on flat surfaces. This model provides insight into the heterogeneous nature of coal particles.

#### ACKNOWLEDGEMENTS

The authors wish to acknowledge the U. S. Department of Energy, Pittsburgh Energy Technology Center, Grant No. DE-FG22-86PC90507

#### REFERENCES

1. R. J. Good, Surface and Colloid Science, R. J. Good and R. R. Stromberg, Eds., Plenum Press, New York, 11, 1-30, 1979.
2. W. A. Zisman, Contact Angle, Wettability and Adhesion, ACS, Adv. in Chem. Series, R. F. Gould, Ed., 43, 1-51, 1964.
3. B. K. Parekh and F. F. Aplan, Recent Developments in Separation Science, CRC Press, Florida, 4, 107-113, 1978.
4. G. C. C. Yang, Ph.D. Thesis, University of California, Berkeley, 1983.
5. D. W. Fuerstenau, M. C. Williams and J. Diao, AIME Annual Meeting, New Orleans, March 1986.
6. D. W. Fuerstenau and M. C. Williams, Colloids and Surfaces, 22, 87-91, 1987.
7. J. Diao, MS. Thesis, University of California, Berkeley, 1987.
8. D. W. Fuerstenau, J. L. Diao, K. S. Narayanan and R. H. Urbina, Int. Symp. on Interfacial Phenomena in Biotechnology and Materials Processing, Boston, MA, August 1987, accepted for publication.
9. A. W. Neumann, R. J. Good, C. J. Hope and M. Sejjal, J. Col. Interfac. Sci., 49, 291-304, 1974.
10. A. B. D. Cassie and S. Baxter, Trans. Farad. Soc., 40, 546-551, 1944.
11. J. M. Rosenbaum and D. W. Fuerstenau, Int. J. Minl. Proc., 12, 313-316, 1984.
12. D. V. Keller, Jr., Colloids and Surfaces, 22, 21-35, 1987.
13. D. Olsen, R. Moravec and A. Osteraas, J. Phys. Chem., 7, 4464-4466, 1967.
14. A. S. K. Osoka, Ph.D. Thesis, University of California, Berkeley, 1983.
15. J. M. Rosenbaum, Ph.D. Thesis, University of California, Berkeley, 1981.

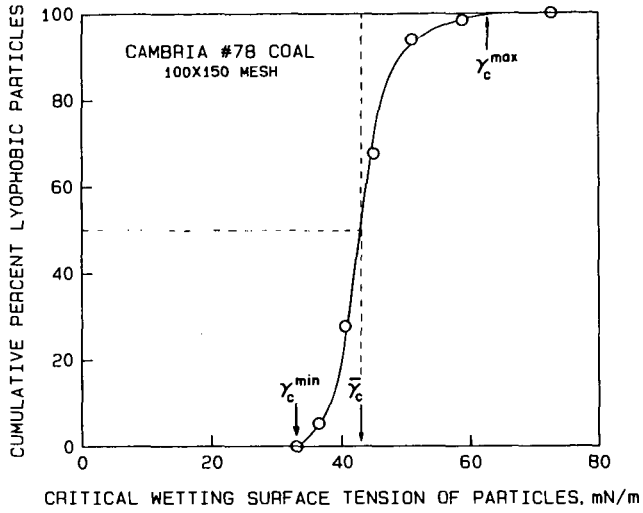


Fig. 1- The cumulative distribution of Cambria #78 coal particles as a function of their critical wetting surface tension obtained from film flotation with aqueous methanol solutions.

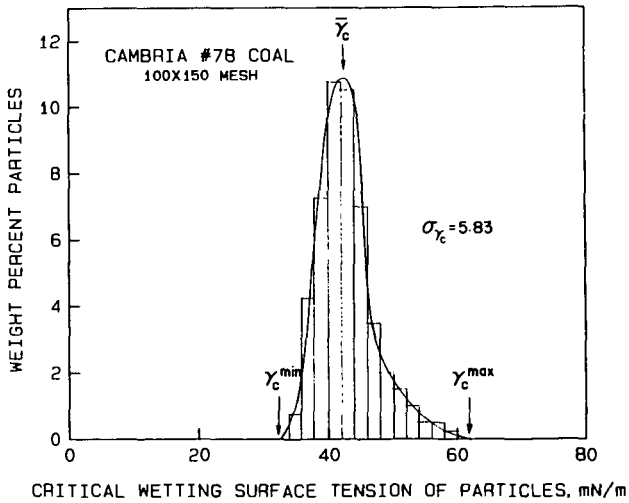


Fig. 2- Frequency distribution of Cambria #78 coal particles as a function of their critical wetting surface tension determined from film flotation with aqueous methanol solutions.

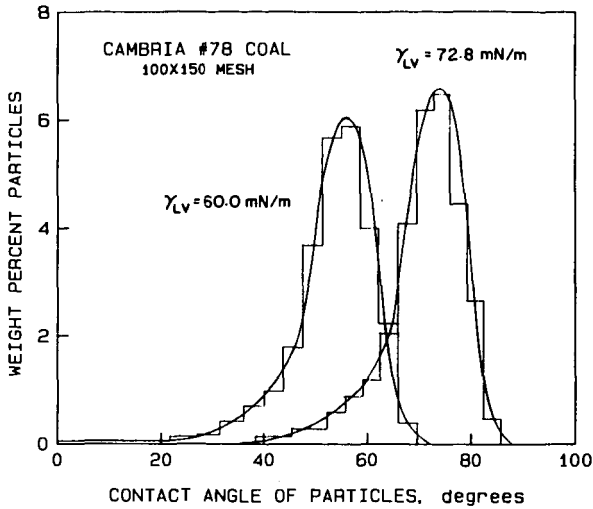


Fig. 3- Frequency distribution of Cambria #78 coal particles as a function of their contact angle in the liquid with surface tension of 60.0 and 72.8 mN/m, respectively.

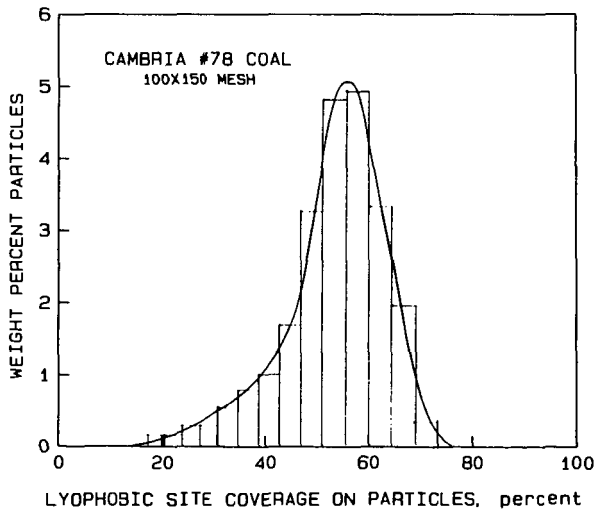


Fig. 4- Frequency distribution of Cambria #78 coal particles as a function of lyophobic sites on the surface of the particles.

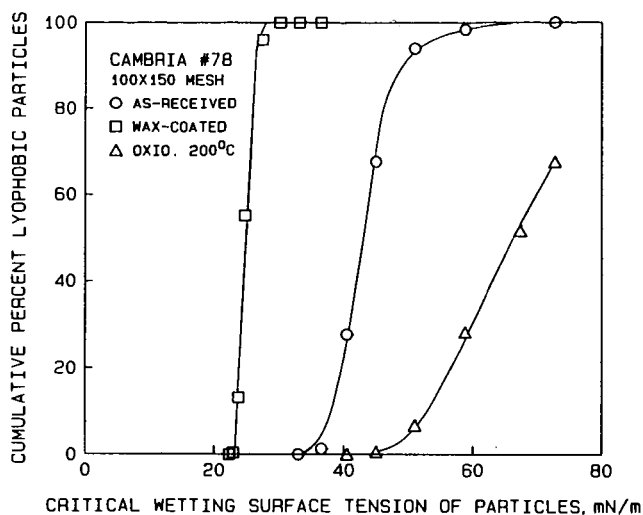


Fig. 5- Cumulative distribution of as-received, wax-coated, and oxidized (200°C, for 19 hours) Cambria #78 coal as a function of their critical wetting surface tension determined from film flotation with aqueous methanol solutions.

Oil Agglomeration of Coal in Salt Solutions:  
Effects of Hydrophobicity and Other Parameters on Coal Recovery

C.-W. Fan, R. Markuszewski, and T. D. Wheelock

Ames Laboratory and Department of Chemical Engineering  
Iowa State University  
Ames, Iowa 50011

Abstract

The recovery of fine coal or graphite particles suspended in water by agglomeration with heptane was observed to be highly dependent on the relative hydrophobicity of the solids as indicated by the measured induction time, i.e., the time required for attachment of one or more particles to a small gas bubble when brought into contact. For highly hydrophobic coal or graphite particles, an increase in ionic strength of the suspending medium caused an increase in agglomeration recovery and a decrease in measured induction time. For weakly hydrophobic coal or pyrite particles, an increase in ionic strength caused a decrease in agglomeration recovery and an increase in induction time. Due to the opposing effects of ionic strength on the recovery of a highly hydrophobic coal and pyrite, it was possible to improve the separation of these materials by an increase in ionic strength. On the other hand, because the recovery of pyrite and a weakly hydrophobic coal were affected similarly by ionic strength, it was not possible to improve the separation of these materials by a similar increase.

Introduction

A number of processes have been proposed for cleaning and recovering ultrafine coal particles suspended in water by selective agglomeration of the carbonaceous solids with oil (1-4). Since most of the ever present mineral impurities are unaffected by oil, an agglomerated suspension can be screened to recover the agglomerates and effect a separation from the unagglomerated mineral particles. The method takes advantage of the difference in surface properties of the organic and inorganic components of coal. Generally the organic material is significantly more hydrophobic than the inorganic minerals found in coal. Therefore, the carbonaceous particles are more readily wetted by oil than the mineral particles, and agglomeration occurs when oil-coated particles become connected by oil bridges. Among the common mineral impurities in coal, only iron pyrite appears to be sufficiently hydrophobic to interfere with separation from coal by this technique. However, the hydrophobicity of pyrite is quite variable and depends on treatment conditions.

It has been recognized that strongly hydrophobic coals respond more readily than weakly hydrophobic coals to this method of treatment (1,5,6). Generally, high recoveries of the more hydrophobic coals can be achieved with relatively small amounts of the lighter, paraffinic hydrocarbons such as heptane, whereas high recoveries of the less hydrophobic coals can only be realized by employing heavier, more complex hydrocarbons in larger amounts. Moreover, for highly hydrophobic coals even less oil is required when the material is suspended in a salt solution (7,8).

An improvement in the separation of coal and pyrite as well as a reduction in oil consumption would improve the economic feasibility of the oil agglomeration method. Minimizing oil consumption by adding salt to the system would reduce one of the major costs of the method. However, preliminary indications suggested that this approach would not work with all types of coal. Therefore, this study was undertaken to determine the effect of coal hydrophobicity on oil agglomeration recovery and to determine how the recovery of different types of coal was affected by salt concentration.

While it was known previously that coal hydrophobicity played an important role in oil agglomeration, it was difficult to measure this role quantitatively. The most popular traditional method for determining wettability by measuring the three-phase contact angle for a water drop on a polished coal surface was difficult to apply in practice. Also it was questionable whether the wettability of a polished surface was the same as that of the small granular particles used in oil agglomeration. In addition, the method was not very sensitive.

Another method of investigating wettability which does not suffer the disadvantages listed above is based on measuring the so-called induction time or, more accurately, the time required for attachment of one or more particles to a small gas bubble when brought into sudden contact under water (9). The measured time is believed to be a combination of the time required to thin the water film between a particle surface and an air bubble to the point of rupture (true induction time) and the time required to displace the film (10,11). Since the attachment time or induction time is based on a dynamic measurement, it depends on the kinetics and hydrodynamics as well as the thermodynamic properties of the system (9-12). Therefore, it differs from the equilibrium contact angle which depends only on the thermodynamic properties of the system. Because of this difference, the induction time depends on certain properties which do not affect the equilibrium contact angle such as particle size and density or the ionic strength of the solution in contact with the particles. Thus, Laskowski and Iskra (12) observed that the induction time of a hydrophobic solid was affected by the concentration of potassium chloride in which the solid was suspended whereas the three-phase contact angle was unaffected. Consequently, certain parameters must be controlled carefully when using induction time measurements to study changes in hydrophobicity.

In the present investigation, the surface of coal and graphite particles was characterized by measuring the induction time, and the response of these materials to agglomeration with heptane was determined by measuring the recovery or mass yield. Different types of coal were utilized which appeared to range from weakly hydrophobic to strongly hydrophobic. In addition, the effect of salt concentration on coal recovery and induction time was determined for a strongly hydrophobic coal (Upper Freeport) and a weakly hydrophobic coal (Illinois No. 6). Also the effect of salt concentration on pyrite recovery and induction time was determined.

#### Materials and Experimental Methods

Samples of coal were obtained from various sources as indicated in Table 1. The Upper Freeport coal is a medium volatile bituminous coal whereas the other coals are high volatile bituminous coals. Relatively pure samples of graphite from Sri Lanka and mineral pyrite from Huanzala, Peru, were obtained through Ward's Natural Science Establishment. These materials were ground in the dry state with a high-speed impact mill and then screened. For the agglomeration experiments the materials were suspended in deionized water having a resistivity of 17.9 megohm-cm and agglomerated with n-heptane from Eastman Kodak Company. The specified normal boiling point of this material was 98°C which indicated a high level of purity.

The agglomeration experiments were carried out with a specially designed closed system so that the operation was conducted without air present (13). The system utilized the motor and agitator from a 14-speed kitchen blender, but the open container furnished with the blender was replaced by a 500-ml glass jar which was nearly square in cross section. A small hole had been drilled in the bottom of the jar which was plugged with a rubber septum. During operation the jar was inverted, and heptane was introduced through the septum with a hypodermic syringe. For each experiment the jar was completely filled with an aqueous suspension containing either 10 g coal or graphite or 3 g pyrite. In some experiments a suspension containing a mixture of coal and pyrite was employed. The suspension at its natural pH was conditioned for 3 min. at high speed (about 18,000 rpm), and then a predetermined amount of heptane was introduced. Agitation was continued at high speed for 3 min.

Table 1. Sources and properties of coal samples

	Upper Freeport	Pittsburgh	Illinois No. 6	Iowa
Source	Indiana County, PA	Belmont County, Ohio	St. Clair County, IL	Monroe County, IA
Mean diameter <sup>a</sup> , $\mu\text{m}$	34	39	43	42
Total sulfur, %	2.10	4.03	2.62	3.06
Proximate analysis, %				
Fixed carbon	62.4	48.2	46.5	45.0
Volatile matter	26.8	40.6	34.5	39.1
Ash	10.4	9.8	9.7	12.4
Moisture	0.4	1.4	9.3	3.5
Total	100.0	100.0	100.0	100.0

<sup>a</sup>Mean diameter of particles used for oil agglomeration.

to produce agglomerates. The agglomerates were recovered on a 100-mesh screen (U.S. Standard), dried in an oven at 100–110°C, and weighed. When a mixture of coal and pyrite was treated, the total sulfur and ash contents of the product were determined and sulfur and ash balances were used to calculate the recovery of the coal and pyrite, respectively.

The so-called induction time of the various materials was measured with the apparatus manufactured by Virginia Coal and Mineral Services, Inc., using the procedure described previously (9–11). For this measurement, -100/+140 mesh coal or graphite particles and -200/+325 mesh pyrite particles were employed. The particles were spread in a thin layer under water and a 2-mm diameter air bubble was formed on the end of a capillary just above the layer of particles. The initial gap between the captive bubble and the surface of the particles was set at approximately 0.1 mm. The bubble was subsequently brought into contact with the particles for successively longer contact times, and the number of particles which adhered to the bubble was noted. The induction time was taken to be the contact time which resulted in particle attachment in five out of ten trials.

### Results and Discussion

Graphite and the four coals listed in Table 1 were found to encompass a wide range of hydrophobicity as indicated by the measured induction time. As the results in Table 2 indicate, the induction time ranged from 0.31 ms for graphite (a highly hydrophobic material) to 5.4 ms for Illinois No. 6 coal (a weakly hydrophobic material). For this series of measurements, the particle size was controlled by screening the materials and using only the particles between 100 and 140 mesh. It was necessary to use somewhat larger particles than were used for agglomeration (-200/+400 mesh) to avoid disturbing the bed of particles in the measuring cell when the particles were contacted with a gas bubble. The induction time of the particles used for agglomeration would have been smaller than that of the particles used for determining induction time since the results of Ye et al. (11) indicated that induction time is proportional to particle size raised to a power which depends on particle density. For coal particles of similar density (1.3 to 1.4 g/cm<sup>3</sup>) the dependency of induction time on particle size was second order, whereas for molybdenite particles (density = 4.7 g/cm<sup>3</sup>) the dependency was third order. In the

Table 2. Induction time and agglomeration recovery of various carbonaceous materials with heptane

Material	Induction time, ms	Agglomeration recovery, %	
		5 v/w % C <sub>7</sub> H <sub>16</sub>	10 v/w % C <sub>7</sub> H <sub>16</sub>
Graphite	0.31	94	100
Upper Freeport coal	1.96	32	76
Pittsburgh coal	2.25	29	70
Iowa Coal	4.85	6	21
Illinois No. 6 coal	5.40	4	17

present study the induction times of the different coals used for agglomeration should have been approximately 10% of the values listed in Table 2 because of the smaller particle size, and the induction time of graphite even less. The effect of particle size should have been more pronounced for graphite due to its greater density (2.2 g/cm<sup>3</sup>). Even so, the relative relationship between the induction times of the materials which were agglomerated should have been about as indicated in Table 2.

When the different carbonaceous materials were agglomerated separately with heptane, the recovery decreased monotonically as the induction time of the material increased or, in other words, as the hydrophobicity of the material decreased (see Table 2). This was the case with either 5 or 10 v/w % heptane (i.e., with either 0.5 or 1.0 ml heptane/10 g solids). Thus, there appeared to be a good correlation between recovery and induction time.

The relationship between agglomeration recovery and induction time was explored further by conducting a series of experiments in which different carbonaceous materials were suspended individually in salt solutions and agglomerated with heptane. The results achieved with different salt concentrations are presented in Figures 1 and 2 for Upper Freeport coal and Illinois No. 6 coal, respectively. In the case of the highly hydrophobic Upper Freeport coal, the recovery increased markedly as the salt concentration was raised to 1.5 M, but then it increased only slightly as the salt concentration was raised further to 3.0 M. At this salt concentration, a recovery of 77% was achieved with only 3 v/w % heptane. To obtain a comparable recovery of Illinois No. 6 coal required using 40 v/w % heptane or more. For this weakly hydrophobic coal, the highest recovery was realized when the material was suspended in deionized water, and the recovery decreased when the material was suspended in a salt solution. Moreover the recovery decreased as the salt concentration was increased, and an increase in salt concentration from 0 to 1.5 M produced a greater change in recovery than a further increase from 1.5 to 3.0 M.

The effect of increasing salt concentration on induction time was to reduce the induction time of the highly hydrophobic Upper Freeport coal and increase the induction time of the weakly hydrophobic Illinois No. 6 coal (see Figures 1 and 2). Consequently, the resulting induction time curves were almost mirror images of the recovery curves for the corresponding coals; thus again there seemed to be a close correspondence between recovery and induction time.

The recovery curves and induction time curves for Pittsburgh coal and graphite, while not presented here, were generally similar to those noted above for Upper Freeport coal. Therefore the recovery and induction time of all of these highly hydrophobic materials were affected in the same way by salt concentration. For such materials it appears that the underlying effect of increasing salt concentration or ionic strength of the suspending medium is to compress the electrical double layer surrounding the individual particles (7,8). This in turn destabilizes the water film in contact with the solid according to Laskowski and Iskra (12). Consequently the water film is more easily ruptured between colliding particles and oil droplets or between oil-coated particles. In a similar way the induction time is reduced because the water film between any given particle in contact with a gas bubble also is more easily ruptured.

A different mechanism is required to explain the behavior of Illinois No. 6 coal since an increase in salt concentration produced results which were opposite to those produced in the case of the more hydrophobic coals. One plausible explanation is that the Illinois No. 6 coal adsorbed hydrated sodium ions from the salt solution which made the coal particles more hydrophilic. This would increase the induction time and reduce the agglomeration recovery. Adsorption of sodium ions could likely be due to the presence of oxygen functional groups on the surface of the coal. It is well known that Illinois No. 6 coal has a higher oxygen content than the more hydrophobic coals. Therefore, it would have a greater affinity to adsorb sodium ions.

Pyrite is also known to adsorb sodium ions, with the quantity adsorbed being proportional to the concentration in solution (14). As in the case of Illinois No. 6 coal, this could explain why the pyrite induction time increased and agglomeration recovery decreased when the salt concentration was increased (see Figure 3). Although the curves for pyrite in Figure 3 appeared similar to those for Illinois No. 6 coal in Figure 2, the pyrite was less hydrophobic than the coal. Since pyrite is much denser than coal, smaller particles had to be used for measuring induction time. Because of differences in density and particle size, the induction time of pyrite is therefore not directly comparable with that of the carbonaceous materials. However, the induction time for pyrite was relatively high. Also the agglomeration recovery of pyrite was relatively low, even when 50 v/w % heptane was used.

The opposing influences of salt concentration on the agglomeration recovery of pyrite and Upper Freeport coal suggested a series of experiments in which a mixture of these materials was agglomerated with heptane. The results which were presented in an earlier publication (8) show that coal recovery increased and pyrite recovery decreased as the salt concentration was raised (see Figure 4). Thus the results achieved with the mixture corresponded well with the results of agglomerating the materials separately. Also shown in Figure 4 is the separation efficiency as defined below:

$$\text{Sepn. Eff. (\%)} = \text{Coal Recov. (\%)} - \text{Pyrite Recov. (\%)}$$

It can be seen that the separation efficiency increased with salt concentration until the concentration reached 1.5 M and then remained constant. When a similar set of agglomeration experiments was conducted with a mixture of Illinois No. 6 coal and pyrite, the results were surprising in that the recovery of pyrite was greater than the recovery of coal (see Table 3). On the other hand, when salt was added to the system, the recovery of both materials decreased as expected and the separation suffered.

### Conclusions

When aqueous particle suspensions of graphite or various types of coal were agglomerated individually with heptane, the recovery correlated well with the measured induction time which seemed to reflect the natural hydrophobicity of the

Table 3. Results of agglomerating a mixture of Illinois No. 6 coal (5 g) and pyrite (5 g) with heptane

Heptane ml	NaCl M	Final pH	Recovery, %		Separation Eff., %
			Coal	Pyrite	
0.5	0	4.3	15	47	-32
1.0	0	4.3	27	73	-46
2.0	0	4.2	37	87	-50
0.5	1.5	4.1	12	28	-16
1.0	1.5	4.1	19	40	-21
2.0	1.5	4.0	23	43	-20

material. A close correspondence between agglomeration recovery and induction time was also observed in other experiments in which the carbonaceous materials or pyrite were suspended separately in salt solutions of various concentrations. In these experiments, increasing salt concentrations enhanced the recovery and shortened the induction time of highly hydrophobic solids but reduced the recovery and lengthened the induction time of weakly hydrophobic solids. The effect of salt concentration on the highly hydrophobic solids appeared to be due to compression of the electrical double layer surrounding individual particles, whereas the effect on weakly hydrophobic particles seemed to be due to adsorption of hydrated cations. Because of these differing effects, it was possible to improve the separation of highly hydrophobic Upper Freeport coal and pyrite by increasing the salt concentration of the agglomeration system, but it was not possible to improve the separation of weakly hydrophobic Illinois No. 6 coal and pyrite.

#### Acknowledgement

Ames Laboratory is operated for the U.S. Department of Energy by Iowa State University under contract No. W-7405-Eng-82. This work was supported by the Assistant Secretary for Fossil Energy, through the Pittsburgh Energy Technology Center.

#### Literature Cited

1. C. E. Capes and J. R. Germain, "Selective Oil Agglomeration in Fine Coal Beneficiation," Chapter 6 in: Physical Cleaning of Coal, Y. A. Liu (ed.), Marcel Dekker, New York, 1982.
2. V. P. Mehrotra, K. V. S. Sastry and B. W. Morey, "Review of Oil Agglomeration Techniques for Processing of Fine Coals," International Journal of Mineral Processing, 11, 175-201 (1983).
3. T. D. Wheelock and R. Markuszewski, "Coal Preparation and Cleaning," Chapter 3 in: The Science and Technology of Coal and Coal Utilization, B. R. Cooper and W. A. Ellingson (eds.), Plenum Press, New York, 1984.
4. W. G. Steedman and S. V. Krishnan, "Oil Agglomeration Process for the Treatment of Fine Coal," Chapter 8 in: Fine Coal Processing, S. K. Mishra and R. R. Klimpel (eds.), Noyes Publications, Park Ridge, New Jersey, 1987.
5. R. Venkatadri, R. Markuszewski, and T. D. Wheelock, "Oil Agglomeration of Weakly Hydrophobic Coals and Coal/Pyrite Mixtures," Energy & Fuels, 2 (2), 145-150 (1988).

6. Z. Sadowski, R. Venkatadri, J. M. Druding, R. Markuszewski, and T. D. Wheelock, "Behavior of Oxidized Coal during Oil Agglomeration," Coal Preparation (in press).
7. G. C. C. Yang, R. Markuszewski and T. D. Wheelock, "Oil Agglomeration of Coal in Inorganic Salt Solutions," Coal Preparation, 5 (3-4), 133-146 (1988).
8. C.-W. Fan, R. Markuszewski, and T. D. Wheelock, "Coal and Pyrite Separation by Oil Agglomeration in Salt Solutions," Fizykochemiczne Problemy Mineralurgii, 19, 17-26 (1987).
9. J. L. Yordan and R. H. Yoon, "Induction Time Measurements for the Quartz-Amine Flotation System," Preprint No. 86-105 for Society of Mining Engineering Annual Meeting, New Orleans, March 2-6, 1986.
10. Y. Ye and J. D. Miller, "Bubble/Particle Contact Time in the Analysis of Coal Flotation," Coal Preparation, 5, 147-166 (1988).
11. Y. Ye, S. M. Khandrika and J. D. Miller, "Induction-Time Measurements at a Particle Bed," presented at 117th AIME Annual Meeting, Phoenix, Arizona, Jan. 25-28, 1988.
12. J. Laskowski and J. Iskra, "Role of Capillary Effects in Bubble-Particle Collision in Flotation," Transactions Institution Mining and Metallurgy, Sec. C Mineral Processing and Extractive Metallurgy, 79, C6-C10 (1970).
13. J. Drzymala, R. Markuszewski and T. D. Wheelock, "Influence of Air on Oil Agglomeration of Carbonaceous Solids in Aqueous Suspension," International Journal of Mineral Processing, 18, 227-286 (1986).
14. A. M. Gaudin and W. D. Charles, "Adsorption of Calcium and Sodium on Pyrite," Transactions of AIME, 196, 195-200 (1953).

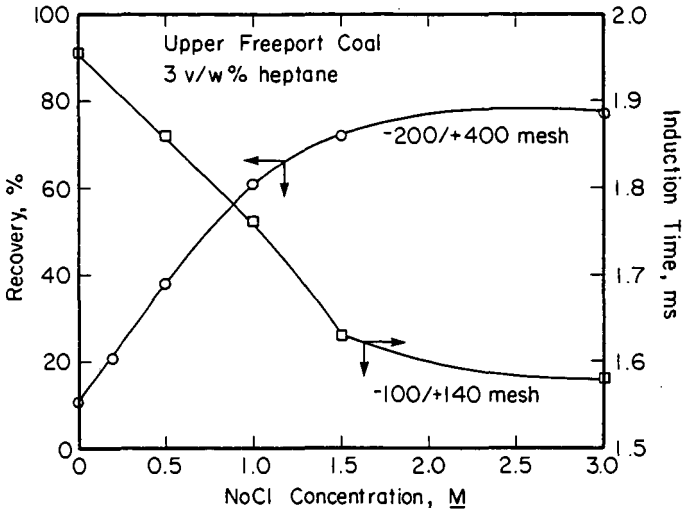


Figure 1. Effect of salt concentration on Upper Freeport coal recovery and induction time.

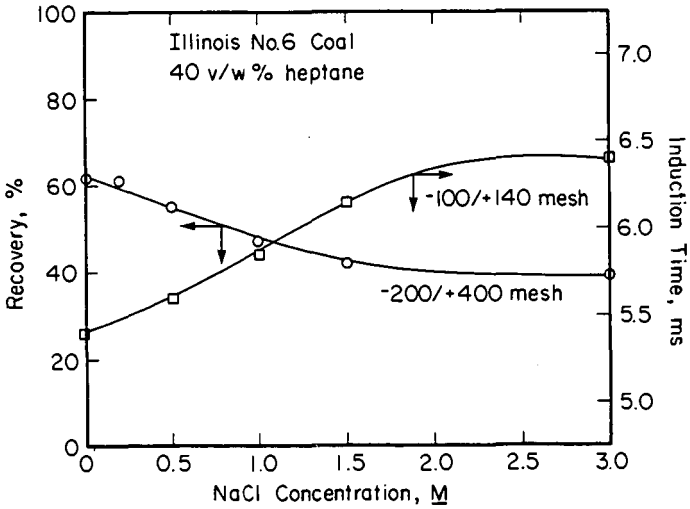


Figure 2. Effect of salt concentration on Illinois No. 6 coal recovery and induction time.

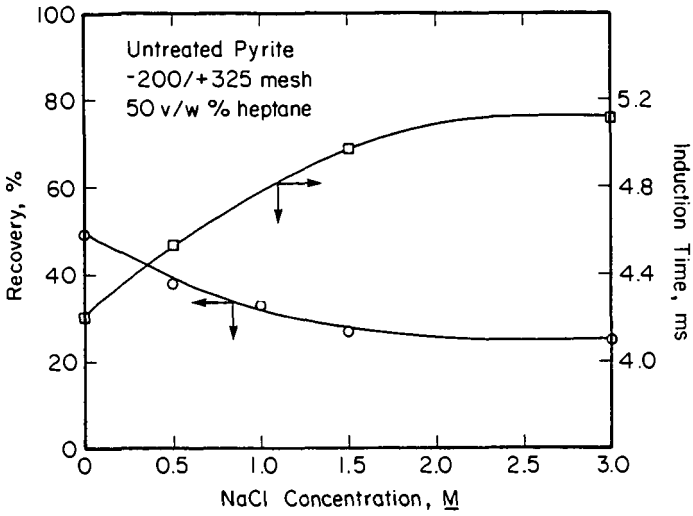


Figure 3. Effect of salt concentration on mineral pyrite recovery and induction time.

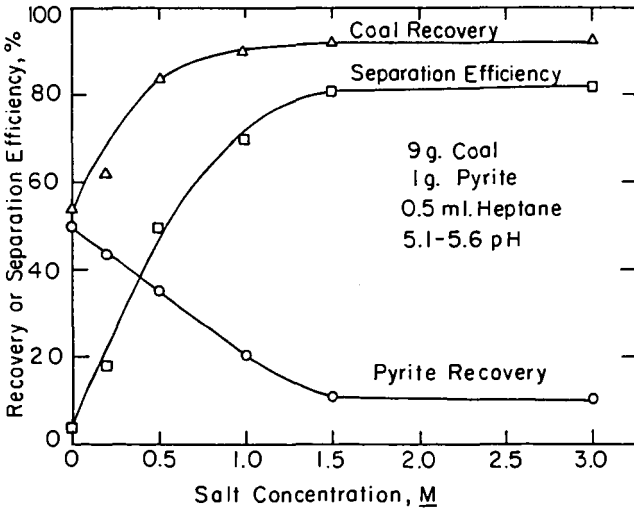


Figure 4. Results of agglomerating a mixture of Upper Freeport coal and pyrite (Ref. 8).

## Surface Properties of Coal-Oil Agglomerates in the Floc Regime

K. Darcovich, C.E. Capes\* and F.D.F. Talbot

*Department of Chemical Engineering, University of Ottawa,  
Ottawa, Ontario, Canada, K1N 9B4*

*\* National Research Council of Canada,  
Division of Chemistry, Chemical Engineering Section,  
Ottawa, Ontario, Canada, K1A 0R6*

### 1 Introduction

Agglomeration processes bring together fine powders into larger masses in order to improve powder properties. In conventional coal mining procedure, much of the fine coal (typically -100 mesh) is rejected with tailings as it is impractical to recover. Due to the heterogeneous nature of coal, smaller particles tend to be individually richer in ash or carbonaceous matter compared to the overall composition of the coal. This discretization facilitates effective separation. The tailings are handled in water slurry form and in an agglomeration/separation treatment, an immiscible oil phase (usually any liquid hydrocarbon of size  $C_7$  or greater) is added under high-shear mixing conditions to enhance surface wetting. The oil selectively adheres to the carbonaceous surfaces and also acts as a bridging liquid to consolidate several oiled coal particles into an enlarged agglomerate. The ash is excluded and is separated via screening or by selective bubble flotation. [1,2,3] Yield-ash results are shown for the agglomeration flotation of a Pennsylvania coal in Figure 1. [4] The results compare well with other recovery methods.

The agglomerate flotation technique has been known since the turn of the century [5], but to date, there is a considerable gap in understanding of the fundamentals involved. Since the coal-oil agglomerates in this context are a product of an upstream formation process, the material properties of the system are more or less fixed, and work has shown that such properties are favourable for flotation. [6] Flotation performance depends on both hydrodynamic and surface chemical interactions. [7,8]

Thus, it is the objective of this study to investigate the surface properties of a coal-oil agglomerate system to provide a database for subsequent work on their flotation properties.

## 2 Experimental

The coal selected for this work was a high-grade metallurgical coal provided by the Cape Breton Development Corporation. It contains 2.18% ash by weight (proximate analysis), and hence can be used as is to study its agglomeration properties.

### 2.1 Agglomerate Preparation

Prior to making any surface property measurements, the procedure for agglomerate preparation had to be established.

Agglomerates were prepared at a 10% pulp density. The coal (density = 1.3 g/cm) was mixed with distilled water and stirred under vacuum in a baffled flask for about 90 minutes to remove complications arising from the presence of air in the system. [9] After de-airing, a required volume of hexadecane was added and the mixing continued for a further thirty minutes to form the agglomerates. Agglomerates were prepared at hexadecane levels ranging from (based on weight percent of coal) 0.25% to 10.0%.

### 2.2 Surface Tension Measurements

The surface properties of the agglomerates were determined by the adhesion technique. [10,11]

Briefly, this technique involves measuring the extent of particle adhesion to various solid substrates as a function of the composition (surface tension) of the suspending liquid. A water-methanol system was used, since hexadecane is immiscible across their entire binary composition range. [12] Thus the agglomerate structure is not interfered with. Surface tensions of binary water-methanol mixtures span possible coal and/or oil surface tensions. For cases where the surface tension of the suspending liquid differs from the particle surface tension, adhesion should be a function of the substrate surface tension,  $\gamma_{SV}$ . For the case where  $\gamma_{LV} = \gamma_{PV}$  the change in free energy due to particle adhesion is zero. Thus the  $\gamma_{LV}$  where the adhesion is not a function of  $\gamma_{SV}$  will be equal to  $\gamma_{PV}$ .

The adhesion method surface tension measurements were carried out as described in detail by Absolom *et al.* [10,11]

Four different polymer film substrates were used to span the possible surface tensions of the coal-oil system. These polymers were polystyrene, sulfonated polystyrene, polyethylene and polyethyleneterephthalate. The adhering agglomerates on these films were then recorded on video tape through a stereo microscope. Using image analysis, the area percent adhesion was determined. Each experiment was duplicated.

### 2.3 Particle-size distribution Measurements

The particle-size distributions for the agglomerates were obtained using a Malvern model 2600 laser diffraction particle-size analyser. This instrument measures the largest dimension of the particles as they are instantaneously positioned in the laser path, and determines an average over at least 500 pulses. Several measurements were made at each oil level.

Additionally, the particle-size distributions of agglomerates were determined suspended in a mixture of 95% CH<sub>2</sub>OH and 5% H<sub>2</sub>O, at several oil levels to verify that the methanol in the suspending liquid did not influence the particle-size distributions.

## 3 Results

Results were obtained for the surface tension of the agglomerate particles and the particle-size distributions at several oil levels.

### 3.1 Surface Tension Results

The adhesion method was employed to determine the surface tension of hexadecane-coal agglomerates at several oil levels. The procedure outlined in [10] was used to determine  $\gamma_{PV}$  at each oil level. Figure 2 shows the agglomerate surface tensions versus oil level. The surface tension of the unoiled coal was 62.0 dyne/cm, in agreement with other published results for bituminous coal. [10,13,14] At 10 weight% oil, the agglomerate surface tension closely approximates that of pure hexadecane.

### 3.2 Particle-Size Distribution Results

Figure 3 shows the agglomerate particle-size distributions for each measured oil level. The mean particle-size of the unagglomerated coal is 33  $\mu\text{m}$ . As one would expect, the mean size increases as more oil is added to the system.

## 4 Discussion

In light of the dependence of the surface tension and the mean size of the agglomerates on oil level, the corresponding three-phase contact angles and bond volumes were evaluated.

### 4.1 Determination of the Three-Phase Contact Angle

Measured and tabulated surface tension values were used along with an equation of state approach to determine the three-phase contact angle. The addition of

adsorbing oil was not considered to have caused a step change in the agglomerate surface properties at low oil levels since problems such as incomplete wetting and surface roughness [15] will contribute some coal character to the surface.

Neumann *et al.* [16,17,18] have developed an equation of state relating an interfacial tension to two known surface tensions. This is coupled with Young's Equation to determine the system.

Neumann's surface tension equation of state is,

$$\gamma_{SL} = \frac{(\sqrt{\gamma_{SV}} - \sqrt{\gamma_{LV}})^2}{1 - 0.15\sqrt{\gamma_{SV}\gamma_{LV}}} \quad (1)$$

and Young's equation,

$$\gamma_{SV} - \gamma_{SL} = \gamma_{LV} \cos \theta \quad (2)$$

Equation 1 gives interfacial tensions for the coal, oil and water system at each agglomerate oil level. Now using equation 2, the three-phase contact angle can be calculated. In Figure 4, the three-phase contact angle is plotted against the agglomerate oil level.

## 4.2 Calculation of Bond Volumes

It has been shown that bonding structure of agglomerates is determined by the volume ratio of binding liquid to solid present in the system. At the binder levels considered in this work, the bonding should be exclusively pendular. [19,20] Pendular bonds are discrete lens-shaped rings at the point of contact of two particles. With different three-phase contact angles at the different oil levels, the oil bond profile will vary. If the effect of gravity is neglected, the binder-liquid interface will assume a profile of constant curvature and thus can be represented by an arc of a circle of radius  $b$ . (Figure 4, inset)

The meridian angle,  $\theta_m$  can have a maximum size of  $45^\circ$  in the pendular regime, or else neighbouring bonds will coalesce. Now assume the particle has a unit radius, defined by the equation  $x^2 + (y - 1)^2 = 1$ . With  $\theta_m$  equal to  $45^\circ$ , the three-phase junction will occur at the point  $x = 1/\sqrt{2}$ ,  $y = 1 - 1/\sqrt{2}$ .

The meniscus surface can be defined by an arc of a circle defined as,

$$(x - a)^2 + y^2 = b^2 \quad (3)$$

Equation 3 along with the particle profile and  $\theta_c$  determine the parameters  $a$  and  $b$ . Thus for a given contact angle, the meniscus profile is defined.

The absolute bond volume,  $V_{BA}$ , can be then taken as a volume of revolution of the meniscus area. Let the meniscus surface be  $\mathcal{F}_2(y)$  and the particle surface be  $\mathcal{F}_1(y)$ .  $y_c$  is the three-phase contact point  $y$ -coordinate.

$$V_{BA} = 2\pi \int_0^{y_c} |\mathcal{F}_2(y)|^2 dy - 2\pi \int_0^{y_c} |\mathcal{F}_1(y)|^2 dy \quad (4)$$

Equation 4 was integrated numerically with a 15-point Gaussian quadrature routine. The bond volume as a function of contact angle is plotted in Figure 4. Newitt and Conway-Jones [20] define the bond volume as a function of meridian angle  $\theta$  as,

$$V_{BA} = 2\pi r^2 (\sec \theta - 1)^2 \left[ 1 - \left( \frac{\pi}{2} - \theta \right) \tan \theta \right] \quad (5)$$

The  $V_{BA}$  calculated for  $\theta_C = 0^\circ$  is exactly the same result as predicted by equation 5. Define  $V_{OB}$  as the ratio of  $V_{BA}$  to the volume of two particles.

### 4.3 Interdependence of the Surface Tension, Oil Level and Enlargement Factor

An informative way of expressing agglomeration data is with an enlargement factor,  $F$ .  $F$  can be defined as,

$$F = \frac{d_p}{d_{p_0}} \quad (6)$$

where  $d_p$  is a mean agglomerate diameter at a given oil level and  $d_{p_0}$  is the mean diameter of the unagglomerated coal.

Figure 5 shows  $F$  plotted against oil level.

Assume that at low oil levels, only single particles and doublets will contribute to the resulting enlargement factor. Now say that there are  $n$  particles and one of them is double size (an agglomeratè). Thus,

$$F - 1 = \frac{1}{n} \quad \text{or,} \quad n = \frac{1}{F - 1} \quad (7)$$

One bond will exist for every  $n + 1$  individual particles, so the fraction of the total solid volume that is bonded in doublets,  $V_{SB}$ , is,

$$V_{SB} = \frac{2}{n + 1} \quad (8)$$

Thus the bonding volume of oil,  $V_{OB}$ , relative to the volume of the two bonded particles is,

$$V_{OB} = \frac{V_O (n + 1)}{2} \quad (9)$$

where  $V_O$  is the total volume of oil expressed as a fraction of the total solids volume. However, for a given volume of solids, the oil will first be consumed in wetting the solid surface, then any excess will be used up in forming bonds. The total oil volume,  $V_O$ , will be composed of two parts, a bonding volume,  $V_B$ , and a wetting volume  $V_W$ . Thus,  $V_B$  is substituted for  $V_O$  in equation 9 to account for the wetting volume.

It is of interest to determine how the oil distributes itself to bring about the observed agglomeration results.

Recall equation 9. Since  $1/n = F - 1$ , it may be re-expressed as,

$$V_{OB} = \frac{V_B F}{2(F-1)} \quad (10)$$

Assume that at low oil levels only pendular bonds will exist. Thus the volume of one bond  $V_{OB}$ , is known and can be used to calculate  $V_B$  and  $V_W$ . Assuming  $V_W$  is constant for all oil levels, equation 10 may be used to determine the bond volume per particle pair.

Denote  $V_{OB}$  from equation 10 as real volume  $V_R$ , and  $V_T$  as the theoretical volume. The ratio  $V_R/V_T$  will give a mean value of bonds per particle. If  $V_R/V_T > 1$ , then this implies that agglomerates larger than doublets exist. Figure 5 shows this ratio plotted versus oil level. One may note the similarity between Figures 5 and 2. At an oil level of about 1 to 2 weight%, the slopes on these plots significantly change. The underlying reason for this change should be a fundamental change in the agglomerate structure. Based on the size data and the surface approximating that of hexadecane, it appears that beyond 2 weight% oil, larger, more compact agglomerates are formed.

A number of factors constrain the system. The result must conform to a mass balance of solids, an oil balance, and a weighted sum of various agglomerate sizes that accounts for the observed size. A system of three linear equations may be written which determine the distribution of singlets, doublets and triplets at each oil level based on the above criteria. They may be expressed as follows,

$$\begin{aligned} a_{11}q_1 + a_{12}q_2 + a_{13}q_3 &= F \\ a_{21}q_1 + a_{22}q_2 + a_{23}q_3 &= 1 \\ a_{31}q_1 + a_{32}q_2 + a_{33}q_3 &= V_B \end{aligned} \quad (11)$$

where the  $q_i$ 's are the fraction of singlets, doublets and triplets, the  $a_{1i}$ 's are the mean size of each type of agglomerate, the  $a_{2i}$ 's are all equal to 1 by mass balance and the  $a_{3i}$ 's are the bond volumes per agglomerate based on the oil level.

This system of equations was solved and it gave positive element solution vectors up to 2 weight% oil. At that point, the number of doublets predicted was negative (physically impossible) thereby indicating agglomerates larger than doublets are present which require substantially more oil due to the increased number of bonds per agglomerate.

The system was remodeled to include four-particle agglomerates that were considered to be in tetrahedral form having six bonds. This required an additional linear equation, and one was formulated based on the strength of the agglomerates. Consider each agglomerate in terms of the probability that it will break up,  $P_b$ . In general  $P_b$  should be proportional to the inverse of the number of bonds present. That is,

$$P_b \propto \frac{1}{nb}$$

where  $n$  is the number of bonds in the agglomerate and  $b$  is the bond strength. The probability of break-up of the singlet may be expressed as  $k_0 b$ , where  $k_0$  is some unknown constant. Thus for singlets through quadruples we have,

$$P_b = k_0 q_1 b + \frac{q_2}{b} + \frac{q_3}{3b} + \frac{q_4}{6b} \quad (12)$$

The strongest system, or minimum probability of break-up will occur when,

$$\frac{\partial P_b}{\partial b} = k_0 q_1 - \frac{q_2}{b^2} - \frac{q_3}{3b^2} - \frac{q_4}{6b^2} = 0 \quad (13)$$

Rewriting equation 13 we obtain,

$$k_0 b^2 q_1 - q_2 - \frac{q_3}{3} - \frac{q_4}{6} = 0 \quad (14)$$

In this form, the coefficient  $a_{41}$  of the new  $4 \times 4$  matrix is indeterminate. However, in view of the agglomerate data, it can be assumed that at 1 weight% oil, the solution element  $q_4$  will be zero and  $a_{41}$  can be calculated from the  $3 \times 3$  system results. The  $4 \times 4$  system was then solved and gave positive solution element vectors from 1 weight% through 10 weight% oil. Interestingly, the  $4 \times 4$  system predicts essentially the same distribution of sizes at 2 weight% oil as does the  $3 \times 3$  system, indicating that the omission of quadruples from the model at very low oil levels is justified.

Figure 6 is a plot of the frequency of each agglomerate size versus oil level as calculated by the system of linear equations. It can be seen from Figure 6 that the frequency of singlets as a function of oil level is a smooth curve supporting the above assumptions.

The above development was also calculated with the assumption of a zero contact angle at the three-phase interface, as assumed in previous papers. [21,22] The results predicted overly large particles at low oil levels as the zero contact angle bond is about half the volume of the finite contact angle bond. Correspondingly the wetting volume with a zero contact angle was found to be much larger as well.

## 5 Conclusions

The adhesion surface tension method and a laser diffraction particle sizer provided means of measuring respectively the surface tension and particle-size distributions of agglomerates formed from metallurgical coal and *n*-hexadecane in an aqueous suspension of the agglomerates.

From this study it can be said that the amount of oil introduced to a coal-water slurry for forming agglomerates determines several properties on the agglomerate surface. The net agglomerate surface tension was found to approach that of the pure oil at increased oil levels, and as such the three-phase contact

angle between the agglomerate, the oil meniscus and the suspending water decreased. Thus at oil levels below 2 weight%, the bond volumes were great enough to consume the available oil in forming agglomerates no larger than doublets and triplets. With smaller contact angles at higher oil levels, the particle bonding is more economical and larger more compact oil-wetted agglomerates are seen. A constraining system of linear equations was developed to illustrate this.

A more complete analysis would involve a statistical approach encompassing the entire particle-size distribution instead of the mean particle size used here.

## References

- [1] Capes, C.E., Coleman, R.D., Croteau, S., Jonasson, K., Thayer, W.L., *Agglomerate recovery methods and yield-impurity relationships in oil agglomeration, Proc. Coal Liq. and Alternative Fuel Tech. Meeting*, Halifax, NS, Sept. 29-Oct. 3, (1986).
- [2] Wojcik, W., Al Taweel, A.M., *Powder Tech.*, 40, (1984), pp. 179-185.
- [3] Hirajima, T., Chan, E., Whiteway, S., Stefanski, M., Stewart, I., *Coal Prep.*, 5, (1987), pp. 85-108.
- [4] Capes, C.E., Coleman, R.D., Thayer, W.L., in *World Congress III of Chemical Engineering*, Tokyo (1986), vol. 1, paper 6b-301, pp. 525-528.
- [5] Froment, A., *U.K. Patent No. 12,778*, June 4, (1902).
- [6] Brown, D.J., in *Aerodynamic Capture of Particles*, E.G. Richardson (Ed.), Pergamon Press, London, (1960), pp. 35-43.
- [7] Sutherland, K.L., *J. Phys. Chem.*, 52, (1948), pp. 394-425.
- [8] Deryagin, B.V., Dukhin, S.S., Rulev, N.N., *Surf. and Coll. Sci.*, 13, (1984), pp. 71-113.
- [9] Drzymala, J., Markuszewski, R., Wheelock, T.D., *Int. J. Mineral Process.*, 18, (1986), pp. 277-286.
- [10] Absolom, D.R., Eom, K., Vargha-Butler, E.I., Hamza, H.A., Neumann, A.W., *Coll. and Surf.*, 17, 2, (1986), pp. 143-157.
- [11] Absolom, D.R., Zingg, W., Thomson, C., Policova, Z., Van Oss, C.J., Neumann, A.W., *J. Coll. Intf. Sci.*, 104, 1, (1985), pp. 51-59.
- [12] Stephen, H., Stephen, T., *Solubilities of Inorganic and Organic Compounds*, Volume 2: Ternary and Multicomponent Systems, Part 2, No. 5160, p. 1740.
- [13] Vargha-Butler, E.I., Kashi, M., Hamza, H.A., Neumann, A.W., *Coal Prep.*, 3, (1986), pp. 53-75.
- [14] Sablik, J., *Pol. J. Chem.*, 59, 4, (1985), pp. 433-438.
- [15] Pietsch, W.B., *Nature*, 217, (1968), pp. 736-737.
- [16] Neumann, A.W., Good, R.J., Hope, C.J., Sejpal, M., *J. Coll. Intf. Sci.*, 49, 2, (1974), pp. 291-304.

- [17] Neumann, A.W., Absolom, D.R., Francis, D.W., van Oss, C.J., *Sep. Purif. Methods*, 9, 1, (1980), pp. 69-163.
- [18] Spelt, J.K., Absolom, D.R., Neumann, A.W., *Langmuir*, 2, 5, (1986), pp. 620-625.
- [19] Germain, R.J., Masters Thesis, U. of Waterloo, (1977), 93 pp.
- [20] Newitt, D.M., Conway-Jones, J.M., *Trans. Instn. Chem. Engrs.*, 36, (1958), pp. 422-442.
- [21] Rumpf, H., in Agglomeration, Intl. Symp., W.A. Knepper, (Ed.), Philadelphia, PA, Apr. 12-14, (1961), pp. 379-418.
- [22] Capes, C.E., Germain, R.J., in Drying '80, Hemisphere Publ. Corp., New York, (1980), v. 2, pp. 460-466.

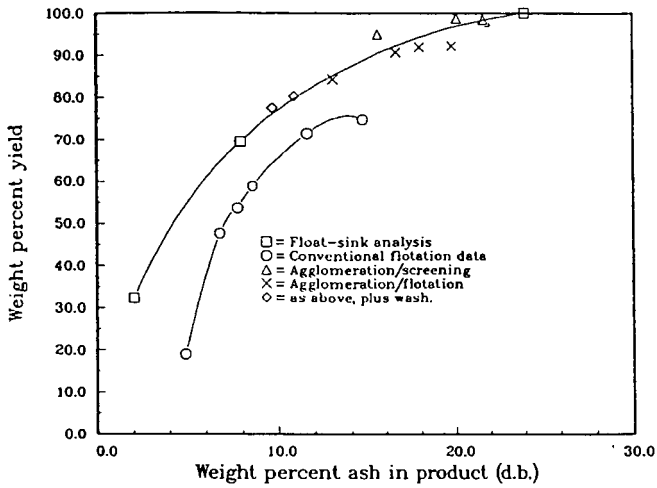


Figure 1: Yield-ash results for a minus 28 run of mine coal from Pennsylvania. (Wt.% reagent levels are based on feed solids).

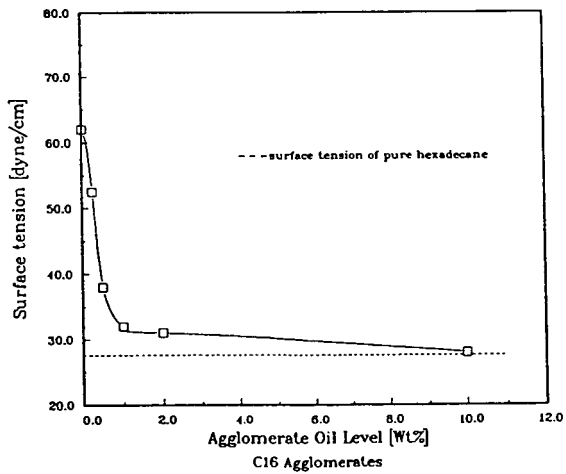


Figure 2: Agglomerate Surface Tension vs. Oil Level

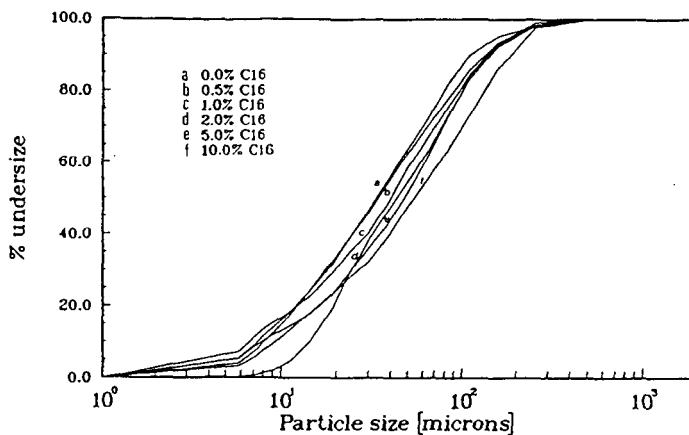


Figure 3: Particle-size distributions of agglomerates for  $n\text{-C}_{16}\text{H}_{34}$  levels from 0 to 10 weight%

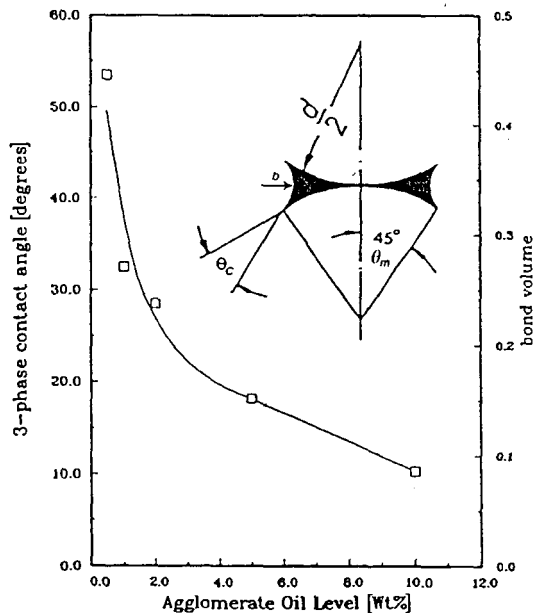


Figure 4:  $\theta_C$  and  $V_{BA}$  vs. Oil Level.  
- inset is schematic of 3-phase contact angle in particle-bonding context

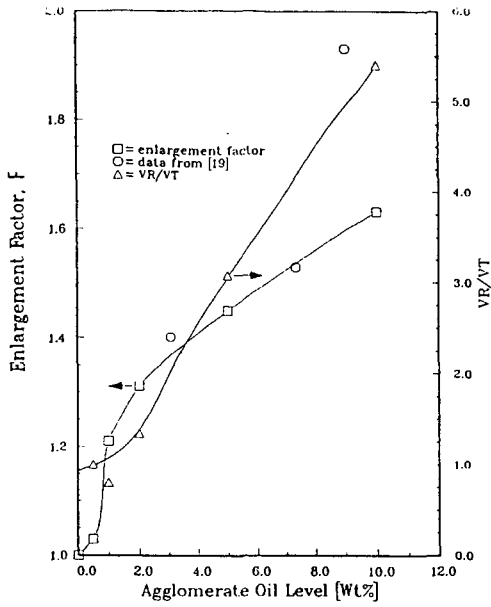


Figure 5: Enlargement Factor and  $V_R/V_T$  vs. Oil Level

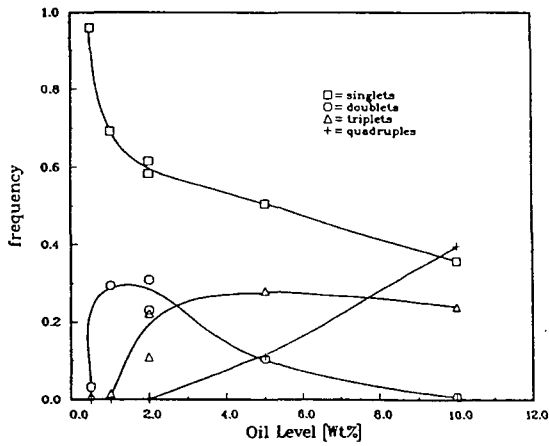


Figure 6: Agglomerate Size Frequency vs. Oil Level

INTERFACIAL PROPERTIES OF LIGNITE, GRAPHITE, KAOLIN, AND  
PYRITE

S.H. Chiang, Alec Richardson, Anni Wong

Chemical/Petroleum Engrng. Dept., University of  
Pittsburgh  
Pittsburgh, PA 15261

This project consists of four major experiments, in which the surface/interfacial and adsorption properties, particle size, and specific surface area of Lignite (35-, 200-, and 400-mesh), Graphite Powder, Kaolin, and Pyrite, are measured. The first two experiments are minor and yield preliminary results that are combined with later results for specific purposes. These experiments involve measuring the external specific surface area of the six powdered samples using the BET volumetric adsorption apparatus with  $N_2$  as the adsorbate, and measuring five average characteristic particle diameters and the particle size distribution of these samples with the Omnicon Alpha Particle Field Image Analyzer. From these results, a correlation is determined between particle size and specific surface area. The third experiment involves obtaining the adsorption and desorption isotherms of the samples and determining the effect of pressure, temperature, particle size, and intrinsic nature of the coal mineral on these isotherms. Adsorption isotherms per unit weight and per unit surface area (in conjunction with the surface area results of the BET experiment) of adsorbent are determined with the  $CO_2$  gravimetric spring adsorption apparatus. The relative film pressure, which is proportional to the area under the equilibrium adsorption isotherm on a semilogarithm plot, is also estimated.

Finally, the fourth experiment consists of two parts: 1) The pendant drop method, involving a water pendant drop in the presence of a  $CO_2(g)$  or  $CO_2(l)$  medium, in which the liquid-vapor and liquid-liquid interfacial tensions are measured as functions of  $CO_2$  pressure (relative to its saturation pressure), temperature, and  $CO_2$  phase used, based on the drop's physical dimensions at equilibrium. 2) The sessile drop method, involving a water sessile drop in equilibrium on a pelletized sample of the coal mineral in a  $CO_2(g)$  or  $CO_2(l)$  environment. In this three-phase system, the equilibrium advancing contact angle of the drop is measured as a function of  $CO_2$  relative pressure, temperature, and  $CO_2$  phase for each of the six samples. Then, with the preliminary particle size and surface area data, a correlation is drawn between the contact angle and particle size/intrinsic nature of the sample. Using the

contact angle and pendant drop data, the solid-vapor and solid-liquid interfacial tensions are calculated as functions of the above system parameters, using Young's equation and the thermodynamic equation of state:

$$\gamma_{sv} = \gamma_{sl} + \gamma_{lv} \cos \phi \quad 1)$$

$$\gamma_{sl} = \{[(\gamma_{sv})^{0.5} - (\gamma_{lv})^{0.5}]^2 / [1 - 0.015(\gamma_{sv} * \gamma_{lv})^{0.5}]\} \quad 2)$$

Then the works of adhesion and cohesion are calculated from Dupre's relation; and the equation of Boyd and Livingston is used to calculate the equilibrium spreading coefficient, which, like the equilibrium contact angle, is a direct measure of the wetting tendency of the three-phase system under given system conditions:

$$W_{ad} = \gamma_{sv} + \gamma_{lv} - \gamma_{sl} = \gamma_{lv} (1 + \cos \phi) \quad 3)$$

$$W_{co} = 2 \gamma_{lv} \quad 4)$$

$$S = \gamma_{sv} - (\gamma_{lv} + \gamma_{sl}) = W_{ad} - W_{co} \quad 5)$$

Then the contact angle and spreading coefficient data are compared for consistency. A system with incomplete wetting is characterized by a high contact angle and negative spreading coefficient at equilibrium; and one with complete wetting is reflected by a zero contact angle and a zero (or positive, indicating the effect of film pressure caused by impurities or an adsorbed vapor film) spreading coefficient. The ultimate objective of this project is to determine the effect of the system parameters (i.e. CO<sub>2</sub> pressure, temperature, CO<sub>2</sub> phase) and nature of the coal minerals (i.e. intrinsic and particle size/surface area) on the relative wettability of the three-phase system of coal mineral-water-CO<sub>2</sub> through an analysis of the interfacial and adsorption properties of the coal minerals.

### Results, Discussion, and Conclusions

In the first experiment, involving measurement of the dispersed particle size and size distribution, it is found that all six samples agree in relative magnitude of the five characteristic diameters: Length-, Volume-, Surface-, Surface-Volume-, and Weight-Diameters (Table 1). Pyrite has the largest average diameter of the six samples in all five categories, with the values of 16.9, 30.6, 23.5, 52.7, and 72.5 um, respectively. The sample with the smallest overall particle size is 400-mesh Lignite, with the respective values of 7.5, 12.4, 9.7, 20.6, and 31.1 um. The sizes of the other four samples fall within the ranges of these extreme values. The order of average particle size, from largest to smallest, is determined to be: Pyrite, 35-mesh Lignite, Graphite Powder, Kaolin, 200-mesh Lignite, and 400-mesh Lignite. As expected among the Lignite samples, the 35-mesh sample has the largest particle size; and 400-mesh has the smallest. Prior to this project, the 35-mesh sample is

already provided; and the 200- and 400-mesh samples are prepared by grinding the 35-mesh particles over a controlled time period. Thus, it is concluded that the initial preparation of these samples is successful.

The weight percent and number percent particle size distributions, based on Gaussian and log-normal distribution theory, are also calculated and agree well with the results of the average particle size data. These two curves lie furthest to the right for Pyrite, indicating that the particle size distribution in the Pyrite sample is toward the largest relative sizes. Furthermore, these curves lie farthest to the left for 400-mesh Lignite; and the relative positions of the curves for all the samples agree reasonably well with the order of the average particle sizes of the six samples. The purpose of this experiment is to obtain a relative picture of the particle sizes of the samples, to compare this data with the specific surface area data from the BET experiment to determine a possible correlation, and to later use these results with the interfacial and adsorption results to determine the effect of particle size on the interfacial phenomena of the coal minerals.

From the BET volumetric  $N_2$  adsorption experiment, it is found that Pyrite has the lowest specific surface area of all the samples:  $17.4 \text{ m}^2/\text{g}$ . In contrast, 400-mesh Lignite is found to have the highest value:  $21.1$ . The general order of the samples, from lowest to highest surface area, is: Pyrite ( $17.4$ ), 35-mesh Lignite ( $17.8$ ), Graphite Powder ( $18.1$ ), Kaolin ( $18.9$ ), 200-mesh Lignite ( $19.9$ ), and 400-mesh Lignite ( $21.1$ ). This order is the exact same order as that obtained from the dispersed particle size analysis. Thus, it is concluded that an inverse relationship exists between particle size and specific surface area for the six coal minerals (Table 1). Although this is only a measure of the external (i.e. available) surface area, this relation is still valid because it is safely assumed that, as a sample is ground to smaller particle sizes, the internal surface area (which is found inside micropores) remains constant. Thus, the purpose of this test is coupled with that of the particle size test; and a further purpose is to later use the surface area results to obtain the adsorption/desorption isotherms per unit surface area of adsorbent, from the corresponding isotherm results per unit weight of adsorbent, in order to eliminate the effect of surface area (or particle size) and determine any effect of the solid sample's intrinsic nature on the adsorption properties (i.e. to determine whether adsorption is an extensive or an intensive property).

The goal of the third experiment, using the CO<sub>2</sub> gravimetric spring adsorption apparatus, is to measure the specific amount of CO<sub>2</sub> adsorbate adsorbed on the powdered sample of coal mineral (both per unit weight and unit surface area) as a function of CO<sub>2</sub> relative pressure and temperature for the six samples. Four temperatures (10, 15, 20, and 25°C), and the CO<sub>2</sub> relative pressure in increments of 20% (from 0 to 100%, based on the saturation pressure of CO<sub>2</sub>) were tested; and each system parameter was varied independently: CO<sub>2</sub> pressure, temperature, and sample. The specific amount adsorbed ranged from about zero at 0% relative pressure to the order of 0.08 g/g adsorbent (at 10°C) or 0.12 g/g adsorbent (at 25°C) at 100% relative pressure for the six samples. Both the adsorption and desorption isotherms are measured, and it is found in all cases that significant hysteresis occurs, which reflects the energy lost in the adsorption-desorption cycle and hence the "irreversibility" of the process. Figures 1 and 2 show the adsorption/desorption isotherms for 35-mesh Lignite at 10 and 25°C. Similar results are obtained for the other five samples in terms of curve shape and magnitude of hysteresis. The hysteresis is attributed to the pore structure of each of the samples (all of which have mesopores or macropores) and the phenomenon that the vapor pressure of an adsorbate in a pore decreases as the pore size (i.e. radius r) decreases (Kelvin equation):

$$P/P_0 = \exp(-2V \gamma \cos \phi / rRT) \quad 6)$$

According to the Ink Bottle Hypothesis, which pictures a pore as having an entrance channel of smaller radius than its bulk volume, adsorption occurs in a pore when the CO<sub>2</sub> relative pressure rises to equal the vapor pressure corresponding to the radius of the "bulk" pore. However, on the desorption curve, as the pressure is reduced, the corresponding desorption does not occur until the pressure reaches a lower value, corresponding to the lower vapor pressure present in the "bottle-neck" of smaller radius, because a meniscus of adsorbate has formed in the bottle-neck. Thus, for a given amount adsorbed, the desorption isotherm lies to the left (i.e. toward lower pressures) of the adsorption isotherm.

This phenomenon also explains the general shape (i.e. concave upward) of the isotherms and the observed change in shape from concave to sigmoidal as the temperature is increased (Figures 1 and 2). Generally, the specific amount adsorbed increases as temperature increases, indicating that some chemisorption (as well as physical adsorption) is present at higher temperatures. The pressure at which the maximum slope of the isotherm occurs decreases as

temperature increases, indicating that the "effective pore radius" decreases: As pore radius decreases, vapor pressure decreases, so that adsorption can occur at lower relative  $\text{CO}_2$  pressures; and an increase in temperature increases the vapor pressure in a given pore radius. Since each solid sample is characterized by a pore size distribution, adsorption occurs in different parts of the sample at different pressures, as reflected by the isotherm's shape at equilibrium. The slope is a measure of the increment of adsorption that occurs in response to an increment of  $\text{CO}_2$  relative pressure, and thus measures the frequency of pores with a given radius. Thus, for a given sample, it is observed that the adsorption isotherm becomes more sigmoidal (i.e. more like a BET isotherm) as temperature increases: the pressure of maximum adsorption shifts to lower values, indicating that the vapor pressure and "effective" pore size both decrease.

A final observation of this experiment is that the specific amount adsorbed per unit weight of adsorbent increases as particle size decreases (or specific surface area increases) among the six samples and among the three Lignite samples of different particle size. At  $20^\circ\text{C}$  and 100% relative pressure, Pyrite showed the lowest specific amount adsorbed (about 0.09 g/g); and 400-mesh Lignite showed the highest amount (about 0.12 g/g). Generally, the order of the amount adsorbed corresponded to the order of specific surface area (or inverse order of particle size) for the six samples at a given temperature and  $\text{CO}_2$  pressure (Tables 2 and 3). Finally, these results (per unit weight of adsorbent) are divided by the specific surface area of the corresponding sample (from the BET results) to obtain the adsorption isotherms per unit surface area of adsorbent at each temperature and  $\text{CO}_2$  pressure. It is found that this specific amount adsorbed varied very little among the six samples, indicating that the intrinsic nature (i.e. hydrophobicity) of the sample has a very little effect on its adsorption properties. Thus, it is concluded that adsorption at equilibrium is an extensive property (i.e. depends on the amount of sample, or the availability of surface area).

The final experiment involves measuring the equilibrium advancing contact angles and several types of interfacial tension as a function of sample,  $\text{CO}_2$  pressure, temperature, and  $\text{CO}_2$  phase. As before, each parameter is varied independently to isolate its effect on the interfacial properties. Four temperatures (10, 15, 20, and  $25^\circ\text{C}$ ) and  $\text{CO}_2$  relative pressure in increments of 25% (from zero to 100%) are tested; and  $\text{CO}_2(\text{g})$  and  $\text{CO}_2(\text{l})$  are used separately. In

the pendant drop experiment, it is found that the liquid-vapor interfacial tension (Table 4) decreases dramatically as pressure increases (i.e. at 25°C: from 72.03 dyne/cm at 0% to 33.01 dyne/cm at 100% relative CO<sub>2</sub> pressure), decreases slightly with temperature (i.e. at 100% relative pressure: from 35.38 dyne/cm at 10°C to 33.01 dyne/cm at 25°C), and decreases significantly as a switch is made from CO<sub>2</sub>(g) to CO<sub>2</sub>(l). For example, at 10°C, the tension decreases from 35.38 to 27.09 dyne/cm when the switch is made to CO<sub>2</sub>(l). These changes are reflected by the changes in the pendant drop's equilibrium physical dimensions (De, Ds, S = De/Ds, and Hs = f(S)) and by the change in density difference (p<sub>2</sub> - p<sub>1</sub>) between the water drop and surrounding CO<sub>2</sub> medium. The physical picture is explained mathematically by Laplace's equation of capillarity and the criteria that the surface and gravitational forces are equal at equilibrium:

$$p'' - p' = \gamma \cos \phi (1/r_1 - 1/r_2) = 2 \gamma \cos \phi / r \quad 7)$$

$$F_g = mg = pVg = pg(4/3 \pi r^3) = 2 \pi r \gamma = F_s \quad 8)$$

Recognizing the nature of curved surfaces, an increase in pressure or temperature decreases the pressure difference across the curved interface and thus decreases the surface force and hence the interfacial tension. As the pendant drop grows in radius, gravitational force increases more rapidly than the surface force. Because of the depressed surface force, the drop has smaller dimensions and a lower interfacial tension at equilibrium, as a result of a pressure or temperature increase. When the switch is made from CO<sub>2</sub>(g) to CO<sub>2</sub>(l), the density difference between the water drop and CO<sub>2</sub> phase decreases; CO<sub>2</sub>(l) has a density comparable to (but still less than) that of water (0.80 vs. 1.00 g/cm<sup>3</sup> at 25°C), as compared to CO<sub>2</sub>(g). According to Andreas, Hauser, and Tucker, the interfacial tension in this two-phase system is proportional to this density difference:

$$\gamma = g (p_2 - p_1) D_e^2 / H_s \quad 9)$$

Thus, a decrease in interfacial tension is expected when a switch is made from CO<sub>2</sub>(g) to CO<sub>2</sub>(l) at 100% CO<sub>2</sub> relative pressure.

In the sessile drop experiment, the equilibrium advancing contact angle is measured versus CO<sub>2</sub> pressure, temperature, and CO<sub>2</sub> phase. Generally, it is found that the contact angle increases when: CO<sub>2</sub> pressure increases, temperature decreases, or CO<sub>2</sub>(l) is used. These trends can similarly be explained by the above argument, Laplace's equation, and the equilibration of surface and gravity forces at equilibrium. According to Padday, a sessile drop is in equilibrium when the top is flat and at maximum height. For most samples, except the hydrophobic Graphite Powder, the contact angles at all temperatures are

essentially zero at relative pressures less than 50%, indicating a completely wettable system. Thus, the optimal system conditions for enhancing incomplete wetting for a given sample are a high pressure (preferably 100%), low temperature, and the use of  $\text{CO}_2(l)$  as the surrounding medium. It is also found that, among the Lignite samples, contact angle increases when particle size decreases. At  $10^\circ\text{C}$  and 100% relative pressure, the average contact angle values for 35-mesh, 200-mesh, and 400-mesh Lignite are, respectively:  $87.50^\circ$ ,  $96.25^\circ$ , and  $107.50^\circ$  with  $\text{CO}_2(g)$ ; and  $103.75^\circ$ ,  $117.50^\circ$ , and  $128.75^\circ$  with  $\text{CO}_2(l)$ .

Furthermore, among all six samples, no correlation is found between particle size and equilibrium contact angle. Graphite Powder, known to be hydrophobic in nature, is found to have the largest overall contact angle values, ranging (at  $10^\circ\text{C}$ ) from  $90.00^\circ$  at 25% to  $147.50^\circ$  at 100% with  $\text{CO}_2(g)$ , and  $152.50^\circ$  with  $\text{CO}_2(l)$ . Thus, Graphite Powder is the most incompletely wettable sample. Pyrite shows more intermediate contact angle values, its highest value being  $95.00^\circ$  at  $10^\circ\text{C}$  with  $\text{CO}_2(l)$ , and is found to have the second lowest average contact angle at a given temperature,  $\text{CO}_2$  pressure, and  $\text{CO}_2$  phase. The sample with the lowest average value (i.e. the most hydrophilic sample) is the clay-like Kaolin, which shows a zero contact angle (i.e. complete wetting) even up to 100% relative pressure with  $\text{CO}_2(g)$ . Its largest value is  $30.00^\circ$ , at  $10^\circ\text{C}$  with  $\text{CO}_2(l)$ . Thus, the general order of wetting is, from complete to incomplete: Kaolin, Pyrite, Lignite (35-mesh, 200-mesh, 400-mesh), and Graphite Powder, because the magnitude of the equilibrium advancing contact angle is inversely related to the tendency of a three-phase system toward complete wetting. Thus, contact angle is found to be an intensive property, because it depends not only on particle size (or specific surface area) but also on the sample's intrinsic nature (i.e. hydrophobicity).

Using the two-phase equilibrium interfacial tension and contact angle data, the solid-vapor and solid-liquid interfacial tension are calculated using Equations 1 and 2. It is generally found that the solid-vapor tension first decreases and then increases with pressure. This is explained by the fact that complete wetting (i.e. a zero contact angle) is predominant at the lower relative pressures, and film pressure is still negligible; thus, the solid-vapor tension is first constant or decreases slightly. At higher pressures, incomplete wetting sets in; and film pressure (i.e. the presence of an adsorbed vapor film on the solid surface) becomes significant. Thus, based on the interfacial tension of a clean, pure solid in a vacuum, the solid-vapor tension increases with pressure to reflect the

film pressure increase. Generally, as incomplete wetting becomes significant, the solid-vapor tension increases. This argument also explains the observation that this tension increases when the switch is made from  $\text{CO}_2(\text{g})$  to  $\text{CO}_2(\text{l})$  at a given temperature.

This tension is also found to be relatively constant with temperature as a result of the cancellation effect of temperature on contact angle and the liquid-vapor tension in Young's equation: As temperature increases,  $\theta$  decreases,  $\cos \theta$  increases, and the liquid-vapor tension decreases; so the product  $\gamma_{\text{lv}} \cos \theta$  is essentially constant with temperature. Among the six samples, the solid-vapor tension is lowest for Kaolin (about 88.0 dyne/cm with  $\text{CO}_2(\text{l})$ ) and highest for Graphite Powder (about 107.0 dyne/cm with  $\text{CO}_2(\text{l})$ ). The order of magnitude for this tension (averaged over the four temperatures) is, in increasing order: Kaolin (88.0 dyne/cm), Pyrite (99.0 dyne/cm), 35-mesh Lignite (101.0 dyne/cm), 200-mesh Lignite (102.5 dyne/cm), 400-mesh Lignite (104.5 dyne/cm), and Graphite Powder (107.0 dyne/cm). This is the same order of increasing contact angle and of decreasing wettability. Thus, among the Lignite samples, this tension decreases as particle size increases. Like the contact angle, the solid-vapor interfacial tension is an intrinsic property, because it depends on contact angle.

Another interfacial tension that is calculated is the solid-liquid tension, which is found to increase with  $\text{CO}_2$  pressure continuously (because of the corresponding increase in contact angle and decrease in the system's wetting tendency, and the insignificant effect of film pressure on this tension), remain constant with temperature (because the term  $\gamma_{\text{lv}} \cos \theta$  is essentially constant with temperature), and increases when  $\text{CO}_2(\text{l})$  is used (because of the enhancement of incomplete wetting). It is observed among the Lignite samples that the solid-liquid tension decreases as particle size increases. Among the six samples, the order of magnitude for this tension parallels that for solid-vapor tension (reflecting the trend toward incomplete wetting) and is, in increasing order (averaged over the four temperatures): Kaolin (63.0 dyne/cm), Pyrite (98.0 dyne/cm), 35-mesh Lignite (106.0 dyne/cm), 200-mesh Lignite (111.0 dyne/cm), 400-mesh Lignite (120.0 dyne/cm) and Graphite Powder (128.0 dyne/cm). Thus, solid-liquid tension is an intensive property, reflecting hydrophobicities as well as particle size.

The main conclusion obtained from this project is the optimization of reaction conditions to enhance the system's tendency toward incomplete wetting and thus enhance the

potential for separation. Graphite Powder has the highest tendency; and, among the Lignite samples, 400-mesh Lignite has the highest incomplete wetting tendency. For a given sample, incomplete wetting is favored at high relative  $\text{CO}_2$  pressures, low temperatures, and the presence of  $\text{CO}_2(\text{l})$ . It is found that, while equilibrium adsorption is an extensive property (i.e. depends only on particle size and thus available specific surface area), the contact angle and interfacial tensions are intensive properties. From the preliminary results, an inverse relation exists between particle size and specific surface area of a powdered sample; and these results make possible and more complete the study of the adsorption and interfacial properties of the six coal minerals.

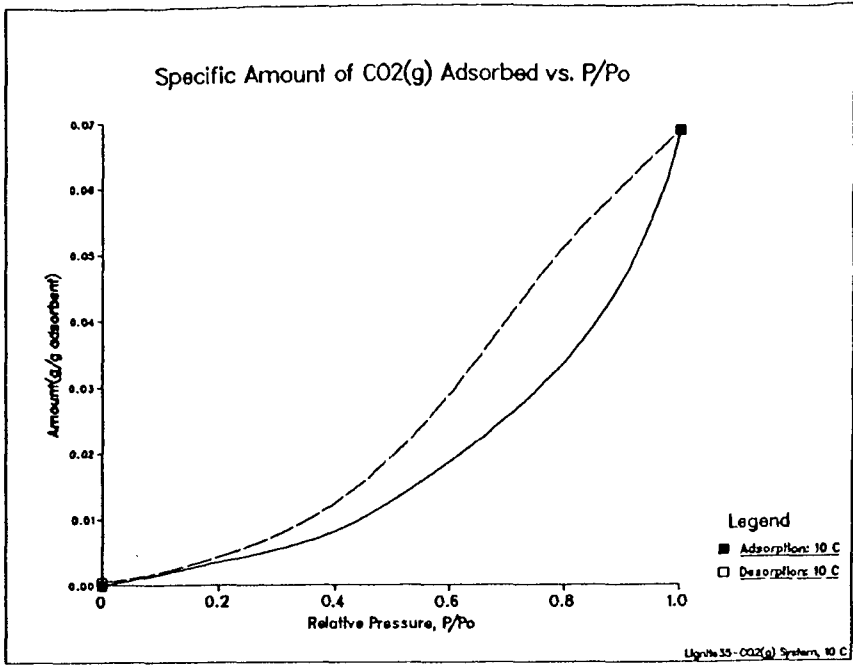


Figure 1 Adsorption and Desorption Isotherms vs. CO<sub>2</sub> Pressure for 35-Mesh Lignite at 10<sup>o</sup> C

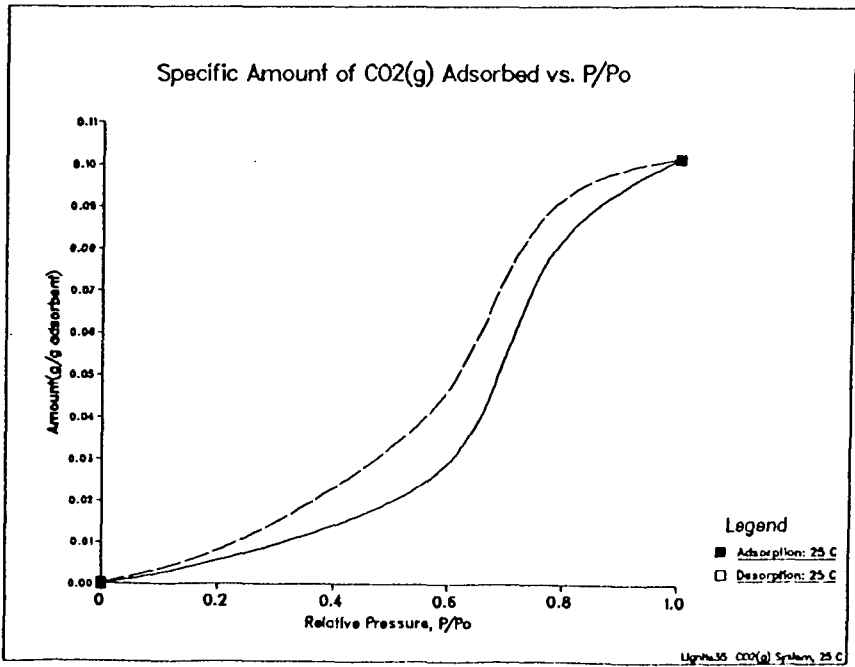


Figure 2 Adsorption and Desorption Isotherms vs. CO<sub>2</sub> Pressure for 35-Mesh Lignite at 25<sup>o</sup> C

Table 1  
Average Characteristic Diameters and Specific Surface Areas of Powdered Particle Samples of Lignite (35-, 200-, and 400-Mesh), Graphite Powder, Kaolin, and Pyrite

Sample	Length Diameter (um)	Volume Diameter (um)	Surface Diameter (um)	Surface Volume Diameter	Weight Diameter	Specific Surface Area (m <sup>2</sup> /g)
35-Mesh Lignite	9.2	17.6	12.8	33.7	54.2	17.8
200-Mesh Lignite	7.6	14.5	10.3	28.9	56.2	19.9
400-Mesh Lignite	7.5	12.4	9.7	20.6	31.1	21.1
Graphite Powder	8.8	16.2	12.0	29.8	46.0	18.1
Kaolin	9.1	15.1	11.6	25.8	44.5	18.9
Pyrite	16.9	30.6	23.5	52.7	72.5	17.4

Table 2  
Specific Amount of CO<sub>2</sub> Adsorbed (per unit weight of adsorbent) Along the Adsorption Isotherm for Lignite (35-, 200-, and 400-Mesh) (g/g adsorbent)

Temp. (°C)	35-Mesh Lignite			200-Mesh Lignite			400-Mesh Lignite					
	0.00	0.20	0.40	0.60	0.80	1.00	0.00	0.20	0.40	0.60	0.80	1.00
10	0.00	0.00330	0.00817	0.01854	0.03367	0.06576	0.00	0.00411	0.00928	0.02012	0.03630	0.07236
15	0.00	0.00403	0.01094	0.02007	0.03578	0.06830	0.00	0.00432	0.01119	0.02187	0.03635	0.09600
20	0.00	0.00538	0.01205	0.02723	0.07121	0.09384	0.00	0.00574	0.01303	0.03114	0.07820	0.09905
25	0.00	0.00568	0.01403	0.02895	0.08239	0.10107	0.00	0.00613	0.01635	0.03278	0.08916	0.10980
Temp. (°C)	35-Mesh Lignite			200-Mesh Lignite			400-Mesh Lignite					
10	0.00	0.00426	0.00980	0.02140	0.03810	0.07622	0.00	0.00426	0.00980	0.02140	0.03810	0.07622
15	0.00	0.00471	0.01259	0.02303	0.05957	0.09908	0.00	0.00471	0.01259	0.02303	0.05957	0.09908
20	0.00	0.00591	0.01376	0.03172	0.10813	0.11794	0.00	0.00591	0.01376	0.03172	0.10813	0.11794
25	0.00	0.00648	0.01790	0.03359	0.09855	0.12426	0.00	0.00648	0.01790	0.03359	0.09855	0.12426

Table 4  
Equilibrium Liquid-Vapor and Liquid-Liquid Interfacial Tensions from the  
Pendant Drop Method (dyne/cm)

Temp. (°C)	Liquid-Vapor Interfacial Tension		
	0.00	0.25	0.50
10	74.27	63.84	53.59
15	73.77	63.51	52.42
20	72.73	61.89	52.87
25	72.03	61.39	51.84

Temp. (°C)	Liquid-Liquid Interfacial Tension		
	1.00 CO <sub>2</sub> (g)	0.75	1.00 CO <sub>2</sub> (l)
10	35.36	43.42	27.09
15	35.07	43.91	26.42
20	34.33	44.15	25.37
25	33.01	43.40	23.32

Temp. (°C)	Work of Cohesion (twice the interfacial tension)		
	0.00	0.25	0.50
10	148.54	127.67	107.17
15	147.54	127.02	106.83
20	145.47	123.78	105.74
25	144.07	122.78	103.69

\* The first four columns tabulate the liquid-vapor interfacial tensions, whereas the last column lists the liquid-liquid interfacial tensions. They are distinguished by the phase of CO<sub>2</sub> surrounding the pendant drop.

Table 3  
Specific Amount of CO<sub>2</sub> Adsorbed Along the Adsorption Isotherm for  
Graphite Powder, Kaolin, and Pyrite (g/g adsorbent)

Temp. (°C)	Graphite Powder			
	0.00	0.20	0.40	0.60
10	0.00	0.00768	0.00878	0.01891
15	0.00	0.00794	0.01081	0.02013
20	0.00	0.00532	0.01198	0.02711
25	0.00	0.00563	0.01411	0.02934

Temp. (°C)	Kaolin			
	0.00	0.20	0.40	0.60
10	0.00	0.00382	0.00891	0.01990
15	0.00	0.00415	0.01121	0.02096
20	0.00	0.00548	0.01232	0.02751
25	0.00	0.00571	0.01601	0.03098

Temp. (°C)	Pyrite			
	0.00	0.20	0.40	0.60
10	0.00	0.00340	0.00780	0.01816
15	0.00	0.00376	0.01070	0.01959
20	0.00	0.00580	0.01170	0.02695
25	0.00	0.00551	0.01343	0.02789

## EFFECTIVE SURFACE AREAS OF COALS MEASURED BY DYE ADSORPTION

Donald P. Spitzer  
American Cyanamid Company  
Stamford, CT 06904

### INTRODUCTION

Coals are well known to be more or less porous structures, but just how much porosity and surface area is measured depends very much on the measurement technique. For example, even though  $N_2$  and  $CO_2$  molecules are essentially the same size, surface areas measured by  $CO_2$  adsorption are  $>100 \text{ m}^2/\text{g}$  for most coals, but less than  $10 \text{ m}^2/\text{g}$  when measured by  $N_2$  adsorption. This is attributed to the fact that the  $N_2$  measurements are made at  $77^\circ\text{K}$  while the  $CO_2$  measurements are made at much higher temperatures, up to  $298^\circ\text{K}$ . That is, most of the pores in coals are so small that rate of diffusion of even such small molecules into the pores becomes a limiting factor. This is clearly because most of the surface area in coals is in micropores,  $<2\text{nm}$  diameter, and even in ultra-micropores,  $<0.8\text{nm}$  diameter (1).

Similarly, use of other small molecules such as methanol vapor (2, 3), water, or butane (3) at temperatures of  $273\text{--}298^\circ\text{K}$  also gives high surface areas of  $30\text{--}400 \text{ m}^2/\text{g}$ , compared to nitrogen surface areas of only  $0.1\text{--}1.5 \text{ m}^2/\text{g}$  for the same coals. This quotation from (2) is relevant: "It is apparent from past work that no absolute method of total surface area measurement exists and that any method will only give the surface area accessible to the adsorbate molecules at the temperature of adsorption." A very similar statement is made by Fuller (4).

Since most coal processing is done in aqueous slurries, adsorption from water is generally of more practical interest than adsorption of vapors. A considerable number of papers dealing with adsorption from aqueous solutions are in print and we can only give some principal conclusions here. The solutes examined include: 1) a variety of surfactants (5-9), which are of interest for dewatering and for coal/water slurries; 2) alcohols which are used as frothers (10-14); 3) polysaccharides such as dextrin and guar, used for coal depression (15, 16); 4) substituted dioxanes (flotation promoters) (17); 5) phenol (10, 18-20); 6) organic acids (14, 21); 7) dyes (22, 23); etc.

In these various publications, establishment of equilibrium adsorption is stated to require anywhere from one hour to  $>100$  hours. One point of agreement is that adsorption of most reagents on most coals is generally within the range  $0.1 - 10 \text{ mg}$  of reagent per gram of coal, for a wide variety of types of reagent. Also, it is consistently concluded that nonionic molecules, e.g. alcohols or weak acids, adsorb via their hydrocarbon portion and adsorption therefore decreases as coal is oxidized, although adsorption of stronger acids can occur via the polar end and increase with oxidation. Ionic surfactants apparently adsorb both on fresh and on oxidized surfaces, either via electrostatic or hydrophobic interactions (5, 6).

An extensive study of dye adsorption on coals is given by Nandi and Walker (23). Using 24 hour equilibration times, adsorption for either an anionic dye, metanil yellow, or a cationic dye, methylene blue was found to be approximately related to nitrogen surface areas for most of the coals examined. Two obvious exceptions, however, were lignites, where dye adsorptions were approximately 20-100 times those expected from nitrogen surface areas.

Most studies of adsorption are concerned with "equilibrium" measurements. Since equilibrium, however, usually requires a day or more, such results may have little relevance to most real coal processing problems, where the time that the coal spends in an aqueous slurry is generally less than one hour (an obvious exception is the case of coal/water slurries, where coals are expected to be stably dispersed in aqueous slurries for weeks or months). Our primary interest has been to examine adsorption behavior especially at short contact times, ten minutes to an hour, to determine whether such measurements might give useful data on effective surface areas - i.e., the surface that would be accessible to reagents within times comparable to those typical of most coal processing. Accordingly, most of our emphasis is on the effect of time on adsorption, rather than on traditional adsorption isotherms.

Although most literature on cationic dye adsorption (mostly on carbons) uses methylene blue, it happened that we originally used safranin O instead because this dye was reported to be useful in distinguishing oxidized coals from fresh coals (24). Many of our experiments were repeated using methylene blue (in water), with very similar results. It was noted early that swelling of coals in water was common, especially for more oxidized or lower rank coals, and adsorption experiments were also done in another solvent, namely methanol. This produced quite striking differences for some coals.

#### EXPERIMENTAL

For the aqueous dye solutions, the amount of mixing during adsorption had a considerable effect on the results. Best mixing appeared to be when bottles containing dye solutions plus coal were placed on rollers. A shaker generally gave lower results, since the coals tended to stay at the bottom of the bottle. On the other hand, more vigorous mixing with a magnetic stirring bar gave some results that were far too high, especially in the case of the oxidized coals, indicating breakup from the combination of swelling by the water and the mechanical agitation. For example, stirring of Coals B or C for only an hour in aqueous solution gave some apparent adsorptions greater than 40 mg/g. Adsorptions from methanol solution were little affected by mixing conditions.

Except for the adsorption isotherms (shown here only for Coal A), adsorptions were done from 100ppm safranin O (Kodak Chemical) solutions at room temperature ( $23 \pm 2^\circ \text{C}$ ), with from 0.1 to 10.0 gm of coal per 100ml of solution, as necessary to give a readily measurable adsorption. Coals were afterwards separated either by centrifuging

or rapidly filtering through a small millipore filter attached to a plastic syringe. Dye concentrations were determined from absorption at 520nm, after appropriate dilution to less than 10ppm.

## RESULTS AND DISCUSSION

Adsorption isotherms for Coal A (Fig. 1) are shown from both water and methanol for 16 hour and for one hour adsorptions. From Fig. 2, 16 hours appears adequate to give "equilibrium" adsorption from the aqueous solutions. The one hour curve in Fig. 1 is clearly far from equilibrium, but it is considered significant that a surface area corresponding to just under 0.4 mg/g adsorption is very readily covered by the dye and further adsorption does not take place until high concentrations are reached or longer times are allowed;  $N_2$  area of this coal is 0.4  $m^2/g$ . Isotherms from methanol solutions are nearly independent of time and the maximum adsorption is not too different from that which is quickly attained from water solutions.

The oxidized Coals B and C show the most striking differences between adsorption from water or from methanol. As noted above, such coals are considerably swollen by water; for Coal C, adsorption from water is more than an order of magnitude greater than from methanol. From methanol, there is again nearly a 1:1 correspondence between  $N_2$  surface area and the amount of dye that is quickly adsorbed: for Coal B, S.A. = 1.2  $m^2/g$ , while adsorptions are 1.0 and 2.1 mg/g at ten minutes and one hour, respectively; for Coal C, S.A. = 0.67  $m^2/g$ , and adsorptions are 0.23 and 0.47 mg/g at ten minutes and one hour, respectively.

To demonstrate that the steep initial increase in adsorption on Coals B and C from aqueous solution was due to swelling by the water rather than just slow diffusion of the dye, the following comparison was made: For Coal B, adsorption from 100ppm aqueous safranin for one hour was 13.5±1.5 mg/g; similarly, adsorption from 100ppm aqueous safranin for ten minutes was 5.4±0.5 mg/g; contacting the coal with water for 50 minutes, followed by only ten minutes contact with safranin gave adsorptions of 12.5±1.5 mg/g (i.e., coal plus water for 50 minutes, then an equal volume of 200ppm safranin was quickly mixed in and kept another ten minutes). Contact with the water is clearly more important in determining adsorption on such coals than is diffusion of the dye. Such swelling must also be responsible for the high adsorption on lignites reported by Nandi and Walker (23), as was suggested by them, but not demonstrated.

For the PSOC coals 217 and 315, adsorptions from aqueous solutions at short times again give numbers that are close to the nitrogen surface areas for these coals, 1.6 and 1.4  $m^2/g$ , respectively. For PSOC 217, adsorption from methanol gives much lower values; it may be that the water helps to open up the pores, but in an experiment similar to that done with Coal B above, we found no obvious swelling.

Note that all of the coals discussed above had quite low surface areas. We did have two other coals with somewhat higher surface areas (3.4 and 7.1  $m^2/g$ ) and we also examined two pure clay minerals,

kaolin and illite, and two natural coal/clay mixtures. These latter four samples had surface areas from 15 to 61 m<sup>2</sup>/g; unlike high area coal samples, however, the surfaces of the clay would be all external and readily accessible, and the surface areas of the mixtures were undoubtedly determined mainly by the clay minerals. As expected from non-porous particles, adsorption on these samples was essentially constant after only an hour. Quantities of safranin adsorbed from the aqueous solutions again showed a close correspondence with the nitrogen surface areas. Adsorptions from methanol on these clays or clay-rich samples gave distinctly lower capacities, by factors of four to six.

Short term safranin adsorption data for all samples in Table 1, from aqueous or from methanol solutions, are summarized in Figs. 5 and 6, respectively. In Fig. 5 especially, the correspondence between safranin adsorptions from water and nitrogen surface areas is surprisingly good. The only two points that clearly do not fit in are for the Coals B and C, where anomalously high adsorptions were shown to be related to swelling by water.

Correlation of N<sub>2</sub> area with adsorption from methanol solutions shows the general trend, but is not as good as from water. Many of the samples show significantly less adsorption from methanol. In the case of highly oxidized coals, however, these lower values from methanol were seen to be much closer to the N<sub>2</sub> areas.

From the correlation in Fig. 5, it happens that 1.0 mg/g of adsorbed safranin is essentially equivalent to 1.0 m<sup>2</sup>/g of N<sub>2</sub> surface area. This would require an area of only 0.58 nm<sup>2</sup> per safranin molecule, which is considerably less than the 2.2 nm<sup>2</sup> we estimate for the molecule lying flat. The 0.58 nm<sup>2</sup> would be consistent with an edge adsorption, or alternatively, may indicate multilayer adsorption (3-4 layers stacked flat). Since there is no apparent reason why a 3-4 multilayer configuration would be particularly stable, an edge adsorption is more likely.

Our coal samples were all of rather low surface areas, 0.2-7 m<sup>2</sup>/g; the only higher surface areas were for essentially non-porous particles. It is expected that as coal surface areas increase above about ten m<sup>2</sup>/g, pores are necessarily smaller and less accessible and the ratio of dye adsorbed to N<sub>2</sub> area must decrease. This is essentially what was found in (23) for coals with surface areas of 10-100 m<sup>2</sup>/g. We expect to extend this present work to also include higher surface area coals. In addition, we have some preliminary results using adsorption of a proprietary reagent that selectively adsorbs only on the coals and not on the ash minerals, permitting a separation of the contributions of the coal and ash to the surface area.

#### SUMMARY

Coal surfaces that are readily accessible to adsorption by safranin are found to correlate well with N<sub>2</sub> surface areas, with adsorption of 1.0 mg safranin per gram of coal corresponding to essentially a

surface area of  $1.0 \text{ m}^2/\text{g}$ . Highly oxidized coals were found to swell considerably in water, with correspondingly increased adsorption. Areas of such coals can be estimated by adsorption of safranin from methanol solutions.

#### References

1. Walker, P. L. Jr., Phil. Trans. Royal Soc. London, A300, 65-81 (1981).
2. Carpenter, D. L. and Sergeant, G. D., Fuel, 45, 429-446 (1966).
3. Anderson, R. B., Hall, W. K., Lecky, J. A., and Stein, K. C., J. Phys. Chem., 60, 1548 (1956).
4. Fuller, E. L. Jr., Coal Structure, Gorbaty, M. L. and Ouchi, K., eds., Adv. Chem. Series 192, American Chemical Society, Washington, D. C. (1981).
5. Laskowski, J. and Konieczny, E., Arch. Gorn., 15, 26-36 (1970).
6. Latiff Ayub, A., Al Taweel, A. M., and Kwak, J. C. T., Coal Preparation, 2, 1-17 (1985).
7. Aston, J. R., Deacon, M. J., Furlong, D. N., Healy, T. W., and Lau, A. C. M., Proc. Aust. Coal Prep. Conf. (1981) 358-378.
8. Esumi, K., Meguro, K., and Honda, H., Bull. Chem. Soc. Japan, 55, 3021-2 (1982).
9. Aston, J. R. and Furlong, D. N., Colloids and Surfaces, 4, 121-129 (1982).
10. Przhegorlinskaya, R. V. and Zubkova, Yu. N., Khim. Tverd. Topliva, 12, 125-128 (1978).
11. Kelebek, S., Salman, T., and Smith, G. W., Coal: Phoenix of the 80's, Proc. 64th CIC Coal Symp., Al Taweel, A. M., ed., 145-152 (1982).
12. Fuerstenau, D. W. and Pradip, Colloids and Surfaces, 4, 229-243 (1982).
13. Nogly, J. and Laskowski, J., Arch. Gorn. 17, 199-208 (1972).
14. Butuzova, L. F. and Kucher, R. V., Khim. Tverd. Topliva, 11, 119-125 (1977).
15. Huang, H. H., Calara, J. V., Bauer, D. L., and Miller, J. D., Recent Devel. Separation Science, 4, 115-133 (1978).
16. Miller, J. D., Laskowski, J. S., and Chang, S. S., Colloids and Surfaces, 8, 137-151 (1983).
17. Petukhov, V. N., Khim. Tverd. Topliva, 13, 12-20 (1979).
18. Al Taweel, A. M., Farag, H. A., Kwak, J., Hanza, H. A., and Falk, M., Coal: Phoenix of the 80's, Proc. 64th CIC Coal Symp., Al Taweel, A. M., ed., 125-130 (1982).
19. Ayub, A. L., Al Taweel, A. M., and Kwak, J. C. T., Coal Preparation, 1, 1-13 (1984).
20. Eveson, G. F., Ward, S. G., and Worthington, F., J. Inst. Fuel, 29, 540-544 (1956).
21. Zubkova, Yu. N., Basenkova, V. L., and Kucher, R. V., Khim. Tverd. Topliva, 13, 32-37 (1979).
22. Glanville, J. O., Haley, L. H. Jr., and Wightman, J. P., Fuel, 62, 1310-1314 (1983).
23. Nandi, S. P. and Walker, P. L. Jr., Fuel, 50, 345-366 (1971).
24. Gray, R. J., Rhoades, A. H., and King, D. T., Trans. S. M. E., 260, 334-341 (1976).

Table 1. Samples Used

Sample	%C	%H	%O	%N	%S	%Ash	N <sub>2</sub> area m <sup>2</sup> /g
Coal A -Virginia	83.0	4.8	10.7	0.9	0.6	7.1	0.4
Coal B -W.V.stockpile	67.4	3.6	27.7	0.9	0.5	16.2	1.2
Coal C -British Columbia surface outcrop	75.4	3.9	19.9	0.6	0.2	18.2	0.67
PSOC 217 -Kentucky	78.9	5.6	8.0	1.8	5.5	17.7	1.6
PSOC 315 -Colorado	76.7	5.8	14.8	2.0	0.8	11.6	1.4
Coal A, oxidized, 200hrs.@150°C	73.7	3.3	21.5	0.9	0.6	6.4	3.4
Coal D -Arizona							7.1
Coal/Ash Mix 1-Kentucky						50.	30.6
Coal/Ash Mix 2-Kentucky						33.	15.1
Kaolin							23.2
Illite							61.2

Figure 1. Adsorption isotherms for safranin on Coal A, from water and from methanol solutions and for 16 hour and one hour contact times.

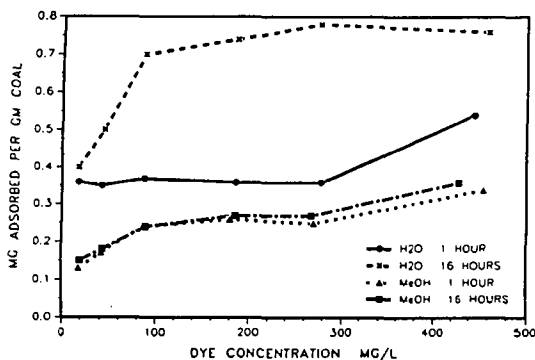
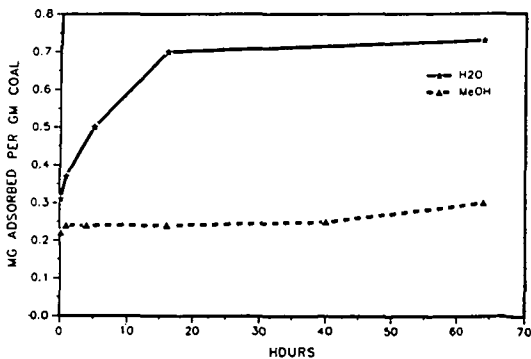


Figure 2. Adsorption on Coal A vs. time, from 100ppm safranin solutions in water and in methanol.



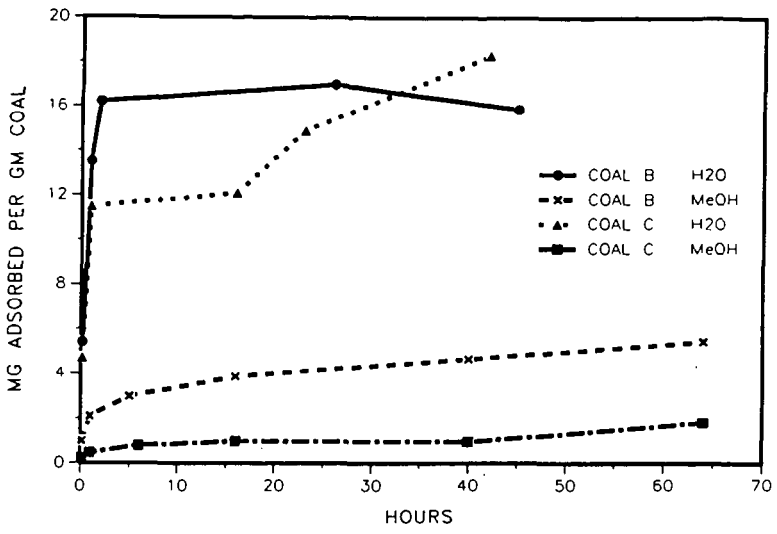


Figure 3. Adsorption on Coal B and Coal C vs. time, from 100ppm safranin solutions in water and in methanol.

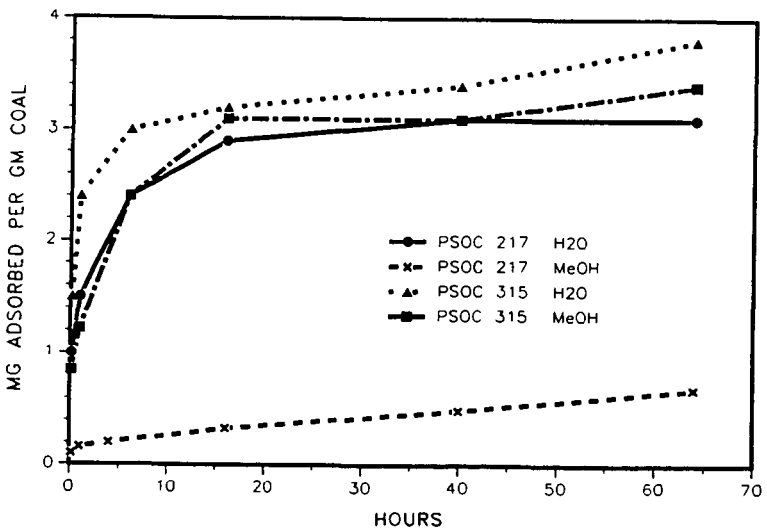


Figure 4. Adsorption on PSOC 217 and PSOC 315 vs. time from 100ppm safranin solutions in water and in methanol.

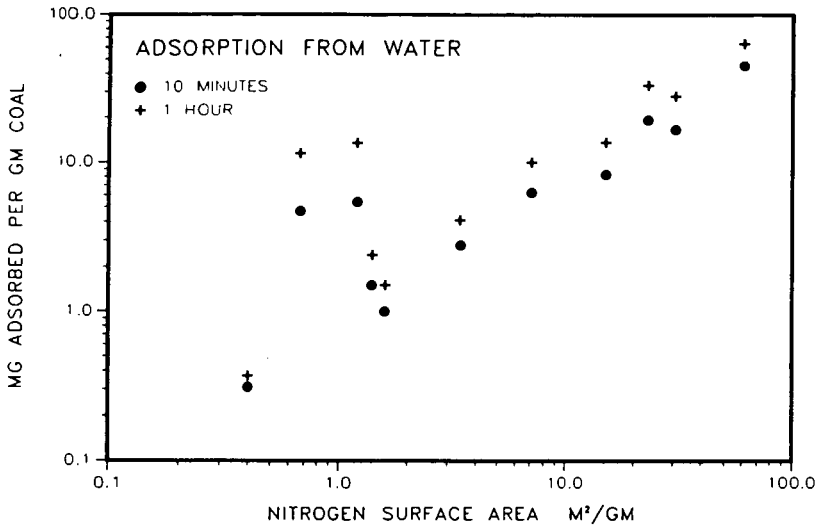


Figure 5. Ten minute and one hour adsorptions of 100ppm safranin from water onto samples of Table 1 vs. nitrogen surface area.

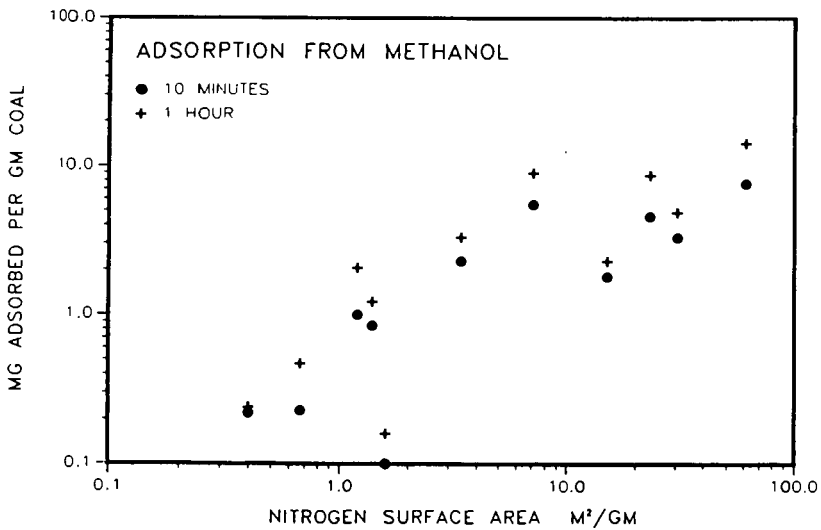


Figure 6. Ten minute and one hour adsorptions of 100ppm safranin from methanol onto samples of Table 1 vs. nitrogen surface area.

## CHARACTERIZATION OF MINERAL AND COAL SURFACES BY ADSORPTION OF DYES

Bogdan J. Slomka, M. Robert Dawson and William H. Buttermore,

Ames Laboratory, Iowa State University, Ames, Iowa 50011

### ABSTRACT

A dynamic method is described for dye adsorption measurements to characterize mineral and coal surfaces for the evaluation of coal cleaning processes. Samples of increasing mineral content were prepared by density separation of a narrowly sized (300 to 425  $\mu\text{m}$ ) wet-sieved coal. The rates and extents of the adsorption of ionic dyes on Illinois No. 6 coal were observed to be highly dependent on mineral content and particle size of ground coal samples. A linear correlation was observed between the adsorbed quantity of dye and the total mineral content of coal samples. Dry-sieved coals were found to be coated by fine material of high mineral ash content which adsorbed greater than 20 times more methylene blue per gram than wet-sieved particles. In preliminary experiments with methylene blue dye, clay was found to adsorb significantly more dye than quartz, pyrite, calcite or low-ash specific gravity fractions of coal.

### INTRODUCTION

Adsorption of dyes from solutions has been extensively used for the determination of surface areas and examining the accessibility of porous structures to dye molecules; and has become a standard practice in the qualitative evaluation of active carbons in industry (1, 2, 3). It is well known that surface properties of solid adsorbents govern the adsorption of molecules from liquid solutions. Generally, increasing the surface polarity of active carbons (e.g., by oxidation) causes an increase in adsorption of the more polar component in binary liquid mixtures (4). For instance, adsorption of stearic acid by nonporous carbons, free from surface oxygen complexes, results in a closely-packed monolayer, whereas on surfaces bearing oxygen complexes, the formation of a complete monolayer is not accomplished, even at the highest possible concentrations of the acid solution (5). Similarly, surface acidity of active carbons strongly influences adsorption of aromatic amines and phenol derivatives from organic solutions (6).

For coals, it has been argued that a portion of the mineral matter of coal, predominantly pyrite and alkali metal compounds, interacts with dye molecules, affecting adsorption results. However, adsorption of dyes is not influenced by surface oxygen groups, except in the case of lignites (7).

Literature references dealing specifically with the use of adsorption methods to evaluate either cleanability of coals or the effects of coal-cleaning processes on coal surface properties have not been found. However, adsorption of surfactants has been used for predicting how easily a stable slurry can be made using a given coal (8). With careful selection of an adsorbate (with respect to polarity, acidity, surface activity, molecular area in the adsorbed state, etc.), adsorption from solutions could become a sensitive 'molecular probe' for investigating coal and mineral surfaces. In particular, adsorption from liquid phases appears to

have the potential to become a useful tool for detecting changes in surface properties (e.g., hydrophobicity) which are important for coal preparation processes.

The primary goal of this study was to develop a practical method for quantifying the selective adsorption of dye on coal and mineral surfaces. In these preliminary tests, adsorption profiles were obtained for: coal samples of different total mineral content, specific mineral species, and coal samples of different particle size.

## EXPERIMENTAL

### Materials

Non-buffered 64.0 mg/l aqueous solutions of methylene blue were prepared by drying the dye under nitrogen at 110°C for 2 hours and dissolving in deionized distilled water.

A bulk sample of coal with a narrow range of particle size was obtained by dry-sieving Illinois No. 6 coal to obtain 330 to 425  $\mu\text{m}$  coal particles. Test samples were then prepared by wet-sieving to remove undersize material from the particle surfaces. Samples of increasing mineral content were prepared by density separation of the wet-sieved particles using aqueous solutions of CsCl at several specific gravities between 1.30 and 1.80 g/cc. Mineral samples for analysis included a single pyrite cube from Ward's Natural Science Establishment; kaolinite flint-clay from A. P. Green quarries of Mexico, Missouri; and single crystals of calcite and quartz obtained from the Department of Earth Sciences at Iowa State University. Mineral samples were ground using a mortar and pestle, and 330 to 425  $\mu\text{m}$  particles were obtained by wet-sieving. Preliminary tests were performed to determine the applicability of the dynamic adsorption technique to fine particle sizes. Illinois No. 6 coal was pulverized and dry-sieved to obtain samples smaller than 150  $\mu\text{m}$  and 44  $\mu\text{m}$ .

### Procedures and Analysis

A continuous-flow apparatus was developed for dynamic measurements of adsorption from liquid phases on solids. Figure 1 shows the configuration of the main components. In a typical experiment, a pre-weighed sample of coal is placed in a sample cell and fixed between two 0.5- $\mu\text{m}$  stainless steel frits. The sample cell is then connected to a six-port switch valve and evacuated to remove air. The valve is set initially to direct the solution of dye to by-pass the cell containing the sample, causing it to flow directly through the ultraviolet/visible detector (Varian UV-50). As soon as a baseline is established for the dye solution, the flowing solution is directed through the sample of coal to the UV/Vis detector. The absorbance measured for the effluent leaving the sample cell is due only to dye not adsorbed by the coal sample. The apparent absorbance is recorded at a fixed wavelength as a function of time using an A/D converter at a sampling rate of 2  $\text{sec}^{-1}$ . This dynamic method of adsorption measurement allows for continuous replacement of the fluid phase in contact with the coal sample, which is not possible in a closed, static system. The rates of adsorption can be continuously measured as a function of time, giving characteristic profiles of adsorption rate, while the total adsorbate uptakes are obtained by integration of the rate profiles over the

time of adsorption. The detector response to dye concentration was linear for the concentrations and wavelengths used in the experiments. The detector was operated in the visible range at 610 nm. Based on preliminary results, two flow rates of solutions were selected, 1 and 0.5 ml/minute, according to the sample size of the materials tested.

To evaluate the adsorptive components of coal and mineral surfaces, coal samples of uniform particle size and increasing mineral content were analyzed. Total mineral content was determined by standard ash analysis. Samples with very low ash content were used to approximate a non-mineral coal surface. To evaluate specific mineral adsorptive characteristics, mineral samples of uniform particle size and composition were analyzed. Ground coal samples of different mean particle size were analyzed to determine the effect of particle surface area.

## RESULTS AND DISCUSSION

Figure 2 shows the correlation between dye uptake and available mineral surface (measured as total ash content) for several coal samples. Quantitative data is presented in Table 1. As shown in Figure 2 and Table 1, increased dye uptakes and adsorption rates are observed for coals with higher mineral content. This implies that methylene blue dye is preferentially adsorbed on mineral surfaces. Figure 3 presents adsorption profiles for samples of different specific gravity (3a), different mineral species (3b), and different particle size (3c). In each graph, the adsorption curve for the head sample of wet-sieved, 300 to 425  $\mu\text{m}$  Illinois No. 6 coal is provided for reference. Data presented in Figure 3a suggest that specific gravity fractions heavier than 1.55 g/cc contain highly adsorbing constituents. Tests are currently underway to identify these constituents from known components of coal mineral matter by testing their behavior during dye adsorption. Figure 3b presents the results of methylene blue adsorption on several common coal mineral species compared to the adsorption pattern for the 300 to 425  $\mu\text{m}$  wet-sieved Illinois No. 6 coal head sample. Based on these data, clay minerals are the most probable single constituent responsible for the high adsorption values reported. Contrary to suggestions by Nandi and Walker (7), pyrite showed the smallest adsorption per gram of sample. In our experiments, pyrite was found to adsorb less methylene blue (Figure 3b) than the coal fraction of 1.30-1.35 specific gravity (Figure 3a).

Early attempts to correlate the extent of adsorption with total coal mineral content using dry-sieved coal samples were unsuccessful. It was later determined that fine-sized material high in mineral content adhered to larger particles and very strongly adsorbed the dye. Figure 3c shows the methylene blue adsorption profiles for dry-sieved and wet-sieved samples of the 300 to 425  $\mu\text{m}$  Illinois No. 6 coal. The integrated uptakes of the dye (Table 1) indicate that the coating of fine material, constituting 20.2% by weight of the dry-sieved sample, adsorbs about 20 times more dye than the wet-sieved coal. Consequently, for later experiments only wet-sieved coals were used.

#### ACKNOWLEDGMENTS

Ames Laboratory is operated for the U. S. Department of Energy by Iowa State University under Contract No. W-7405-ENG-82. This work was supported by the Assistant Secretary for Fossil Energy through the Pittsburgh Energy Technology Center. We gratefully acknowledge Dr. Robert Cody and the Department of Earth Sciences at Iowa State University for mineral samples and helpful discussions.

#### REFERENCES

1. Kudo, K., H. Hosada, S. Honma, and M. Komatsu. Journal of the Fuel Society of Japan, 1973, 52:335.
2. Hassler, J. W. "Active Carbon", Brooklyn Chemical Publishing Co., 1951.
3. Rist, L. P. and D. P. Harrison. "Surface Area and Pore Development During Lignite Activation", Fuel, March, 1985, 64:291-7.
4. Jankowska, H., A. Swiatkowski, J. Oscik, and R. Kusak. Carbon, 1983 No. 2, 2:117
5. Kipling, J. J. "Adsorption from Solutions of Non-Electrolytes", Academic Press, New York, 1965, p. 115.
6. Oda, H. and C. Yokokawa. Carbon, 1983 No. 5, 21:485.
7. Nandi, S. P. and P. L. Walker, Jr. "Adsorption of Dyes from Aqueous Solutions by Coals, Chars, and Active Carbons", Fuel, October, 1971, 50:345-66.
8. Liang, W. and L. Jiang. "Effect of Wettability and Adsorptability of Coal on the Slurryability of Coal", Journal of Coal Quality, April, 1987, 44-8.

Table 1. Adsorption of Methylene Blue Dye on Minerals and Illinois No. 6 Coal (adsorption time: 10 minutes)

<u>Sample</u>	<u>Adsorption, mg/g</u>
<b><u>Minerals</u></b>	
Pyrite	0.017
Quartz	0.030
Calcite	0.135
Clay	0.577
<b><u>Coal</u></b>	
- 45 um, dry grind	4.07
-150 um, dry grind	3.09
-425 + 300 um	
dry-sieved	2.50
wet-sieved	0.51
<b><u>Specific Gravity Fractions of Coal</u></b>	
> 1.80	1.15
-1.80 + 1.65	0.671
-1.65 + 1.55	0.585
-1.55 + 1.50	0.535
-1.50 + 1.45	0.462
-1.45 + 1.40	0.357
-1.40 + 1.35	0.291
-1.35 + 1.30	0.185
< 1.30	0.142

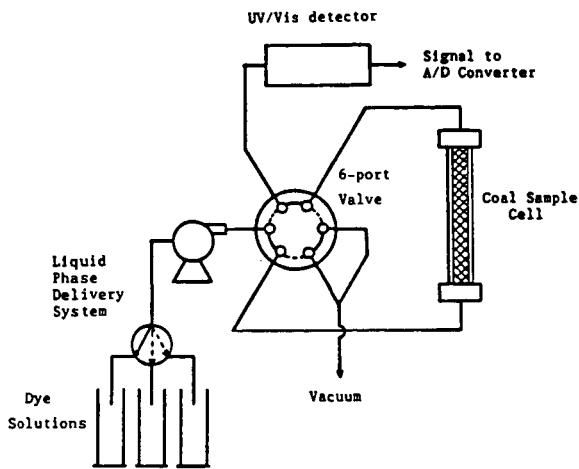


Figure 1. Continuous Flow Dye Adsorption Apparatus

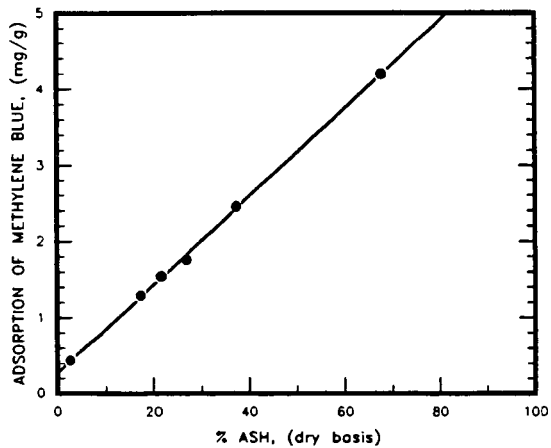
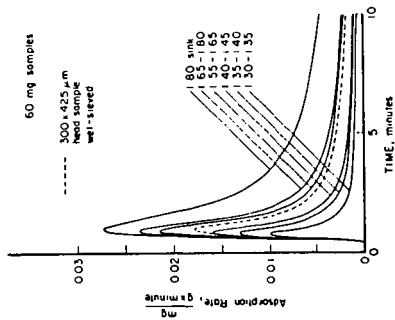
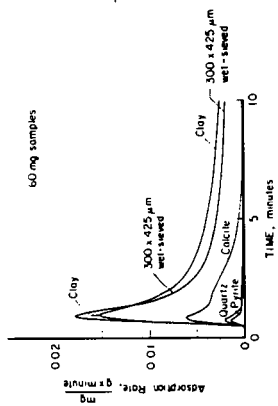


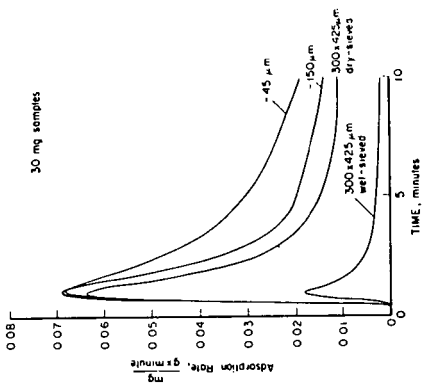
Figure 2. Dye Uptake vs Coal Ash Content (Adsorption time: 6 hours, Flow Rate: 1. ml/min.)



3a. Specific Gravity



3b. Mineral Species



3c. Particle Size

Figure 3. The Effects of Sample Characteristics on Methylene Blue Dye Adsorption.

ASSESSMENT OF THE HYDROPHOBICITY OF FINE COAL PARTICLES  
IN VARIOUS AQUEOUS MEDIA BY VISCOSITY MEASUREMENTS.

Geatesh K. Tampy, David H. Birlingmair, and Lawrence E. Burkhart  
Ames Laboratory, Iowa State University  
Ames, Iowa 50011

ABSTRACT

Viscosity measurements have been shown to provide a good indication of the relative hydrophobic and hydrophilic nature of fine coal particles in various aqueous media. Slurries of float and sink fractions of pulverized Upper Freeport run-of-mine coal in various electrolytes showed evidence of structure formation under the influence of shear. This structuring reaches a steady state at very high shear rates; by examining the viscosities at the higher shear rates, the inter-particle interaction effects and hydrodynamic effects may be distinctly determined. When the particles are more hydrophobic, the tendency for structure formation is greater. This is reflected in the response of the slurry to shear. Viscosity measurements of  $\alpha$ -alumina particles in slurries of various pH, and corresponding zeta potential measurements, confirmed that the highest viscosity and the maximum structure formation occurred at the PZC, when the particle surfaces are most hydrophobic.

INTRODUCTION

The rheological properties of slurries are influenced both by the surface characteristics of the particles, and by the properties of the suspending liquid(1-4). Measurement of the appropriate rheological parameters offers a simple means of comparing the relative hydrophobicity of particles in different aqueous media and also of comparing the effect of different chemical treatments on the hydrophobicity of the particles. Current work in our laboratories involves surface modification by chemical pretreatment of coal during the size-reduction stage that typically precedes beneficiation in most advanced coal cleaning processes. The rheology measurements can be used to characterize the changes to the particle surfaces that have been brought about by the pretreatment.

THEORY

In the Einstein equation(5) for suspensions of non-interacting spherical particles, the viscosity increase due to the presence of the particles is a function only of the volume fraction of the particles. The equation is valid only for relatively dilute suspensions(6). In a simple shear field, this still represents Newtonian flow, in the sense that shear stress is linearly related to shear rate.

For more concentrated slurries, particle interactions also affect the viscosity of the suspension since various degrees of aggregation or 'structuring' of the particles will occur(7). If the particles are suspended in an aqueous medium and have strongly hydrophobic surfaces, the preference of the water molecules to associate with other water molecules, rather than with the particle surfaces, will promote aggregation. Ionic or polar surfaces on the

other hand, can associate more freely with the polar water molecules and are thus hydrophilic(8). The presence of an electrostatic charge at the surface reduces the tendency for such particles to aggregate. Aggregation causes the viscosity of the suspension to increase for two reasons. The particle assemblages tend to entrap liquid within themselves, increasing the effective volume fraction of the solids, and thus increasing the viscosity in accordance with the Einstein equation(9). Additional energy is also dissipated when the particle assemblages interact with each other during shear flow.

In most slurries containing particles of a few micrometers or smaller in size, the basic flow units are considered to be small clusters of particles and entrapped liquid called flocs(10,11). At rest, the flocs are grouped into larger flow units called aggregates. As shear is imposed on the slurry, the aggregates break down into individual flocs, until at sufficiently high shear, a linear shear stress-shear rate relationship is observed, as shown in Figure 1. This linear portion of the curve represents a steady-state energy relationship between the tendency of the flocs to form doublets, and the tendency of the shear forces to break-up the doublets. The curve is characteristic of pseudoplastic shear-thinning behavior. The Bingham yield stress,  $\tau_B$ , is defined as the extrapolated intercept of the linear portion of the curve and the apparent viscosity,  $\eta$ , is the ratio of the shear stress to the shear rate at any point on the curve.

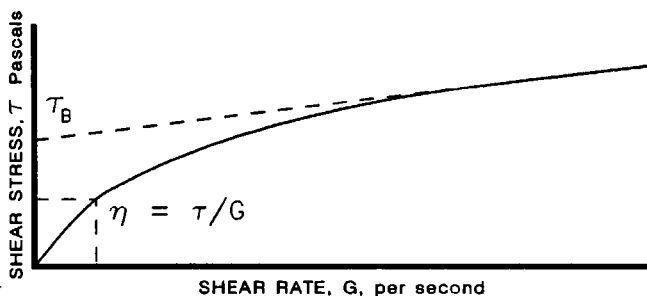


Figure 1. Typical shear stress-shear rate relationship showing pseudoplastic shear-thinning behavior.

Michaels and Bolger(10) found that  $\tau_B$  increased with the square of the floc volume fraction ( $\phi_F$ ), and with the strength of the interparticle interactions. The relationship is expressed as:

$$\tau_B = \frac{A}{a d_F^2} \phi_F^2 \quad 1)$$

where A is a constant which depends on the net force of attraction between the particles. The parameter,  $d_F$ , is the average floc diameter, and 'a' is the distance between flocs and is thus a measure of the attraction between flocs. They also found that the ratio  $A/d_F^2$  was constant and independent of the chemical composition of the liquid used. Thus  $\tau_B$  depended only on 'a', which is a measure of the degree of interaction between flocs, and on  $\phi_F$ , the floc volume. Since the tendency of particles to aggregate is

greater when they are more hydrophobic, this implies that greater hydrophobicity would yield a higher value of  $\tau_b$ .

Hunter and co-workers(11), who extended the "aggregate-collision" theory of Michaels and Bolger(10), showed that  $\tau_b$  varied as the square of the zeta potential of the particles in the suspension.  $\tau_b$  was a maximum when the zeta potential was zero. The tendency for particles to aggregate is also a maximum at this point.

#### EXPERIMENTAL

To study the effects of the different treatments on the surface properties of the organic and mineral portions of Upper Freeport run-of-mine coal, the coal was first ground to an average particle size of about 10  $\mu\text{m}$ , separated into an organic-rich fraction which had only 4.9% ash, and a mineral-rich fraction which had 55.3% ash. This was done by centrifugal float-sink separation using a liquid of specific gravity 1.4. The organic and mineral-rich fractions were filtered, vacuum dried, and then used to form a variety of different slurries each of which had the same solid concentration (volume fraction). However, the pH of the suspending solutions was different. For each fraction, one additional slurry was made using a 0.1M solution of sodium dithionite. The viscosities of the slurries were measured using a Haake concentric cylinder viscometer. The viscosities of the suspending electrolytes were measured using a Cannon-Fenske capillary viscometer, and very little variation among them was noticed.

As a further test of the method, viscosity and pH measurements were also made on slurries of  $\alpha$ -alumina particles, which had more homogenous surfaces. The alumina was obtained from Fisher Scientific Company, and was further ground to an average particle size of about 10  $\mu\text{m}$ .

#### RESULTS

The results of beneficiation tests on separate samples of the same Upper Freeport run-of-mine coal used in this work are given in an accompanying paper(12). Separation was carried out by oil agglomeration, microbubble frit flotation, and microbubble foam flotation. They were made at different pH levels and also in the presence of 0.1M sodium dithionite. In each case the coal which had been pretreated with sodium dithionite ( $\text{Na}_2\text{S}_2\text{O}_4$ ) yielded substantially better results than when only pH control was used. To understand the changes to the surfaces of the particles that might have caused such a response, the viscosity curves obtained in this work were examined.

The shear responses of the mineral-rich fractions of Upper Freeport coal in the various electrolytes are shown in Figure 2. The only difference between the curves is in the liquid used for making each slurry. The curves are all typical of shear thinning behavior. The initial nonlinear portion of the curves represents increasing break-up of aggregates. When these are all destroyed, the curve becomes linear and represents a steady-state relation between the formation and break-up of floc doublets. The slopes of the linear part of the curve is a function only of the

floc volume. These slopes, and hence the floc volumes of the slurries, are essentially equal. This is not unreasonable since each slurry has the same particle concentration, and was subjected to the same shear cycle in the viscometer.

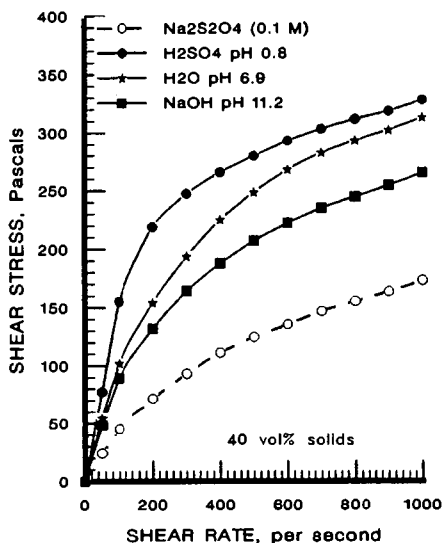


Figure 2. Shear response of slurries of the mineral-rich fraction.

Table 1.  $\tau_B$  values for slurries of the mineral-rich fraction.

pH	$\tau_B$ , Pascals
0.8	245
6.9	204
11.2	162
0.1M Na <sub>2</sub> S <sub>2</sub> O <sub>4</sub>	85

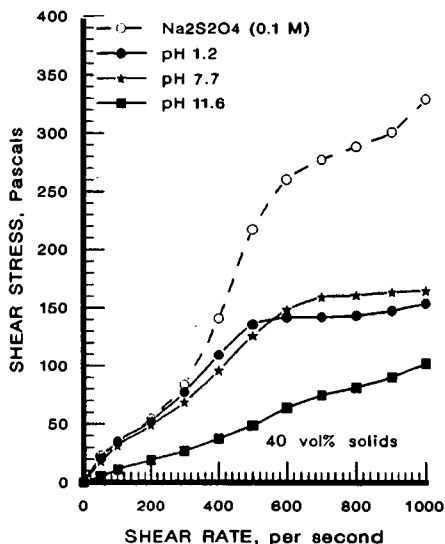


Figure 3. Shear response of slurries of the organic-rich fraction.

Table 2.  $\tau_B$  values for slurries of the organic-rich fraction.

pH	$\tau_B$ , Pascals
1.2	130
7.7	150
11.6	11
0.1M Na <sub>2</sub> S <sub>2</sub> O <sub>4</sub>	217

The Bingham yield stress,  $\tau_B$ , found by extrapolating the linear portion of each curve to zero shear rate, is different for each slurry. The values of  $\tau_B$  are given in Table 1. The Bingham yield stress is a function of both the floc volume and the strength of the net attractive interaction force between flocs. Since the floc volumes are essentially equal for each slurry,  $\tau_B$  should be directly related to the strength of the particle interactions. Lower values of  $\tau_B$  indicate a lower net particle-particle interaction (or more correctly, a greater tendency for particle-medium association), a

lesser tendency towards flocculation, and hence a stronger hydrophilic character of the particle surfaces. Clearly, the particles in the slurry treated with sodium dithionite were most hydrophilic; the curve for this slurry is significantly lower than those slurries in which only pH was varied.

Figure 3 shows the shear response of the slurries formed with the organic rich fractions. Although some shear thickening appears at intermediate shear rates, the slurries still showed shear thinning at low and high shear. This type of behavior is not unusual for hydrophobic systems(3,13). For these slurries, the plastic viscosities are not so nearly equal as they were for the mineral-rich slurries. A clear interpretation of the result is difficult and will not be attempted until more data are available. However, the substantial difference in the  $\tau_B$  values shown in Table 2, for the slurry treated with sodium dithionite, would seem to overshadow any effect of the floc volume difference in reaching a conclusion that the particles in the sodium dithionite slurry were most hydrophobic.

These results suggest that the improved beneficiation results obtained by using sodium dithionite was due to alteration of surfaces of both the organic-rich and mineral-rich coal particles, since the organic-rich particles became more hydrophobic and the mineral-rich particles became more hydrophilic. In other words, the surface characteristics of the two fractions were altered in different ways. Additional evidence, given in the companion paper(12) to this work, is that both sulfur and ash reduction was improved. Reduction of a sulfide surface by an appropriate reductant is known to improve sulfur rejection, but its effect on either carbonaceous surfaces or ash surfaces is less clear and additional work will be required to explain this result.

Figure 4 shows the shear response of  $\alpha$ -alumina slurries at various pH values and is included to demonstrate the variation of  $\tau_B$  with particle interaction effects on slurries made up of particles with more homogenous surfaces. At the point of zero zeta potential, (see Figure 5) the value of  $\tau_B$  (Table 3) is a maximum, showing maximum particle-particle interaction, minimum particle-liquid interaction, and therefore maximum hydrophobicity. This is only expected, since the particles being least charged can least interact with the polar aqueous medium, and also have the least particle-particle repulsion.

**Table 3.** Yield Stress ( $\tau_B$ ) at various pH for  $\alpha$ -alumina slurries. The corresponding zeta potential values ( $\zeta$ ) are also shown.

pH	$\zeta$ , mV	$\tau_B$ , Pascals
6.4	+10	76.6
8.3	0	102.4
9.8	-27	33.6
10.0	-29	18.1

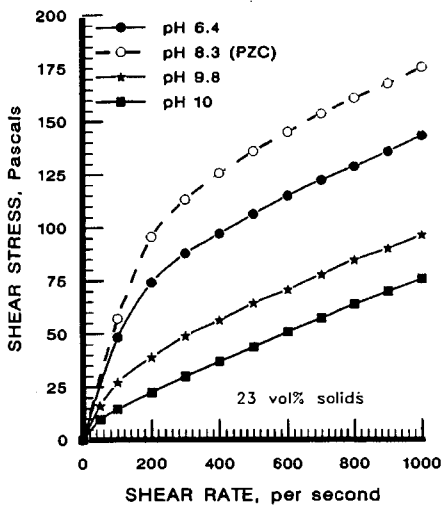


Figure 4. Shear response of slurries of  $\alpha$ -alumina.

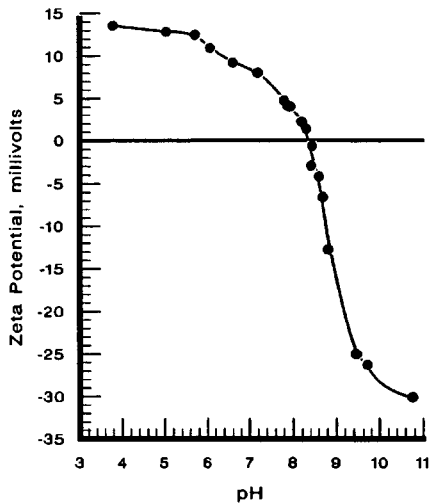


Figure 5. Zeta potential of  $\alpha$ -alumina particles at different pH.

#### CONCLUSIONS

Rheological measurements have been used to study the hydrophobic/hydrophilic behavior of coal and mineral particles in various aqueous media, in an effort to explain why the use of sodium dithionite as an additive during grinding of a coal slurry produced improved beneficiation results. The measurements suggest that this was due to a beneficial effect on the surface properties of both the organic and mineral fractions of the coal. The organic fraction became more hydrophobic and the mineral fraction became more hydrophilic in the slurries containing 0.1M sodium dithionite. These results do not necessarily contradict the contact angle measurements reported earlier(12), if the possibilities of kinetic effects are taken into account. The time taken to prepare the dispersed slurries for viscosity measurements could allow for relatively slow changes to the particle surfaces. These effects would not be expected to show up in the contact angle measurements which did not allow for extended coal-sodium dithionite solution contact. The exact mechanisms that effect these changes are not known at this time. However, additional studies are underway.

#### ACKNOWLEDGEMENT

Ames Laboratory is operated for the U. S. Department of Energy by Iowa State University under Contract No. W-7405-ENG-82. This work was supported by the Assistant Secretary for Fossil Energy through the Pittsburgh Energy Technology Center.

#### REFERENCES

1. Adiga, K.C.; Shah, D.O.; Colloids and Surfaces, **1982**, 4, 271-284.
2. Kesavan, S.K., Powder Technology, **1987**, 50, 15-23.
3. Kaji, R.; Muranaka, Y.; Miyadera, H.; Hishinuma, Y.; AICHE J., **1987**, 33, 11-18.
4. Tadros, E. in "Polymer Adsorption and Dispersion Stability", Goddard, E.D.; Vincent, B. eds.; ACS, Washington, 1984, pp. 411-428.
5. Jeffrey, D.J.; Acrivos, A.; AICHE J., **1976**, 22, 417-432.
6. Heimenz, P.C.; "Principles of Colloid and Surface Chemistry", Marcell Dekker, New York, 1977, pp. 59-80.
7. Hoffman, R.L.; "Science and Technology of Polymer Colloids", vol 2, Poehlein G.W.; Ottewill, R.H.; Goodwin, J.W.; eds., Martinus Nijhoff, Boston, 1983, pp. 570-588.
8. a) Tamy, G.K; PhD Thesis, Ohio University, March 1988. b) Tamy, G.K., Prudich, M.E.; Savage, R.L; Williams, R.R.; Energy & Fuels, 1988, in press.
9. a) Gillespie, T.; J. Colloid Interface Sci. **1966**, 22, 563-572. b) Gillespie, T.; J. ibid., **1983**, 94, 166-173.
10. Michaels, A.S.; Bolger, J.C.; Ind. Eng. Chem. Fundam. **1962**, 1, 153-162.
11. a) Hunter, R.J.; Nicol, S.K.; J. Colloid Interface Sci. **1968**, 28, 250-259. b) Friend, J.P; Hunter, R.J; ibid. **1971**, 37, 548-556. c) Firth, B.A; ibid., **1976**, 57, 257-265. d) Firth, B.A; Hunter, R.J.; ibid., **1976**, 57, 248-256. e) Firth, B.A; Hunter, R.J.; ibid., **1976**, 57, 266-275. f) van de Ven, T.G.M.; Hunter, R.J.; Rheologica Acta, **1977**, 16, 534-543. g) van de Ven, T.G.M.; Hunter, R.J.; J. Colloid Interface Sci. **1979**, 68, 135-143. h) Hunter, R.J.; Frayne, J.; ibid., **1979**, 71, 30-38. i) Hunter, R.J.; Frayne, W.; ibid. **1980**, 76, 107-115.
12. Tamy, G.K; Birlingmair, D; Burkhart, L.E; Prepr. Conf. Am. Chem. Soc. Div. Fuel Chem. **1988**, 33, in press. see accompanying paper.
13. Umeya, K.; Kanno, T. J. Rheol., **1979**, 23, 123-139.

## THE HYDROPHOBIC CHARACTER OF PRETREATED COAL SURFACES

R. Jin, Y. Ye and J.D. Miller  
Department of Metallurgy and Metallurgical Engineering  
University of Utah, Salt Lake City, UT 84112

### INTRODUCTION

In recent years, the production of superclean coal has been of considerable interest in order to partially replace oil and natural gas as fuel sources. Of all the coal-cleaning processes, flotation is one of the most versatile. Carbon dioxide coal flotation is a new technology developed at the University of Utah.<sup>(1)</sup> Compared with conventional flotation, carbon dioxide flotation enhances the ash rejection and increases flotation recovery for coals of different rank with the exception of lignite. However, significant improvement of the hydrophobicity and flotability of lignite has been found after controlled thermal pretreatment. The potential for the production of superclean coal by carbon dioxide has been demonstrated in bench scale flotation experiments.<sup>(2)</sup>

### EXPERIMENTAL

Coal samples and experimental methods of flotation, contact angle measurement and bubble attachment time measurement have been described in a previous paper.<sup>(3)</sup>

In addition, a diffuse reflectance FTIR (DRIFT) technique has been used to characterize the coal surface.<sup>(3)</sup> More recently, an attenuated total reflectance (ATR) accessory, the CIRCLE™ cell with a ZnSe rod from Spectra-Tech Inc., was used in ATR-FTIR spectroscopy. The coal for the ATR-FTIR analysis was ground to minus 1 micron in a ceramic mortar with distilled water at pH 6-6.5 before transferring to the CIRCLE™ cell at a coal/water ratio of 0.5 by weight. A spectrum for each coal was obtained by subtraction of water spectrum from the spectrum of the coal/water suspension. Both spectra were collected under the same conditions with the empty CIRCLE™ cell as a background.

XPS experiments were conducted with the Hewlett-Packard 5950 B instrument using monochromatic Al K<sub>α1,2</sub> radiation at 1487 eV. Power at the X-ray source was 400 watts and the chamber vacuum was controlled at 10<sup>-10</sup> torr. An electron gun at 6 eV supplied a flux of low-energy electrons to the coal surface to minimize heterogeneous charging artifacts in the resulting spectra.

### RESULTS AND DISCUSSION

#### Coal Hydrophobicity

As shown in Figs. 1 and 2, it has been found by reagent-less Hallimond tube flotation and by contact angle and bubble attachment time measurements that the hydrophobicity and flotability of coals increase with an increase in coal rank, reaching a maximum for low-volatile bituminous coal and then decreasing with a further increase in coal rank. These traditional methods are excellent indicators of the macroscopic hydrophobicity of the coal surface. However, to better describe the hydrophobic/hydrophilic balance at a coal surface, it is important to establish the corresponding chemical characteristics of these coals.

DRIFT- and ATR-FTIR spectroscopy can provide a more detailed description of the coal surface than elemental bulk composition or chemically determined acid-group content as used by previous investigators.<sup>(4)</sup> These two FTIR techniques have been used to evaluate the hydrophobicity of fine coals by a spectroscopic criterion--the hydrophilicity index--which contrasts the relative abundance of surface hydrophilic groups OH and COOM with the relative abundance of surface hydrophobic groups ArH and RH.<sup>(3)</sup> Using the hydrophilicity index determined by both DRIFT- and ATR-FTIR spectroscopy, a rank-dependence of coal hydrophobicity can be plotted as shown in Fig. 2. Note that the hydrophobic character of coal estimated by the hydrophilicity index varies with coal rank in much the same fashion as bubble attachment time, contact angle, and flotation recovery. Since the coal rank is essentially classified by the carbon content, the hydrophilicity index determined by FTIR

spectroscopy is obviously a more detailed index for evaluating coal hydrophobicity than coal rank or carbon content.

To ensure the surface sensitivity of the FTIR techniques and confirm the conclusions reached from the FTIR analysis, XPS has also been used to evaluate the hydrophobic character of fine coals. The ratio C/O determined by XPS has also been used to define a hydrophobicity index for the coals. Such a hydrophobicity index for six coals of different rank is presented in Fig.1. Notice that the rank-dependence of coal hydrophobicity estimated by XPS agrees with that evaluated by other methods such as FTIR spectroscopy, flotation response, contact angle and bubble attachment time measurements.

### Enhanced Hydrophobicity of Pretreated Coal

#### Characterization of CO<sub>2</sub>-treated coal

As shown in Table 1, it has been found that CO<sub>2</sub> pretreatment increases coal hydrophobicity. Table 2 indicates that enhanced hydrophobicity of CO<sub>2</sub>-pretreated coals results in an increased flotation recovery and enhanced ash rejection for coals of different rank with the exception of lignite. It has also been found that coals of middle ranks such as high-, medium-, and low-volatile bituminous coals are most amenable to carbon dioxide coal flotation.<sup>(5)</sup>

Oxidation can result in a reduced hydrophobicity of CO<sub>2</sub>-pretreated coals. Figure 3 illustrates that oxidation of a CO<sub>2</sub>-pretreated low-volatile bituminous coal in air reduces the coal hydrophobicity and restores the original lower hydrophobic character after about 20 hours of oxidation. Fortunately, coal oxidation is a slow process. No significant loss in coal hydrophobicity was observed during the first couple hours which was long enough to complete flotation experiments.

The success of CO<sub>2</sub> coal flotation has been attributed to the coal's high adsorption potential for CO<sub>2</sub>.<sup>(6)</sup> It has been found by monitoring the OH absorption band using in-situ FTIR spectroscopy that pore water and hydration water in coal are displaced by CO<sub>2</sub> during pressure treatment, which results in enhanced coal hydrophobicity as shown in Fig.4.

A model for carbon dioxide adsorption by coal is being considered, and a schematic drawing of the microstructure is shown in Fig.5. This drawing represents a final state of the adsorption process, where all the pore water and hydration water have been replaced by CO<sub>2</sub>. Before CO<sub>2</sub> pretreatment, the positions of CO<sub>2</sub> molecules in this drawing are predominantly occupied by H<sub>2</sub>O molecules. Displacement of the H<sub>2</sub>O molecules by CO<sub>2</sub> molecules during pressure treatment and CO<sub>2</sub> nanobubble formation at the coal surface on pressure release are believed to be responsible for the improved flotation performance.

#### Characterization of thermally-treated coal

It has been found that low-temperature thermal treatment significantly increases the hydrophobicity of lignite as suggested by FTIR hydrophilicity index determinations and confirmed by bubble attachment time measurements/flotation response (see Fig.6). It is believed that the increased hydrophobicity of lignite is attributed to the removal of pore water, hydration water and some organic OH functional groups as well as the diffusion of volatile matter to the surface and the reorientation of surface functional groups. As shown in Table 2, it has been found that controlled thermal treatment can also increase the hydrophobicity of subbituminous coal and anthracite. Finally it should be noted that the thermal treatment improves the flotation separation of lignite from mineral matter.

### SUMMARY

Increased hydrophobicity and hence the flotability of coals of different rank has been observed for CO<sub>2</sub> pretreatment and/or controlled thermal pretreatment. DRIFT- and ATR-FTIR and XPS techniques have been used to determine the surface chemical characteristics in order to evaluate coal hydrophobicity. These results agree very well with those determined by traditional methods. The enhanced hydrophobicity of CO<sub>2</sub>-treated coal is attributed to the high specific affinity of coal for CO<sub>2</sub> which results in the displacement of pore water and hydration water by CO<sub>2</sub> and on pressure release leads to nanobubble formation at the coal surface in aqueous suspension. Increased hydrophobicity of

lignite by thermal treatment arises from the removal of pore water, hydration water and some organic OH functional groups as well as the diffusion of volatile matter to the surface and the reorientation of surface functional groups.

The financial support provided by the U.S. Department of Energy under Grant No. DE-FG22-85PC80530 is greatly acknowledged.

#### REFERENCES

1. Miller, J.D. and Misra, M., 1987. U.S. Patent No. 4,676,804.
2. Miller, J.D. and Misra, M., 1985. Coal Preparation, 2:69.
3. Jin, R., Ye, Y. and Miller, J.D., 1987. "Evaluation of coal hydrophobicity by diffuse reflectance FTIR spectroscopy," presented at the 8th National Convention of the Royal Australian Chemical Institute, Aug.24-28, and submitted to Colloids and Surfaces.
4. Miller, J.D., Laskowski, J.S. and Chang, S.S., 1983. Colloids and Surfaces, 8:137.
5. Miller, J.D., Jin, R., Ye, Y. and Sadowski, Z., 1987. "Carbon dioxide for fine coal flotation," Final Report to U.S. Department of Energy, Grant No. DE-FG22-85PC80530.
6. Jin, R., Ye, Y. and Miller, J.D., 1988. "Studies of carbon dioxide adsorption at the surface of coal by in-situ FTIR spectroscopy," presented at the 117th AIME Annual Meeting, Jan.25-28, Preprint No. 88-300, submitted to Fuel.

Table 1 Contact Angle and Bubble Attachment Time for Different Gas Bubbles on a Polished Surface of Low-Volatile Bituminous Coal

Pressure Treatment Using Corresponding Gas Phase at 20 psi	Gas Phase of Bubbles	Contact Angle (degrees)	Bubble Attachment Time (ms)
Yes	Air	49-52	170-190
Yes	N <sub>2</sub>	50-51	140-160
Yes	CO <sub>2</sub>	54-56	20-25
No	Air	47-49	180-200
No	N <sub>2</sub>	50-51	170-190
No	CO <sub>2</sub>	51-53	140-150

Table 2 Enhanced Hydrophobicity and Improved Flotation Performance of Pretreated Coals of Different Rank

Coal Rank	Ratio of Attachment Times $\tau_{CO_2}/\tau_{air}$	Increased Flotation Recovery by CO <sub>2</sub> Pretreatment	Enhanced Ash Rejection by CO <sub>2</sub> Pretreatment	Increased Hydrophobicity by thermal Pretreatment	Enhanced Ash Rejection by thermal, Pretreatment
ANT	0.70	Yes	Yes	Yes	
LVB	0.80	Yes	Yes	No	
MVB	0.69	Yes	Yes	No	
HVB	0.66	Yes	Yes	No	
SUB	1.0	Yes	Yes	Yes	
LIG	1.0	No	No	Yes	Yes

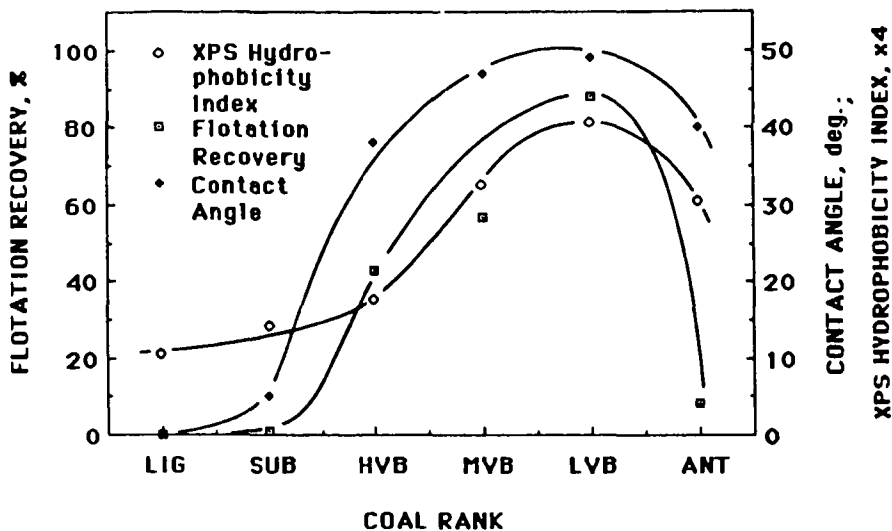


Figure 1 Coal hydrophobicity evaluated by Hallimond tube flotation, contact angle measurement, and XPS analysis as a function of coal rank. ANT = Anthracite, LVB = Low-volatile bituminous coal, MVB = Medium-volatile bituminous coal, HVB = High-volatile bituminous coal, SUB = Subbituminous coal, LIG = Lignite.

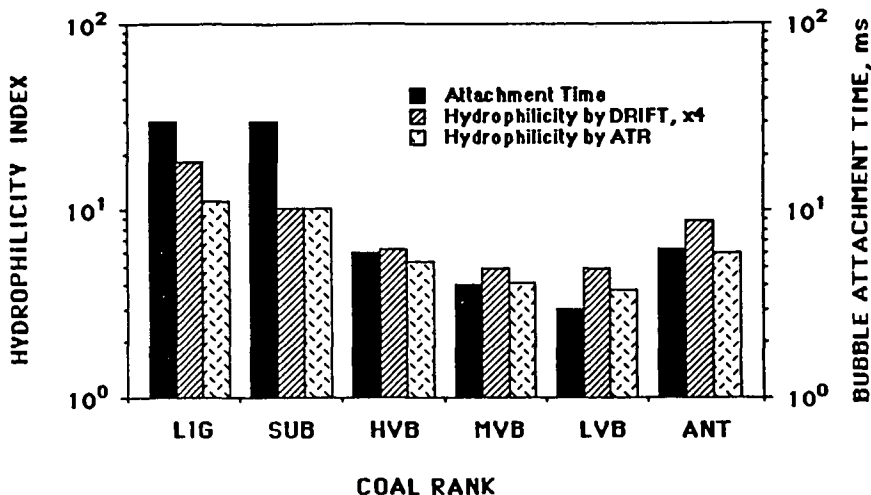


Figure 2 Hydrophobic character of coal as described by bubble attachment time and the hydrophilicity index determined from DRIFT- and ATR-FTIR spectra.

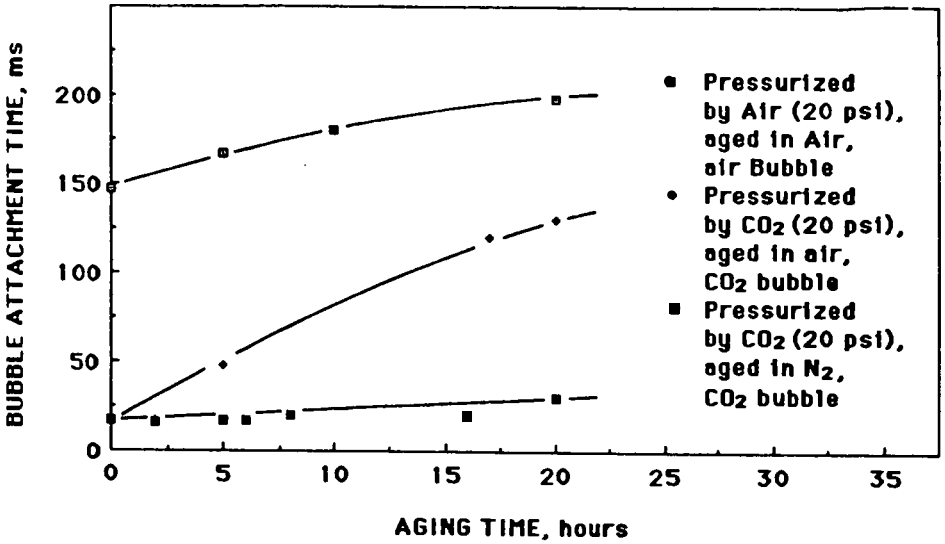


Figure 3 Bubble attachment time measured on the polished surface of a pretreated low-volatile bituminous coal as a function of aging time of the coal.

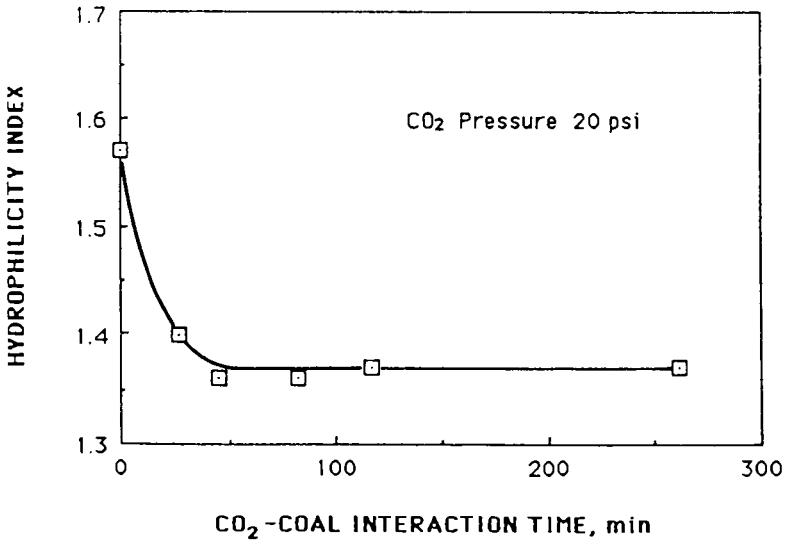


Figure 4 The hydrophilicity index of a CO<sub>2</sub>-pretreated high-volatile bituminous coal (-5 micron) at 302 °K determined by DRIFT-FTIR spectroscopy as a function of CO<sub>2</sub>-coal interaction time.

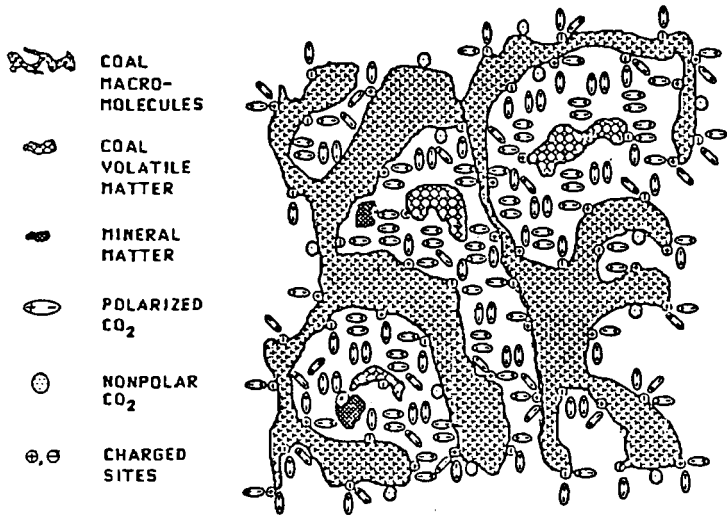


Figure 5 Schematic drawing of carbon dioxide adsorption by coal.

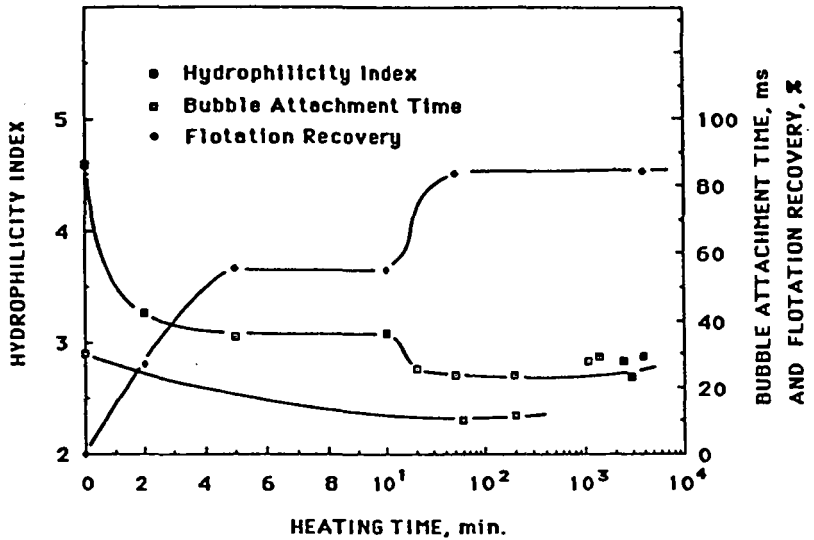


Figure 6 Hydrophobic character of lignite evaluated by the DRIFT-FTIR hydrophilicity index, bubble attachment time and flotation recovery as a function of thermal-treatment time.<sup>(3)</sup>

## IMPROVED SULFUR REMOVAL FROM COALS BY REDOX POTENTIAL CONTROL OF SURFACES DURING GRINDING.

Geatesh K. Tamy, David H. Birlingmair, and Lawrence E. Burkhart  
Ames Laboratory, Iowa State University  
Ames, Iowa 50011

### ABSTRACT

Control of the redox potential of an Upper Freeport run-of-mine coal slurry during wet grinding and subsequent beneficiation gave better sulfur removal, with no decrease in coal recovery, than either potential control during grinding or beneficiation alone. Sodium dithionite, a reducing agent used to depress the sulfur, also gave substantially better results than pH control alone, irrespective of whether the physical beneficiation was by oil agglomeration, foam flotation, or microbubble batch flotation. Three-phase contact angle measurements and pulp potential measurements suggest that slow electrochemical reactions at the particle surfaces may be responsible for the improved results obtained when the reductant is added at the grinding stage.

### INTRODUCTION

The purpose of this work was to alter the surface properties of coal and/or associated mineral particles during grinding to enhance the removal of sulfur-bearing minerals during the beneficiation process. This was done by using reducing agents to alter the electrochemical potential during grinding and beneficiation. The fact that sulfide ores can be depressed by electrochemical techniques is well catalogued in the literature(1-5). Studies(6-9) also have shown that electrochemical effects due to "galvanic interaction" of grinding media during size reduction can affect the flotation of sulfide minerals. In this study, however, electrochemical effects were imposed during grinding by the addition of a chemical reagent. It was presumed that the generation of fresh surfaces, improved contact with the freshly generated surfaces, and the presence of an energy-intensive environment, would all contribute towards promoting surface reactions that could result in enhanced beneficiation.

It should be emphasized that adding oxidizing or reducing agents and monitoring the system by measuring the potential of the pulp relative to a reference electrode, yields a potential which has no real thermodynamic significance. However, it may be used as a guideline, and it has been shown to correlate with laboratory flotation results(10).

### EXPERIMENTAL

#### Materials

##### a) Feed Coal.

A run-of-mine coal sample from the Upper Freeport Seam, Lucerne Mine No. 6, Helvetia Coal Company, Indiana County, Pennsylvania, was used. The sample was dried and reduced to a nominal top size of 9.5 mm (3/8 in) by the Pittsburgh Energy Technology Center. It was further reduced to minus 176  $\mu\text{m}$  in a hammermill, riffled into aliquots, purged with argon, and sealed until use. Its properties are listed in Table 1.

Table 1. Upper Freeport run-of-mine coal, 'as received.

Moisture %	Ash %	Total Sulfur %	Pyritic Sulfur %	Organic Sulfur %	Sulfate Sulfur %	Heating Value Btu/lb	Hardgrove Grindability (0.7% Moisture)
0.85	32.65	2.41	2.04	0.36	0.01	9970	87

b) Additives.

Reagent grade sodium hydroxide, sulfuric acid, and sodium dithionite ( $\text{Na}_2\text{S}_2\text{O}_4$ ) were used. Kerosene was employed as a conditioner and as an agglomerating oil; Dowfroth 150, Accofroth 76, and methylisobutylcarbinol (MIBC) were used as collectors.

Experimental procedure

Grinding.

Samples of the 176- $\mu\text{m}$  feed coal were wet ground (40% solids by weight coal) for 15 minutes in a stirred ball mill using 1/8-in stainless steel balls as the grinding media. The final average particle size was about 10  $\mu\text{m}$ .

Separations.

After grinding in the stirred ball mill, each slurry was separated from the balls and divided into aliquots for separation by three techniques.

1) Microbubble Frit Flotation

The slurry was diluted to 10% solids, conditioned with kerosene (collector) and MIBC (frother), and placed in a flotation cell. Microbubbles were formed in the flotation cell by admitting a regulated gas flow through a porous glass frit at the bottom of the cell. The coal particles, being hydrophobic, attached themselves to the microbubbles and were thus carried to the top of the cell in a fine froth. The overflowing froth (or concentrate) and the material remaining in the flotation cell (i.e., the tailings) were collected, filtered, dried, and analyzed.

2) Microbubble Foam Flotation

In this process the conditioned pulp was transferred to a flotation tube and a microbubble foam was introduced at the bottom of the tube. The foam was prepared by adding either Accofroth 76 or Dowfroth 150 to water in a modified blending chamber at high speed. The concentrate and the tailings were filtered, dried, and analyzed.

3) Oil Agglomeration

A 10% percent coal/water slurry was agglomerated with 15% (by weight of coal) kerosene in a 500-ml blending chamber for 3 minutes at low shear. The agglomerates were separated from the tailings using 100- and 200-mesh test sieves. They were then filtered, dried, and analyzed.

Variations in pretreatment during comminution in the stirred ball mill included the use of NaOH and  $\text{H}_2\text{SO}_4$  for pH adjustments and  $\text{Na}_2\text{S}_2\text{O}_4$  for control of the pulp potential ( $\epsilon$ ). Tests were also conducted with no additives and with the same additives introduced after grinding.

Float/Sink

In another series of tests, portions of the feed coal sample were subjected to float/sink separation using Certigrav at a specific gravity of 1.4 to obtain an organic-rich fraction with a

low mineral content and a mineral-rich fraction with a high mineral content. After separation, the samples were dried at 107°C until no odor of Certigrav remained. The float fraction thus obtained contained 4.7% ash and 0.78% sulfur, and the sink fraction contained 55.4% ash and 8.8% sulfur. Since the ideal separation conditions are those in which the organic fractions are more hydrophobic and the mineral fractions are more hydrophilic, by separating the feed coal into organic-rich and mineral-rich fractions, each fraction may be tested separately to determine the surface characteristics under the conditions used. Flotation results, conducted with coal samples soaked in Certigrav and then dried, were compared with flotation results from samples that had not been soaked in Certigrav to assure that exposure to the Certigrav liquid did not affect the particle surfaces.

#### Contact angle measurements

Three-phase (solid-liquid-water) contact angle measurements at various values of pH and also for an aqueous phase containing sodium dithionite were made using compressed pellets of organic-rich and mineral-rich coal fractions of the Upper Freeport coal which were obtained from the float-sink separation. The pH of the water drops placed on the pellets was adjusted using NaOH and H<sub>2</sub>SO<sub>4</sub>. A 0.1 M solution of sodium dithionite (Na<sub>2</sub>S<sub>2</sub>O<sub>4</sub>) was used. A Rame-Hart contact angle goniometer was used, and the contact angles were measured from enlarged photographs of the drops using a protractor. The contact angles thus obtained were accurate to within 5 degrees, which is the best accuracy that may be expected from a heterogeneous substance like coal.

#### Potential Measurements

Zeta potential measurements were made with a Komline Sanderson Model 12S zeta meter. Measurements were made for both organic-rich and mineral-rich fractions of coal obtained by float-sink separation in solutions of various concentration of sodium dithionite. The pH and the pulp potential ( $\epsilon$ ) were monitored with an Orion Microprocessor Ion Analyzer (Model 901) using a combination pH electrode and a combination Pt-Ag/AgCl electrode (0.044±0.001V vs.SCE).

## RESULTS

### Beneficiation

In the grinding and beneficiation tests, the sample was ground both with and without pH control. The samples ground at pH 3 and pH 7 were each separated at both pH 3 and pH 7. Those ground at the natural pH of 5.5 and at pH 11 were separated at the same pH as during grinding. The results, presented in Table 2, show that under most conditions, the coal recovery was high but with only moderate sulfur reductions and rather poor ash reduction. Since the blender flotation technique yielded poor recoveries, particularly at low pH, some of these tests were repeated using Dowfroth 150 as the frother instead of Accofroth 76. Sulfur removal was poor with Dowfroth, although a slight improvement in coal recovery was obtained.

Table 3 shows the results obtained in replicate runs when sodium dithionite was present during both grinding and separation. This produced significant improvement in the sulfur reduction over those experiments where only pH control was used (Table 2). Average

sulfur reduction values obtained with pH control are compared to those obtained when sodium dithionite was used during both grinding and separation in Figure 1. Figure 2 shows an equally important result; when sodium dithionite was used in only one step, either grinding or separation, lower sulfur reduction was obtained. However, the values still tended to be better than those found during pH control.

Table 2. Results of separations performed under various conditions of pH during grinding and separation.

Grinding pH	Separation		% S Conc.	% S <sup>a</sup> Redn.	% Ash <sup>b</sup> Conc.	% Ash <sup>c</sup> Redn.	% Coal <sup>d</sup> Recov. (additive)
	Type <sup>e</sup>	pH					
Feed			3.64	-	31.3	-	-
Natural	Foam Frit Agg	Natural ~5.5	2.20	39.2	15.9	51.3	84.1 (Accofroth)
			2.20	39.2	19.9	39.0	97.6 (MIBC)
			2.32	35.9	13.4	58.9	95.5 (Kero)
7	Foam Frit Agg	7	2.24	38.1	14.3	56.2	90.3 (Accofroth)
			2.11	41.7	17.6	46.0	97.0 (MIBC)
			2.39	34.0	13.3	59.3	96.0 (Kero)
3	Foam Frit Agg	3	2.19	39.5	15.4	52.8	65.6 (Accofroth)
			2.22	38.7	19.9	32.1	97.7 (MIBC)
			2.27	37.3	12.8	60.8	94.1 (Kero)
3	Foam Frit Agg	3	2.59	28.9	19.3	38.4	89.9 (Dow Froth)
			2.30	36.8	14.3	54.3	88.0 (MIBC)
			2.25	38.1	14.3	54.3	94.1 (Kero)
3	Foam Foam Frit Agg	7	2.22	39.07	16.4	47.8	88.7 (Accofroth)
			3.20	12.41	24.5	15.5	98.7 (Dow Froth)
			2.50	33.1	15.4	50.8	95.9 (MIBC)
			2.34	35.6	14.2	54.8	96.1 (Kero)
11	Foam Frit Agg	11	2.60	28.6	16.5	47.4	95.3 (Accofroth)
			2.31	36.4	14.8	52.6	91.7 (MIBC)
			2.43	33.3	13.5	56.8	96.4 (Kero)

a % S Reduction =  $\frac{\% \text{Feed S} - \% \text{Product S}}{\% \text{Feed S}}$  (all DAF)

b Ash reported on a moisture-free basis; sulfur reported on a moisture- and ash-free basis.

c % Ash Reduction =  $\frac{\% \text{Feed Ash} - \% \text{Product Ash}}{\% \text{Feed Ash}}$ , moisture free.

d % Coal Recovery =  $\frac{100 \times (100 - \% \text{Product Ash}) (\text{Product wt})}{(100 - \% \text{Feed Ash}) (\text{Feed wt})}$

e Foam, Frit, and Agg indicate the type of separation technique used: foam flotation, microbubble frit flotation, or oil agglomeration, respectively.

Table 3. Results of separations performed using 0.1 M sodium dithionite during both grinding and separation<sup>a</sup>. Replicate runs for each technique are shown.

Grinding Condition	Separation		% S Conc.	% S Redn.	% Ash Conc.	% Ash Redn.	% Coal Recov.	
	Type	Condition						
		pH						ε (V)
Feed			3.64	-	31.3	-	-	
0.1 M Na <sub>2</sub> S <sub>2</sub> O <sub>4</sub>	Frit	5.0	-0.39	1.56	57.1	9.3	70.3	68.6
	Frit	4.6	-0.43	2.09	42.6	13.0	59.4	92.4
	Frit	4.3	-0.40	1.96	46.3	12.8	59.3	92.6
	Frit	4.8	-0.40	1.93	46.9	16.1	48.6	90.8
	Foam	5.2	- <sup>b</sup>	1.89	48.3	12.8	59.1	71.5
	Foam	5.2	-	2.05	43.8	12.3	60.8	68.5
	Foam	5.2	-	1.89	48.3	12.1	61.4	65.4
	Foam	5.3	-	1.66	54.5	12.5	60.2	58.0
	Agg	5.0	-0.39	2.02	44.5	12.1	61.4	95.4
	Agg	4.9	-0.40	1.98	45.4	12.4	60.7	84.6

<sup>a</sup> Definitions as in Table 1.

<sup>b</sup> The foam flotation technique does not permit sufficient time for pulp potential measurements.

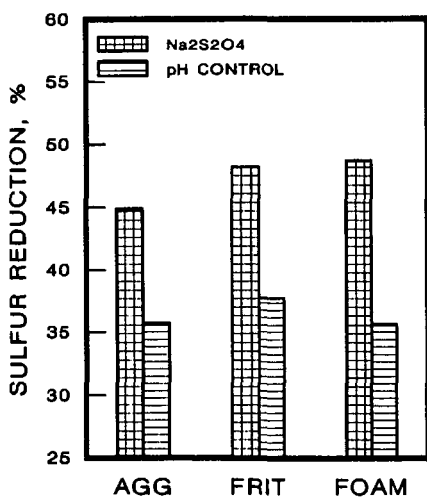


Figure 1. Average sulfur reduction values obtained when Na<sub>2</sub>S<sub>2</sub>O<sub>4</sub> was used during both grinding and separation compared to those obtained with pH control alone.

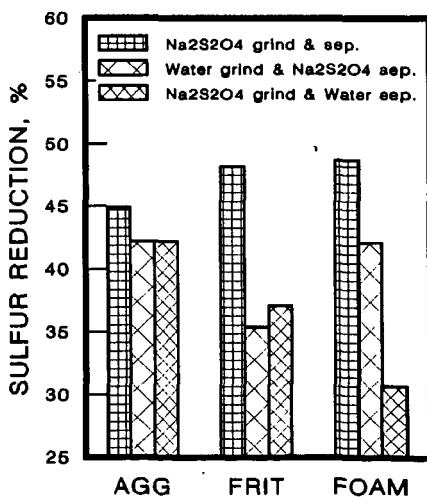


Figure 2. Results obtained when Na<sub>2</sub>S<sub>2</sub>O<sub>4</sub> was used either during grinding or separation only, or during both grinding and separation.

### Surface Characterization Tests

Table 4 depicts the results of contact angle measurements made on pellets prepared with material from the float-sink separations. A smaller angle indicates a surface of greater hydrophobicity (see Figure 3). The contact angles measured for the mineral-rich fraction are consistently larger than those measured for the organic-rich fraction, demonstrating that the mineral-rich fraction is more hydrophilic than the organic-rich fraction. Also, the hydrophilicity of the mineral fraction was a maximum at high pH. These are expected results. However, an unexpected result was that the contact angles measured when the aqueous phase contained 0.1 M sodium dithionite were similar to those with the acidic and neutral aqueous solutions.

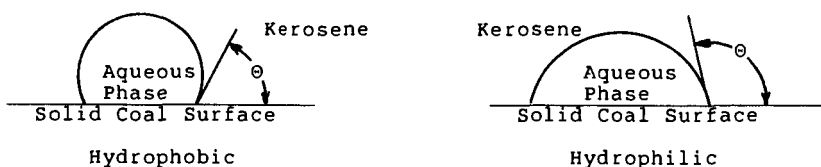


Figure 3. Contact angle measurement.

Table 4. Measured contact angles ( $\theta$ ) of organic-rich and mineral-rich fractions of Upper Freeport coal using the sessile drop technique. Values are averages of 'n' measurements with a standard deviation of  $\sigma$ .

Condition	Mineral-Rich "Sink" Fraction			Organic-Rich "Float" Fraction		
	$\theta$	$\sigma$	n	$\theta$	$\sigma$	n
pH 11.0	27.5	1.69	8	21.2	5.32	8
pH 7.6	27.3	3.58	8	20.3	4.56	8
pH 3.0	24.4	4.72	8	17.5	3.38	8
0.1M $\text{Na}_2\text{S}_2\text{O}_4$	26.1	3.98	8	20.9	2.10	8
pH 4 Buffer	24.5	0.71	2	16.5	2.12	2
pH 7 Buffer	26.5	2.12	2	15.5	0.71	2
pH 10 Buffer	30.0	0	2	20.0	0	2

An attempt was made to determine the effect of ionic strength on the zeta potential of the organic-rich and mineral-rich fractions in solutions of varying sodium dithionite concentration. During these tests, it was found that both the pulp potential, and the pH of the slurry, changed with time. The change continued over several minutes and the rate of change was a function of sodium dithionite concentration. Thus these experiments provided no information about the effect of the ionic double layer. However, they suggest that the kinetics of reactions at the surface may be important and that slow electrochemical surface reactions may have been taking place.

### DISCUSSION

The increased floatability of pyrite and other sulfide minerals is usually attributed to mild oxidation which leads to the formation

of sulfur or sulfur-like entities which enhance the particle hydrophobicity. Hamilton and Woods(11) have explained the effect as the formation of a metal-deficient sulfide; conversely, reduction produces a metal-rich sulfide on the particle surface. These authors state that the attractive interaction between water and the mineral surface is determined by the availability of metal ions in the immediate surface layer (large anions, like sulfide, are generally not hydrated). Thus, removal of metal ions from the surface reduces the opportunity for specific interaction with water molecules. Hydrophobic/hydrophilic effects in solution may also be explained in terms of the free energy of the particle surface(12). When this is done the entropy component of the free energy change of the surface is seen to be significant(12).

Guy and Trahar(13) report that for many sulfides, the oxidation reaction does not proceed rapidly. Firth and Nicol(14) state that a number of factors could affect the rate of reaction on pyrite surfaces. These include: the temperature and humidity, the size distribution and form of occurrence of the sulfides, the time of exposure, and the presence of peculiarities in the crystal lattice, such as sulfur deficiencies and the presence of polymorphs, which may serve as active sites for oxidation reactions. Castro(15) found that, over time the electrode potential of chalcocite decreased when sodium sulfide was added, indicating oxidation of the mineral. More recently, Miley(16) has shown that the electrode potential of a suspension of coal particles in an aqueous solution of a strong oxidizing agent changes over several hours. Thus, observing this change, a general picture of the oxidation process may be obtained, the change being indicative of the "oxidation state" of the coal.

One may envision that the reduction reaction, which has been studied less extensively, may display kinetic effects similar to those observed for oxidation. Chander(17) has reviewed the published literature on the mechanism of reduction of pyrite minerals and states that a unified theory is, as yet, unavailable. According to Chander(17), formation of metastable species in the solution or in the solid phase, nonstoichiometry of the solid phase, and slow reaction kinetics could all lead to nonequilibrium conditions. The variation of the pulp potential and pH with time does suggest slow reaction kinetics.

#### CONCLUSION

The addition of sodium dithionite to control pulp potential resulted in improved ash and sulfur removal from Upper Freeport coal as compared to pH control. The best results were obtained when the reducing agent was present during both grinding and separation. Contact angle measurements indicated that the improvement was not due to a lesser affinity for the organic portion of the coal toward the dithionite solution. The pulp potential and the pH of the slurries containing the organic-rich and mineral-rich fractions of the coal varied with time, indicating the possibility of slow reaction kinetics. This work is an example in which the grinder has been employed effectively in chemical pretreatment. The concept, often discussed in the literature, has rarely been demonstrated.

#### ACKNOWLEDGEMENTS

Ames Laboratory is operated for the U. S. Department of Energy by Iowa State University under Contract No. W-7405-ENG-82. This work was supported by the Assistant Secretary for Fossil Energy through the Pittsburgh Energy Technology Center.

#### REFERENCES

1. Hyde, G.R.; Stojsic, A.; Mining Engineering, 39(7), 481-484, (1987).
2. Nakazawa, H.; Iwasaki, I.; Minerals and Metallurgical Processing, 2, 206-211, (1985).
3. Ogunsola, O.M.; Osseo-Asare, K.; Fuel, 65, 811-815, (1986).
4. Biegler, T.; Swift, D.A.; Electrochimica Acta, 24, 415-420, (1979).
5. Luttrell, G.H., and Yoon, R.H., Int. J. Miner. Proc., 13, 271-283, (1984).
6. Kocabag, D.; Smith, M.R.; in "Complex Sulfides. Processing of Ores, Concentrates and By-Products", Zunkel, A.D.; Boorman, A.S.; Wesely, R.J.; eds., 55-81, 1985.
7. Learmont, M.E.; Iwasaki, I.; Minerals and Metallurgical Processing, 1, 136-143, (1984).
8. Adam, K.; Natarajan, K.A.; Iwasaki, I.; International Journal of Mineral Processing, 12, 39-54, (1984).
9. Pozzo, R.L.; Malicsi, A.S.; Iwasaki, I.; SME Annual Meeting, Phoenix, AZ, Jan 25-28 (1988).
10. Hamilton, I.C.; Woods, R.; Proc. Int. Symp on Electrochemistry in Mineral and Metal Processing, Richardson, P.E.; Srinivasan, S.; Woods, R.; eds., The Electroanalytical Society, NJ, 1984.
11. Hamilton, I.C.; Woods, R.; J. Electroanal. Chem., 118, 327, (1981).
12. a) Tampy, G.K.; PhD Dissertation, Ohio University, March (1988). b) Tampy, G.K.; Prudich, M.E.; Savage, R.L.; Williams, R.R.; Energy & Fuels, in press, 1988.
13. Guy, P.J.; Trahar, W.J.; in "Flotation of Sulfide Minerals", Fossberg, K.S.E.; ed.; Elsevier, 1985, pp. 91-110.
14. Firth, B.A.; Nicol, S.K.; Coal Preparation, 1, 53-70, (1984).
15. Castro, S.; in "Mineral Processing", vol. 2, Laskowski, J.; ed., Elsevier, 1981, pp. 181-202.
16. Milley, J.; Fuel, 67, 143-144, (1988).
17. Chander, S.; Minerals and Metallurgical Processing, 2, 26-35, (1985).

## EXTRACTION RATES AND POROSITY CHANGES OF COALS IN SUPERCRITICAL THF

E.S. Olson, J.W. Diehl, D.K. Horne and H.D. Bale

University of North Dakota  
Energy and Mineral Research Center  
and Department of Physics  
Grand Forks, ND 58202

Important facets of the thermal processing of coals in a dissolving medium, such as that which occurs in liquefaction or extraction, are the rate of dissolution and the concomitant change in the surface structure of the coal. The interaction between these two related parameters is being studied by extracting coals in a flow-through cell under supercritical conditions and measuring the rates of extraction by on-line ultraviolet spectroscopy and the changes in pore structure of the coal by in situ small-angle X-ray scattering. The advantages of utilizing supercritical fluids in this project are the solvent densities, which are similar to liquids, the high solubility parameters, and yet low viscosities, similar to gases. For these experiments the solvent should be composed of first row elements and not have significant absorption in the uv. In addition, alcohols cannot be used since they destroy the aluminum windows of the extraction cell. Several solvents were tested in these investigations, and supercritical tetrahydrofuran (THF) was the only one found satisfactory for both measurements. The supercritical THF gave good yields of extract from even lignites, and the extracted material remained soluble in liquid THF.

### EXPERIMENTAL

The solvent in these studies was uninhibited HPLC grade THF (Fisher), used as received. Coal was dried in an inert atmosphere or in a vacuum prior to the extraction. Ultimate analysis (maf) for the Wyodak subbituminous coal (Clovis Point) was H, 5.2; C, 70.9; N, 0.92; S, 0.60; O (ind.), 22.3. Proximate analysis (mf) was volatile matter, 44.2; ash, 8.4; fixed carbon (ind.), 47.5.

Two different extraction cells have been used for the two types of measurements. The apparatus in which the extraction kinetics were measured by uv absorption consisted of an Isco LC-5000 syringe pump connected to a 5 cm x 4.6 mm (LC precolumn) extraction cell. The cell and steel inlet tubing were heated in a Varian 1400 aerograph GC. The cell capacity was 0.2 g. Effluent from the cell was carried from the oven via a 1/16-inch steel tubing to a 1 m x 0.32 mm fused silica capillary (no phase coating), which served as the cell for the uv detector. The polyimide outer coating was removed from a portion of the capillary which was in the beam path of a Kratos 700 LC detector (254 nm). After passing through the uv detector, the capillary was connected to a Whitney SS-21RS2 restrictor valve to maintain the pressure in the system. The eluent was collected, and the weight of extract was determined after evaporation of the solvent.

Analog signals from the uv detector were digitized with an Omega WB-31 12-bit A/D converter and transferred to a Tandy 2000HD computer via RS-232C. Data was collected and stored to disk at 2 points/s. The area under the uv response curve was divided into 100 equal time segments and the proportional area determined for each segment. The

proportional areas were multiplied by the extract weight, giving the weight of extract per unit time. This normalization assumes that the response across the curve remains constant, which was determined to be true for extraction of 3 g of coal in a large cell where individual fractions were collected and weighed.

The extraction cell for the small-angle scattering studies consisted of two electrically heated flanges which hold the aluminum/beryllium windows and a stainless steel block which gives a sample depth of 0.07 inches between the two windows. Molybdenum  $K_{\alpha}$  radiation was used in these studies. Details of the collimation system and position sensitive detector are available elsewhere (1). Analysis of the scattering data was based on a model developed by Kalliat, Kwak, and Schmidt (2). Pore structure parameters calculated for thermally treated lignites have been shown to be in close agreement with independent measurements (3).

## RESULTS AND DISCUSSION

A series of kinetic experiments were carried out with Wyodak subbituminous coal (Clovis Point) in the flow-through cell with on-line uv detection. In each of these runs, a dewaxing preextraction stage at a temperature of 120°C was utilized to remove an initial surge of material, whose elution was monitored until no detector response was observed. The material extracted at this low temperature (2% mf basis) was mainly aliphatic (fatty acids), similar to the Montan wax, which is normally extracted with noncritical solvents and is not believed to be covalently bonded or "matrix trapped" material.

The X-ray scattering pattern of the Wyodak coal after extraction at 120°C and 4.5 MPa indicated that the dewaxing had an effect on the pore structure, causing a modest increase in the micropore parameters (Table 1). The micropore specific surface increased from 58 m<sup>2</sup>/g to about 290 m<sup>2</sup>/g. The corresponding increase in micropore volume was 0.019 cm<sup>3</sup>/g, which would suggest about a 2% loss of mass if the new pore structure is formed in the wake of the dissolved component.

The supercritical extractions were carried out by rapidly increasing the temperature of the system (30°C/min) in the GC oven to the desired extraction temperature where the temperature was held constant (isothermal stage). UV response data for the Wyodak coal were recorded for four extraction temperatures from 325 to 400°C at 15.2 MPa and flow rates of 1 ml/min. Run times were about one hour. Two extractions were conducted at 380°C at lower pressures (5.5 and 10.3 MPa) for comparison with the 15.2 MPa run. The solvent containing the extracted material was collected after the restrictor valve. The solvent was removed and the extract weighed. The yield data from the four experiments at 15.2 MPa and two experiments conducted at lower pressures are shown in Table 2. The yields at the high temperatures (350° and above) at 15.2 MPa were essentially the same and were approximately three times the yield obtained at either low temperature (325°) or low pressures. We distinguish then, three classes of extracted coal material, the preextraction wax, the low-temperature extract (easily extracted material), and the high-temperature extract (less easily extracted material). The composition of the low- and high-temperature extracts was similar, consisting of high molecular weight aliphatic and aromatic material. The higher yields at the higher pressure may be due to the higher solvating power of the supercritical fluid at higher densities, which are obtained at

higher pressure, or may be due to a physical effect such as solvent being forced into a micropore.

The uv response curve for the 380°C extraction of Wyodak is shown in Figure 1. The curve does not include the preextraction step, instead it begins with the rapid temperature increase. From the uv response curve, the amount of coal material being extracted at each instant and the amount accumulated at each time interval (x) was determined. The natural log of the difference between the total amount of extract (a) and the accumulated amount at each interval (x) was plotted versus time. The first half of the curve was linear, indicating first-order kinetics. The slope of this part of the curve was used to determine an apparent rate constant. Similar curves were obtained for the reactions carried out isothermally at the other temperatures, and the rate constant (k') for each of these is shown in Table 2. It is likely that these rate constant values are a composite of reaction rate constants for bond cleavage reactions and other constants for diffusion and dissolution of the coal macromolecules in the supercritical phase. Because of the variety of bonds in the coal matrix which must be broken to solubilize the coal, the range of individual rate constants for bond cleavages which make up the composite might be quite large. Similarly, the polydispersity of molecular sizes in the material released by bond breakage and the solvation parameters of these materials might result in diffusion constants that vary over a large range. Thus one would not expect to be able to derive an activation energy for bond dissociation from the rate constant data at the different temperatures via an Arrhenius plot.

Comparison of the rate constants for the 350, 380, and 400°C runs show that they increase generally with the temperature as one would normally expect. The rate constant for the 325°C reaction is higher than that for the 350°C reaction, but this is for much less extracted material, a 10% yield versus a 28% yield. Thus at 325°C we observe the rate constant for the easily extracted material (10% yield) and the rate constant for extraction of this material would be expected to increase with temperature. Then at 350°C the less easily extracted material contributes to the extraction products (an additional 20% yield) but with a lower extraction rate constant, hence lowering the overall rate constant observed. At higher temperatures the rate constant for the less easily extracted material increases. At the lower pressures, lower yields are obtained, presumably because of lower solvent density. This may be the same easily extracted material with the higher extraction rate constant, exhibiting the expected increase with temperature. Thus the less easily extracted material made no contribution to the rate constant at the lower pressures.

For the Wyodak coal extracted at 380°C and 4.5 MPa, the micropore surface calculated from the scattering data was  $2.7 \times 10^3 \text{ m}^2/\text{g}$ . This substantial (tenfold) increase was accompanied by a decrease in the transition pore area to  $0.39 \text{ m}^2/\text{g}$ . Progressive isothermal (380°C) extraction as a function of pressure was carried out at 4.5, 7.5, and 10.5 MPa. The curves show an increase in scattering at the intermediate h values, which can be attributed to an increase in the transition pore structure (Table 1). There is also a small increase in the scattering at the larger h values following extraction at 7.5 MPa which suggests additional micropore structure. The progressive changes in the micropore surface area may be due to the increased

solubility of the extract at higher fluid density. The increased transition pore structure is likely a consequence of heterogeneous nature of the coal which results in certain regions dissolving more easily than others.

The change in kinetics as the reaction proceeds may be attributed to an increase in surface area as the micropore volumes develop during the extraction. Thus the greater contact with solvent in the enlarged micropores may result in release of more coal material, even though the activation energies for bond cleavage do not change. Further measurements are needed to confirm this hypothesis.

Experiments were carried out with two additional coals, Beulah (ND) lignite and Pittsburgh #8 bituminous coal (Argonne premium sample), with supercritical THF at 2200 psi and 380°C. The bituminous coal gave a 24% yield of extract in a two-hour run. The uv response had not reached the baseline even after the two hours, indicating that coal-derived material was still being extracted. As expected from this incompleteness of the reaction, the first-order rate constant calculated from the uv response curve for this experiment was considerably lower than that of the Wyodak at the same temperature and pressure, that is 0.014 min<sup>-1</sup>. Thus the bituminous coal is capable of giving good yields of extract but at a much slower rate than the Wyodak subbituminous coal. Under the same conditions of temperature and pressure, the Beulah lignite gave a yield of 12% over a 80-min period, with the uv response returning to baseline. The uv response curve was unlike that of the Wyodak and Pittsburgh #8 in that the maximum extraction rate was reached more slowly. The first-order rate constant calculated from the curve was 0.022, also lower than that of the Wyodak. These data appear to provide an excellent reactivity index for the coal under nonreductive conditions.

#### REFERENCES

1. Bale, H.D. Role of Porosity in Supercritical Fluid Extraction of Coal, Technical Progress Report, January 20, 1987.
2. Kalliat, M.; Kwak, C.Y.; Schmidt, P.W. New Approaches in Coal Chemistry, Symposium Series 169; Amer. Chem. Soc.: Washington, DC, 1981; Chapter 1.
3. Bale, H.D.; Carlson, M.L.; Schobert, H.H; Fuel 1986, 65, 1185-1189.

#### ACKNOWLEDGEMENTS

This research was sponsored by the Department of Energy under DOE contract number DE-FG22-86PC90521.

Table 1  
Scattering Results for Wyodak Coal

Conditions	Specific Surface (m <sup>2</sup> /g)			Specific Volumes x 10 <sup>3</sup> (cm <sup>3</sup> /g)	
	S <sub>ma</sub>	S <sub>tr</sub>	S <sub>mi</sub>	V <sub>tr</sub>	V <sub>mi</sub>
120 C, Ar, 0.2MPa	1.5	3.7	58	2.2	7.1
120 C, THF, 4.5MPa	1.8	3.0	2.9 x 10 <sup>2</sup>	2.2	26
380 C, THF, 4.5MPa	1.6	0.39	2.7 x 10 <sup>3</sup>	0.15	140
380 C, THF, 7.5MPa	1.2	4.5	4.0 x 10 <sup>3</sup>	2.3	250
380 C, THF, 10.5MPa	1.5	10.0	4.3 x 10 <sup>3</sup>	4.0	260

Table 2  
Yield data and apparent rate constants for Wyodak extractions (THF)

Temperature (°C)	Pressure (MPa)	Yield (%mf±2%)	k* (min <sup>-1</sup> )
325	15.2	10	0.041
350	15.2	28	0.028
380	15.2	30	0.041
400	15.2	25	0.064
380	10.3	9	0.053
380	5.5	6	0.052

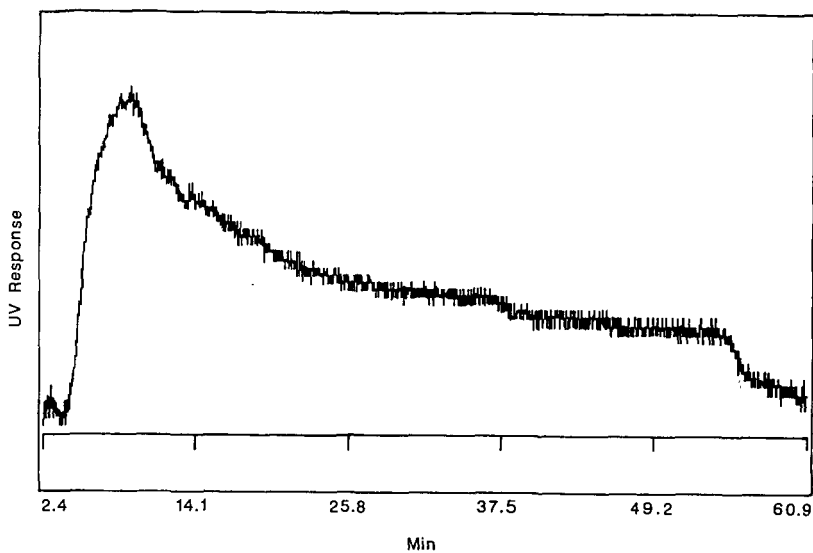


Figure 1: UV response curve for supercritical THF extraction of Wyodak. (THF, 380<sup>o</sup>, 2200 psi, 1 ml/min).

COAL COMMINATION BY HIGH PRESSURE WATER JETS  
MACHINE DESIGN CONCEPTUAL STUDY

Dr. G. Galecki  
Dr. M. Mazurkiewicz  
Mr. L. Wijeratne

Rock Mechanics & Explosives Research Center of the University of Missouri-Rolla,  
1006 Kingshighway, Rolla, Missouri 65401 U.S.A.

ABSTRACT:

In the offered paper the authors present the results of the work conducted on the coal response for high pressure water jets attack. The paper covers different types of water jets such as: solid jets, cavitating jets, and rotating jets and also the results of coal disintegration effectiveness. The concepts of the models of comminuting machines are presented. The mechanism of the coal disintegration in relationship to these models and the process efficiency are discussed.

INTRODUCTION:

With the advances in the high pressure water jet technology, one of the potential applications of this science is in the area of material disintegration. Coal was chosen as the subject of interest because of the ongoing search for an alternative source of energy. Coal has a structure that is very brittle and filled with micro-cracks. Earlier work by Mazurkiewicz [1] show that material is weaker in tension than in compression. Figure 1 shows the stresses that occur as the water jet penetrates a coal crack. The tip tension stress  $\sigma$  maximum is given by the equation

$$\sigma_{\max} = \sigma_0 \left( 1 + \frac{2b}{a} \right) \quad 1)$$

where  $\sigma_0$  is the stagnation pressure developed inside the crack by the jet,  $2b$  the crack length and the  $2a$  the crack width. For even hard coal with a crack dimension ratio,  $b/a = 10$ , the pressure necessary to ensure continued crack growth is 15.7 KPa.

For coal, the practical observation yields a ratio between the compression stress versus the tensile stress to be in the range of 20 to 30 times. Also, the theoretical strain energy comparisons show that the compression tension ratio for coal to be 65 in the perpendicular direction to the coal seam and 62 in the parallel direction to the coal seam. These facts combined with the ability of the water jets to penetrate the micro-cracks, creating a zone of tension at the crack tip enhances crack growth and increases the comminution effectiveness.

The theoretical model for comminution of coal by high pressure water jets was based on Griffith's theory [2,3]. Griffith considered an infinite cracked plate of unit thickness with a central traverse crack of length of  $2a$ . The plate is under tensile stress and fixed at its ends. Crack propagation will occur if the energy released upon crack growth is sufficient to provide all the energy that is required for crack growth, which can be expressed by:

$$\frac{dU}{da} = \frac{dW}{da} \quad 2)$$

where  $U$  is the elastic energy and  $W$  the energy required for crack growth. Griffith defined the crack driving force as  $G = \pi\sigma^2 a/E$ . For crack growth to occur  $G$  must exceed a certain critical value  $G_{IC}$ . Hence the condition for crack growth

$$G_{IC} = \frac{\pi\sigma_c^2 a}{E} + \sigma_c = \frac{E G_{IC}}{\pi a} \quad 3)$$

$$\sigma = \frac{P_o - P_v}{\rho U_o^2 / 2} \quad 4)$$

where  $P_o$  and  $U_o$  are the ambient values of pressure intensity and velocity and  $P_v$  and  $\rho$  are the vapor pressure and the density of the liquid, respectively. For maximum cavitation in the chamber the outlet pressure should be approximately 1% of the inlet pressure. To control these conditions, a specially designed cavitation chamber was used [5].

Two types of nozzles were used. The first series utilized a nozzle that was not point loaded, but rather contains a cylindrical cavity of air in the center of the jet, which causes very high turbulence (Figure 4). For this series the coal was loaded into the cavitation cell and acted by the high pressure water. In the second series a solid water jet nozzle was used combined with a mixing chamber and slurry nozzle.

Using the cavitation nozzle, tests were conducted for jet action time of 5.0 seconds at an inlet pressure of 5,000 psi for a mass of 200 grams. The results showed that an almost linear relationship existed between the initial coal size and the energy consumption. The lowest energy consumption was for the smallest coal particle size of #30 mesh. As the coal size was increased the energy consumption increased. These results can be explained by the fact that for the same coal mass but smaller grain size, the total surface area of coal which comes into contact with the cavitation bubbles is greater. Cavitation is a micro-phenomenon and the area of contact is very important. For this reason, the erosion process observed during the cavitation phenomenon is proportional to the coal grain size.

For the same initial coal size of #30 mesh, as the time of jet action was increased to 10.0 seconds a drastic increase in the energy consumption occurred (13,502 kWh/ton for the 10 second tests as compared to 839 kWh/ton for the 5.0 second test). These results indicate the importance of the slurry concentration. To further emphasize these results, tests were conducted for constant pressures but for different amounts of initial coal of 200, 400 and 600 grams. The results show that as the initial coal mass was increased the energy consumption decreased.

For the next series of experiments the mechanism of coal feeding was identical to that for solid jets (Figure 2). The coal entering the mixing chamber was attacked by the high pressure water jet and exists through the slurry nozzle into the cavitation chamber. Inside the cavitation chamber erosion of the coal particles takes place due to the cavitation phenomenon and high turbulence in the chamber.

The tests were conducted for a nozzle diameter combination of  $d=0.041$ " and  $D=0.120$ " for pressures of 3,500 and 5,500 psi. The initial coal particle size was #30 mesh. The tests were conducted for different back pressures, as shown in Figure 5.

The lowest energy level achieved for a final product size of -75 microns was 407 kWh/ton for an inlet pressure of  $p=3,500$  psi. Also, the results show that no significant changes in the energy level was observed at higher pressures. Slight changes in the back pressure caused no significant change in the energy consumption.

As conclusions from this series of experiments it could be concluded that the coal should not be surrounded by water. A higher slurry concentration would produce better results. The importance of the initial particle size was brought out again. As the initial particle size was decreased the energy consumption decreased.

#### Rotating Water Jets:

A specially designed and machined test rig was used in conducting these experiments. The primary system component was the rotating spindle. Three nozzles were attached to the nozzle head. The rotating spindle was supplied with high pressure water through the rotary coupling. The maximum speed of rotation for this rotary coupling was limited to 600 rpm. The system was driven by an electric motor. A schematic view of the assembly can be seen in Figure 6. The coal was filled into both perforated and imperforated container. The container placed on a mechanical lifter made it possible to give vertical movement to the container.

#### EXPERIMENTAL EQUIPMENT, PROCEDURE AND DISCUSSION OF RESULTS:

No theoretical value of  $G_{IC}$  is given for coal in the literature. The heterogeneous structure of coal would account for this.

To gain a better understanding of material disintegration by water jet action, a model study on material discontinuities has been carried out earlier [4]. The pressure distribution inside a receiving pipe, designed to simulate a representative micro-crack in the material was studied. The results show that the pressure within the receiving pipe depends on the ratio of the injecting nozzle and receiving pipe diameters. As the injecting nozzle diameter increased with respect to the receiving pipe the pressure inside the pipe P 2 increased. Also, the pressure P 2 was strongly dependent on the stand off-distance between the injecting nozzle and receiving pipe. In practice it means that for maximum pressurization of the crack, the jet diameter has to be bigger or equal to the micro-crack. Also, the distance between the jet and the coal is important.

As mentioned, three types of jets were tested, i.e., solid, cavitating and rotating jets. In all tests the comminuted particles below 75 microns (200 mesh) was separated by a wet sieve analysis [4] and the specific energy levels calculated. The calculated specific energy consumption was the energy of the water stream alone and does not include the energy consumed by the system as a whole. In this chapter each series of experimental equipment, experimental procedure and the results achieved will be discussed separately for each kind of jet.

#### Solid Water Jets:

The first series of tests was concerning the use of solid water jets for coal comminution. The apparatus consists of a solid water jet nozzle connected to a mixing chamber and slurry nozzle assembly. The mixing chamber was connected to a long plexi glass tube by a conical shape adaptor. Figure 2 shows a schematic view of the equipment set up. The coal was fed directly into the mixing chamber to be attacked by the jet emerging from the nozzle. The water jet moving through the mixing chamber creates a vacuum inside the chamber which results in a suction at the coal inlet to the mixing chamber. By taking advantage of this suction, it was possible to get an uniform flow of coal into the mixing chamber. The coal after being attacked in the mixing chamber flows through the slurry nozzle and was collected at the end of the tube.

The initial task was to find the dependence of the initial coal particle size. Tests were carried out for #4 and #30 coal. The energy consumption for the #4 coal was almost 7 times as that for the #30 coal (7147 kWh/ton for the #4 coal as compared to 1032 kWh/ton for the #30 coal).

The next series of tests were for different injecting and slurry nozzle combinations. The initial coal particle size was #30 mesh. The results are presented in Figure 3. These test results show that for a pressure increase that no significant change in the energy consumption occurred. This is an important remark from a practical point of view because lower pressures are easier to generate and does not require expensive equipment. Also, as the slurry nozzle diameter was increased a reduction in the energy consumption occurred. This can be explained by the fact that in a bigger nozzle the possibility of the particles hitting the nozzle wall, deflecting and hitting other particles is greater, thereby, increasing the attrition of particles.

As conclusions from this part of the tests it could be stated that as the initial coal particle size was reduced, the energy consumption was reduced. Also, as the slurry nozzles diameter was increased from 0.086" to 0.120" for the same injecting nozzle of 0.041" a reduction in the energy consumption occurred. Increasing the pressure had an adverse effect on the energy consumption.

#### Cavitating Water Jets:

The second series of experiments were for cavitating jets. The cavitation number which defines the inception and subsequent growth and collapse of cavitation bubbles is given by the equation

The initial coal particle size was 0.742"  $<S < 0.525$ ". The tests were conducted for a pressure of 5,500 psi using three nozzles each of diameter 0.032".

The initial tests were carried out with the nozzles oriented at 3, 8 and 20 degree angles. The first task was to investigate the importance of increasing the volume of water to the comminution process. Tests were carried out for jet action times of 15, 30 and 75 seconds using an imperforated container. It was seen that as the time of jet action increased the energy consumption increased. To explain this, consider the water jet action on the coal and the time over which it acts. Increasing the jet action time increases the volume of water utilized. The coal particles tend to become suspended in the excess water. They are in effect, surrounded by a coating of water whose protective ability increases with the volume of water utilized. The water jets lose energy in penetrating this protective coating in order to come in contact with the coal particles. This energy is not used to create new surfaces during direct collision with coal particles and hence is wasted.

For the same series of tests a perforated coal container was used and water jet action times of 75 seconds and 150 seconds investigated with vertical up and down axial movement (8 cycles/minute) of the coal container. A test with a jet action time of 75 seconds was conducted without container movement. The results show (Figure 7) that the energy consumption with coal container movement to be almost half those of the case with rotation only. These results clearly indicate the importance of the kinematic movement of the high pressure water jets, which gives a better opportunity for the coal particles to come in direct contact with the water jets.

In the next series the orientation of the nozzles were changed. The nozzles were now oriented perpendicular to the spindle axis. The effect of vertical movement of the coal container was investigated for both 3 and 12 full cycles of motion for 2 minute tests. For the purpose of comparison the coal container was also kept stationary. The energy requirements appear almost 20% less for the case when rotating jets were moved up and down 12 times per minutes as compared to other kinematic conditions of the jets for the tests carried out (Figure 8).

As conclusions from this portion of experiments the importance of the slurry concentration was brought out again. The coal particles should not be surrounded by water. Also the kinematics and dynamics of the interaction between the high pressure water jets and the material to be comminuted plays a very important role in the effectiveness of the comminution process.

#### GENERAL CONCLUSIONS:

Based on the experimental results presented in this paper the following conclusions can be formulated:

The energy consumption taken into consideration as a criterion of the effectiveness of the comminution process shows a very strong dependence on:

- jet diameter and pressure
- initial coal particle size
- solid concentration in slurry
- kinematics of the interaction between the high pressure water jets and coal

The minimum specific energy input of 400 kWh/ton achieved to date represents a significant improvement in the comminution technology. Typical specific energy consumption levels associated with fluid energy mills are in the range of 700-800 kWh/ton [6]. It is envisaged that application of the knowledge gained from the tests carried out to date will enable further improvement of the comminution technology.

#### ACKNOWLEDGEMENT:

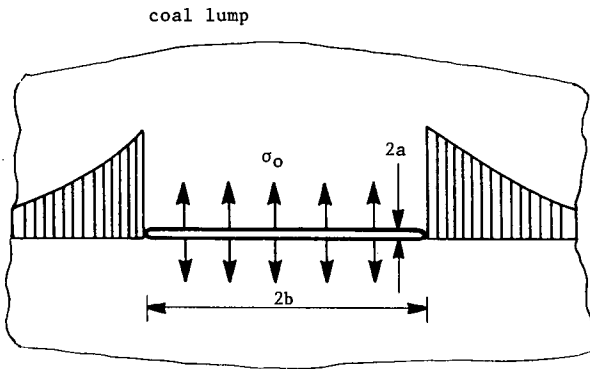
Support for this project was provided by the Department of Energy, Pittsburgh Energy Technology Center under contract No. DOE-DE-AC22-86PC-91271. The authors are grateful for this support.

REFERENCES:

1. Galecki, G., Mazurkiewicz, M., "Coal Comminution by High Pressure Water Jet" 8th International Symposium of Coal Slurry Fuels Preparation and Utilization., May 27-30, 1986, Orlando, Florida, pp 852-861.
2. Griffith, A.A., "The Phenomena of Rupture and Flow in Solids", Phil. Trans. Roy. Soc. of London, A 221 (1921), pp 163-197.
3. Griffith, A.A., "The Theory of Rupture", Proc. 1st Int. Congress Appl. Mech., (1924), pp 55-63.
4. Mazurkiewicz, M., Galecki, G., Technical Progress Report No. 7 on Contract DOE-DE-AC22-86PC-91271, submitted to Department of Energy, Pittsburgh, Pennsylvania, April 1987.
5. Galecki, G., Mazurkiewicz, M., Summers, D.A., "Cavitation Cell" Invention Disclosure 88-UMR-042.
6. Report of the Committee on Comminution and Energy Consumption "Comminution and Energy Consumption", Publication NMAB-364, National Academy Press, Washington, D.C., 1981, pp. 13-39.

For Illinois Coal:

$\sigma_{\perp} = 26.7 \text{ MPa}$       compression  
 $\sigma_{\parallel} = 15.0 \text{ MPa}$   
 $\sigma_{\perp} = 3.3 \text{ MPa}$       tension  
 $\sigma_{\parallel} = 1.9 \text{ MPa}$



$\sigma_0$  - stagnation pressure developed inside the crack by jet

$\sigma_{\max}$  - tip tension stress

$$\sigma_{\max} = \sigma_0 \left( 1 + \frac{2b}{a} \right)$$

For  $b/a = 10$ ,  $\sigma_{\max} = 21 \sigma_0 = 3.3 \text{ MPa}$

The stagnation pressure to grow a micro-crack is

$$\sigma_0 = 15.7 \text{ kPa}$$

Figure 1. Pressure necessary to propagate coal micro-cracks.

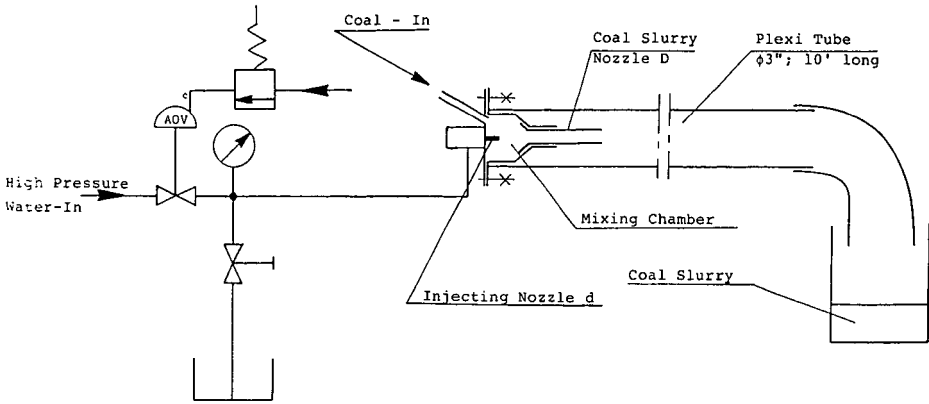


Figure 2. Schematic Drawing of Apparatus for Solid Water Jet Tests with Mixing Chamber.

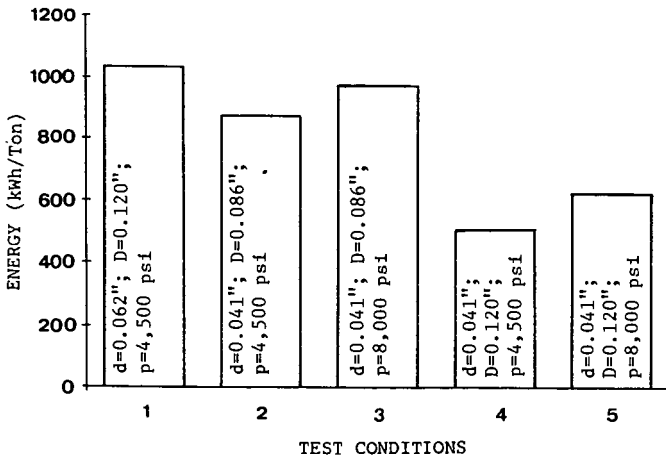


Figure 3. Graph of Energy Versus Different Test Conditions of Pressures and Slurry Nozzle Diameters for Direct Water Jets.

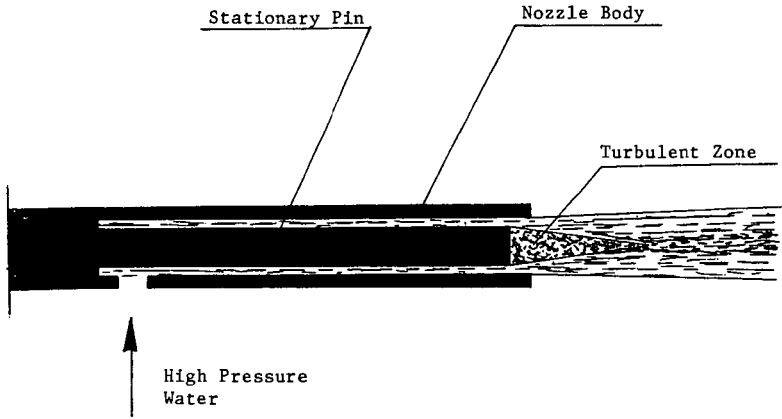


Figure 4. Schematic Drawing of Nozzle with Cylindrical Cavity of Air.

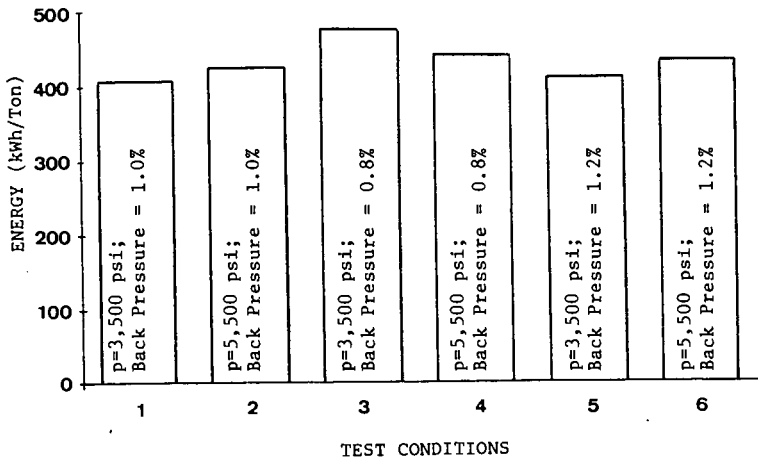


Figure 5. Graph of Energy Versus Different Combinations of Inlet and Back Pressures for Cavitation Tests.

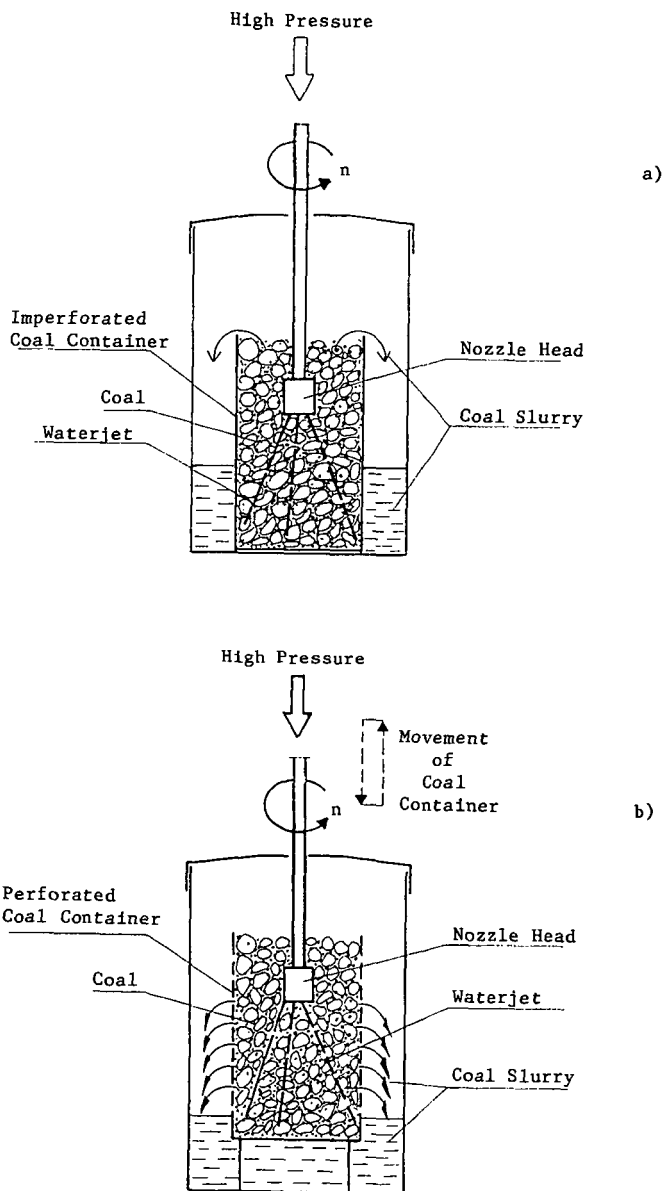


Figure 6. Schematic Drawing of Rotating Water Jet Experimental Equipment.

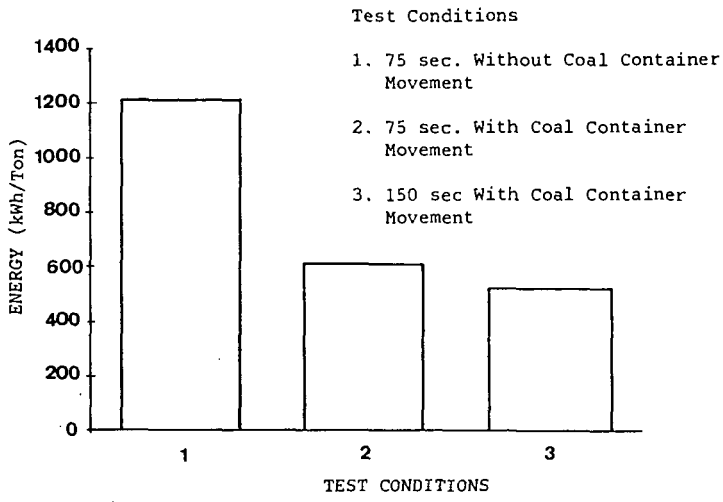


Figure 7. Graph of Energy Versus Different Test Conditions for Nozzles Angled at 3, 8 and 20 Degree Angles.

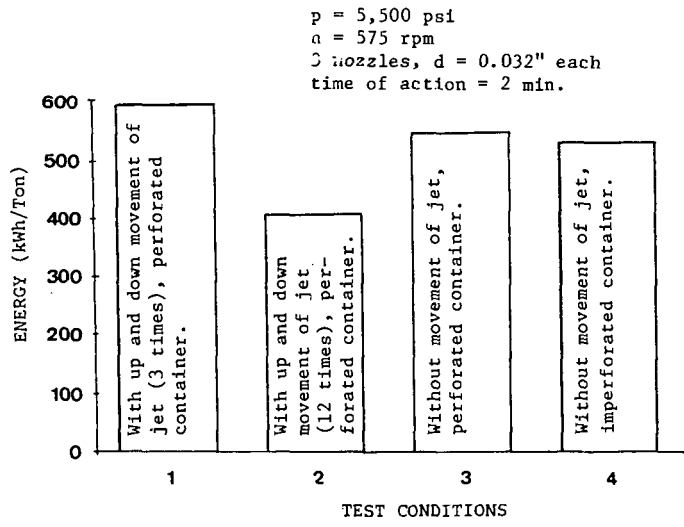


Figure 8. Graph of Energy Versus Different Test Conditions for Nozzles Angled Perpendicular to the Axis of Rotation.